TIN MOLYBDENUM MIXED METAL OXIDES CATALYST FOR OXIDATIVE DESULFURIZATION OF MODEL DIESEL

Fina Lesafi

A Dissertation Submitted in Partial Fulfillment of the Requirements for the Degree of Doctor of Philosophy in Materials Science and Engineering of the Nelson Mandela African Institution of Science and Technology

Arusha, Tanzania

August, 2023

ABSTRACT

This study reports on synthesis, characterization, and catalytic activity of mesoporous mixed metal oxides of tin (Sn) and molybdenum (Mo) for sulfur removal from model diesel. Variable synthesis conditions, namely calcination temperature and Sn/Mo mole ratios, have been on focus**.** Several techniques were used to characterize the catalysts, including powder X-ray diffraction (XRD) for the crystal structure, orientation, and particle size; scanning electron microscopy (SEM)-EDX for examining the morphological properties of the materials, N_2 adsorption-desorption isotherms for textural properties, thermal gravimetric analysis (TGA) for thermal stability, the Fourier transform infrared spectroscopy (FT-IR) for functionality.

Characterization results show that the adsorption-desorption isotherms are of type IV, indicative of mesoporous materials. The surface area of the synthesized materials decreased as calcination temperature increased due to the Ostwald ripening process and increased with the mole ratio Sn/Mo increase. The X-ray diffraction structural analyses revealed that the synthesized catalyst had a tetragonal structure. The presence of Mo=O and Sn–O–Mo bonds, which are responsible for the catalytic reaction, is confirmed by FT-IR and Raman analyses. The activity of the catalysts prepared at various calcination temperatures and mole ratios was analyzed for oxidative desulfurization of model diesel, dibenzothiophene (DBT). The optimal synthesis conditions were the calcination temperature of 450 °C and the mole ratio of Sn/Mo of (2:1). Other multiple parameters affecting the reduction of sulfur compounds were also investigated, including reaction temperature, catalyst loading, oxidant/sulfur ratio, and reaction time. The (DBT) removal efficiency was 99.8 % at 60 °C, 100 mg, 5, and 30 min, correspondingly. This high catalytic activity was due to the surface defects increase,resulting in a high surface area with high pore distribution around the mesopore region.

Experiments examining the reaction kinetics have indicated that the reaction follows a pseudo-first-order behaviour. The activation energy for the reaction has been determined to be 36 ± 4 kJ mol^{-1}. The rate of the heterogeneous reaction is governed by the Langmuir-Hinshelwood mechanism. Furthermore, the maximum rate constant value of SnO_2-MoO_3 catalyst with Sn/Mo (2:1) molar ratio is 0.057 $min^{-1,}$ which is higher than for pure SnO_2 (0.017 min^{-1}) and MoO_3 (0.007 min^{-1}), confirming a synergy between SnO_2 and MoO_3, promoting oxidative desulfurization efficiency. The catalyst's high activity and reusability indicate enormous promise for industrial catalytic desulfurization.

DECLARATION

I, Fina Lesafi, do hereby declare to the Senate of The Nelson Mandela African Institution of Science and Technology that this dissertation titled *"Tin Molybdenum Mixed Metal Oxides Catalyst for Oxidative Desulfurization of Model Diesel"* is my own original work and that it has neither been submitted nor being concurrently submitted for degree award in any other institution.

Fina Lesafi — 15th August 2023
Fina Lesafi — Date

The above declaration is confirmed by:

Prof. Tatiana Pogrebnaya — 15th August 2023
Prof. Tatiana Pogrebnaya — Date

Prof. Cecil King'ondu — 15th August 2023
Prof. Cecil King'ondu — Date

COPYRIGHT

CERTIFICATION

The undersigned certify that they have read and hereby recommend for examination by The Nelson Mandela African Institution of Science and Technology a dissertation entitled: "Tin Molybdenum Mixed Metal Oxides Catalyst for Oxidative Desulfurization of Model Diesel" in partial fulfilment of the requirements for the degree of PhD Materials Science and Engineering at Nelson Mandela African Institution of Science and Technology.

Prof. Tatiana Pogrebnaya Date

Prof. Cecil King'ondu Date

ACKNOWLEDGEMENTS

First, I'd want to express my gratitude to the almighty God, the Most Merciful, for his unwavering protection, guidance, perseverance, and spiritual healing during my PhD program. My supervisors, Prof. Tatiana Pogrebnaya and Prof. Cecil King'ondu, made a big contribution. I owe a significant debt to their passionate encouragement, patience, drive, knowledge, understanding, helpful critiques, essential assistance, and constant supervision throughout my studies.

I want to express my heartfelt gratitude to Prof. Kelvin Mtei, Dean of the School of Materials, Energy, Water and Environmental Sciences (MEWES) and Prof. Revocatus Machunda (former Dean of the School of Materials, Energy, Water and Environmental Sciences (MEWES)), for their untiring commitment to helping each student. Dr. Mwemezi Rwiza and Dr. Mwema Felix Mwema for their insightful comments and recommendations, MEWES current examination officer Ms. Magreth Sigimba, and former examinations officers namely: Mr. Haji Chomba, Ms. Christina Dominick. Current secretary dean's office Ms. Happiness Mwaihaki, and former secretary at the dean's office namely: Ms. Agnes Mbugamoto, Ms. Hana Geogre, Ms. Florence George and Ms. Eunice Mwakang'ata for their exceptional work in MEWES Dean's Office. Furthermore, I wish to thank Ms. Analyce Ichwekeleza (Dean of Students), Ms. Victoria Ndossi (Students Welfare Office). I also owe the NM-AIST community and all MEWES staff for their support in bringing this project to a successful conclusion.

I want to thank the Nelson Mandela African Institution of Science and Technology (NM-AIST) and the African Development Bank (AfDB) for supporting my PhD studies financially. I am grateful to my employer, the Nelson Mandela African Institution of Science and Technology (NM-AIST), for granting me study leave to pursue PhD studies.

My genuine appreciation goes to Dr. Joyce Elisadick Lyimo, a former student at NM-AIST, for continuous support during the data analysis, manuscript and dissertation writing. I have greatly benefited from her support.

I want to express my gratitude to Dr. Oyedotun Kabir Oyeniran of Pretoria University, Dr. Bernad Kivumbi of Makerere University (former student at NM-AIST), and Mr. Godfrey Pius of the University of Dar es Salaam for coordinating all logistics to ensure that the samples were properly characterized at the University of Pretoria, Makerere University, and University of Dar es Salaam laboratories.

I want to thank Dr. Ramadhani Sinde, Mr. Emmanuel Lyimo, Mr. Paul Sanka and Ms. Irene Tesha, for their technical support and assistance during my laboratory work. Mr. Anthony Kazembe of Modern Inspection and Testing Company Limited (MITLC), and Mr. Festo Nicas of Africa Technical Research Centre (ATRC) were also involved in the sample analysis of the model diesel.

I would also like to thank my fellow students Ms. Sofia Bakili, and Ms. Tusekile Alfred as well as, Dr. Ramadhani Mringo, Dr. Said Mateso, Dr. Kassim Ramadhani, Dr. Stanley Mtavangu, and Dr. Rene Costa (former NM-AIST students), for their courage and moral support.

While I was very busy with laboratory work, it is an honor to convey my heartfelt gratitude to my darling spouse Mr. Angelous Thomas Shokia for his patience, support, and abundant care for me and our sons, Aaron, Ammi, and Abraham. My mother, Ms. Cecilia Joseph Merinyo, my brothers, Mr. Menasi and Straton Lesafi, and my sisters, Ms. Liberia, and Hellen Lesafi, deserve my heartfelt gratitude for their constant support, which has enabled me to pursue my PhD studies.

DEDICATION

My mother, Ms. Cecilia Joseph Merinyo, my loving husband, Mr. Angelous Thomas Shokia, my sons Aaron Angelous, Ammi Angelous, and Abraham Angelous; my father, the late Mr. Justine Lesafi and father-in-law, the late Mr. Thomas Shokia, are all honored in this work.

TABLE OF CONTENTS

LIST OF TABLES

LIST OF FIGURES

LIST OF SCHEME

LIST OF ABBREVIATIONS AND SYMBOLS

Å	Angstrom
BDS	Biodesulfurization
BET	Brunauer–Emmett–Teller
BJH	Barrett–Joyner–Halenda
BNT	Benzonaphthothiophene
BT	Benzothiophene
CMC	Critical micelle concentration
CO	Carbon monoxide
CTAB	Cetyltrimethylammonium bromide
DBT	Dibenzothiophene
DBTO	Dibenzothiophene sulfoxide
DBTO2	Dibenzothiophene sulphone
DFT	Discrete Fourier Transform
DMDBT	Dimethyl dibenzothiophene
EISA	Evaporation-induced self-assembly
EU	European Union
eV	Electron volt
F	Flakes
FT-IR	Fourier Transform Infrared Spectroscopy
h	Planks constant
H_2	Hydrogen
H_2O_2	Hydrogen peroxide
H_2S	Hydrogen Sulfide
HDS	Hydrodesulfurization
IUPAC	International Union of Pure and Applied Committee
JCPDS	Joint committee on Powder Diffraction Standards
L	Liquid
Mo	Molybdenum
MoO_3	Molybdenum oxide
Na	Sodium
nm	Nanometer
NOx	Nitrogen oxide gas
NT	Naphthothiophene
ODS	Oxidative desulfurization

P	Powder
PEO-PPO-PEO	poly (ethylene oxide)-block poly (propylene oxide) poly (ethylene oxide)
ppm	parts per million by weight
PSD	Pore size distribution
PT	Phenanthrene
RT	Room temperature
SEM-EDX	Scanning electron microscope-electron diffraction
Sn	Tin
SnO_2	Tin oxide
SO_2	Sulfur dioxide
SO_3	Sulfur trioxide
SOx	Sulfur oxide
SSA	Specific surface area
TH	Thiophene
US EPA	United States electricity and petroleum agency
UV	Ultraviolet
XRD	X-Ray Diffraction

CHAPTER ONE

INTRODUCTION

1.1 Background of the Problem

Diesel and gasoline are processed petroleum products mainly used as transportation fuels containing various organic sulfides. Diesel fuel is a mixture of hydrocarbons derived from crude oil distillation. The cetane number, fuel volatility, density, viscosity, cold behaviour, and sulfur content are all important properties that characterize diesel fuel (Majewski, 2020). Diesel fuel improves the country's economy by power generation and transportation of goods from cross-country, increasing efficiency on the nation's farms. Other diesel fuel applications include off-road activities such as farming, mining, construction, logging, and electric power generation.

Air pollutants are natural and artificial airborne substances introduced into the environment in a concentration sufficient to have a measurable effect on humans, animals, vegetation, or building materials. These include ozone, volatile organic matter (VOCs), carbon monoxide (CO), nitrogen dioxide (NO_2), and sulfur dioxide (SO_2); among which the SO_2 is produced primarily by the combustion of fuels containing sulfur. On-road and off-road engine fuels are estimated to source less than 3% of the total SO_2 emissions. Due to the depletion of oil reserves, fuel with a high sulfur content is currently extracted (Albayrak & Tavman, 2022; Houda *et al.*, 2018). In 2019, fossil fuels accounted for 84% of global primary energy consumption (Dale, 2019). Due to the presence of a high amount of sulfur fuel, when combusted, releases SO_X chemicals into the surrounding environment, resulting in a variety of problems, including environmental degradation such as structural damage, deterioration of automotive paint finishes, acidification of the soil, and ultimately the loss of forests and other ecosystems, as well as the spread of deadly diseases such as respiratory illnesses, aggravated heart disease, triggered asthma, and contributed to the formation of atmospheric acid (Speight, 2020; Srivastava, 2012).

Moreover, excessive sulfurous oxide concentrations in exhaust streams act as catalyst poison, impairing the effectiveness of vehicle catalytic converters in lowering particulate matter, CO, and NOx concentrations (Harrison & Yin, 2000; Matsumoto *et al.*, 2000). Globally, ultra-low-sulfur diesel production has become a crucial challenge for refineries. In 2006, the US EPA mandated that diesel fuel's sulfur level be decreased to 15 parts per million by weight (ppm). The EU has established a maximum sulfur concentration of 10 ppm for diesel fuel (Kulkarni & Afonso, 2010). However, the levels of sulfur in crude oils are on the rise, resulting in a

notable difference between the high sulfur content found in crude oils and the low sulfur content required for liquid fuels. Consequently, the process of desulfurization has become a more formidable task.

Desulfurization is a chemical process to remove sulfur compounds from fuel (diesel). Diverse processes have been used in the desulfurization of diesel: hydrodesulfurization, bio-desulfurization, adsorptive desulfurization and oxidative desulfurization (Chen *et al.*, 2021; Dong *et al.*, 2021; Liu *et al.*, 2021; Saleh, 2021; Xiao *et al.*, 2016). Hydrodesulfurization, a process used to remove sulfur from substances, necessitates extremely elevated temperatures (300°C–400°C) and pressures (20–100 atm of H_2). However, this method has some drawbacks; the cetane number, which indicates the combustion quality of fuel, is decreased due to accompanying hydrogenation reactions. Moreover, hydrodesulfurization is not as efficient in eliminating stubborn sulfur compounds like dibenzothiophene and its alkyl derivatives, primarily due to steric hindrance (Yansheng *et al.*, 2011). A commercially possible desulfurization process must have a low-energy pathway that involves cheaper and reusable catalysts. Oxidative desulfurization (ODS) has been proposed as a promising alternative method for its high efficiency, mild desulfurization conditions, and low cost (Rafiee & Rahpeyma, 2015). It is considered a supplementary technology to hydrodesulfurization; hence it is necessary to encourage the development of viable technologies for selective oxidation of sulfur compounds. The organic sulfur in fuel oil that can be removed by adsorption or extraction is oxidized by an oxidant. The H_2O_2 is a popular oxidant since it is inexpensive, safe to use and store, and environmentally benign (Alonso *et al.*, 2002; Dartt & Davis, 1994; Goyal *et al.*, 2022; Sato *et al.*, 2001). A suitable catalyst is required to increase the efficiency and activity of the ODS process because the interaction between the active sites of the catalyst and the oxidant generates active radical species that contribute to high performance (Rivoira *et al.*, 2017). A wide range of transition metal oxides like copper (Ahmadian & Anbia, 2022), titanium (Fraile *et al.*, 2016), chromium (Jiang *et al.*, 2022), tungsten (Shen *et al.*, 2018), iron (Al-Abduly & Sharma, 2014), molybdenum (Chen *et al.*, 2018), cobalt (Bhadra & Jhung, 2022) and vanadium (Caero *et al.*, 2005) oxides used as catalytically active phases in oxidative desulfurization process. The SnO_2 and MoO_3 catalysts are widely examined in systems of oxidative reactions. The SnO_2, a semiconducting oxide and a post-transition metal oxide, has been extensively used as an oxidation catalyst, and its valency state can be Sn^{4+}/Sn^{2+} (Batzill & Diebold, 2005; Guo *et al.*, 2020; Liu *et al.*, 2019; Luo *et al.*, 2006). The SnO_2 contains surface-active anions O_2^-, O_2^{2-}, and acidic sites. The close interaction of these acidic sites and anions is the primary reason for their exceptional performance in oxidation reactions (Guo *et al.*, 2019). Study by Liu *et al.* (2019) show an excellent desulfurization reaction using SnO_2

due to the presence of Lewis acid. Metal additives modify this oxide to either increase the charge carrier concentration by donor atoms or increase the gas sensitivity or the catalytic activity (Batzill & Diebold, 2005). Molybdenum oxide is a transition metal oxide catalyst exhibiting high activity due to the possibility of multivalent metal transitions (Tu *et al.*, 2019). Charge transfer kinetics can be improved by doping Mo into the lattice of SnO_2 (Wang *et al.*, 2015). Safa and Ma (2016) reported MoO_3 as the most effective active ingredient for oxidative desulfurization. However, the activity and stability of catalysts can be enhanced by adding other components, altering the loading mechanism, and modifying the synthesis procedure (Rivoira *et al.,* 2017; Tu *et al.,* 2019).

1.2 Statement of the Problem

Dibenzothiophene (DBT) and its alkyl derivatives, which include cyclic sulfide are most prevalent in diesel, and are less effectively removed by hydrodesulfurization (HDS). Extraction, selective adsorption, photocatalytic desulfurization, and oxidative desulfurization (ODS) have all been developed to address the shortcomings of HDS. Due to its excellent efficiency, comfortable operating conditions, and low cost, ODS for fuel oil was recognized as one of the most promising desulfurization technologies. Despite the high ODS activity of the metal oxide catalysts, it has been proven that mixed metal oxide catalysts would show higher catalytic activity in the ODS process, as reported by Alvarez-Amparán *et al.* (2017), Arellano *et al.* (2014), López Luna *et al.* (2022), and Teimouri *et al.* (2018). The combined use of tin and molybdenum mixed-metal oxide catalysts has become increasingly popular for the targeted oxidation of hydrocarbons. These catalysts are receiving considerable interest in the field of heterogeneous catalysis due to their unique acidic and basic properties (Švachula *et al.*, 1991) and redox properties (Okamoto *et al.*, 1981). The different catalytic reactions of tin–molybdenum mixed metal oxides have been reported, such as oxidation of olefin (Takita *et al.*, 1972), dehydrogenation and dehydration of sec-butyl alcohol (Okamoto *et al.,* 1981), fructose conversion (Dos-Santos *et al.*, 2018), reduction of nitroarenes (Sakthikumar *et al.*, 2016), xylose conversion (Dos-Santos *et al.*, 2021). A limited study reports tin–molybdenum mixed metal oxide catalyst for sulfur removal. Hence, the objective of this study was to synthesize catalysts composed of tin and molybdenum mixed metal oxides using the sol-gel technique and examine their effectiveness in oxidative desulfurization (ODS), dibenzothiophene (DBT) was utilized as a representative sulfur-containing compound, while hydrogen peroxide served as the oxidizing agent. The calcination temperature was optimized to obtain the appropriate phase of tin– molybdenum mixed metal oxide catalyst and investigated the impact of the Sn/Mo ratio with high catalytic activity on oxidative desulfurization performance.

1.3 Rationale of the Study

In recent years, serious air pollution in emerging countries has received much attention in the academic and industrial sectors. Automotive emissions cause the majority of air pollution in major cities. Although exhaust treatment devices such as the three-way catalytic converter have long been standard in modern cars for reducing NOx, CO, hydrocarbons, and particulates, SO_2 emitted by the combustion of fuels containing organosulfur compounds mostly remains because sulfur poisons the Pt catalysts in the three-way catalytic converter. During fuel combustion, sulfur compounds are transformed into sulfur oxides (SO_2 and SO_3), resulting in acid rain, acid snow, and health problems worldwide. As a result, sulfur compounds like thiophene (TH), Benzothiophene (BT), dibenzothiophenes (DBTs), and dimethyl dibenzothiophenes (DMDBTs) must be tightly controlled in fuels. Hydrodesulfurization is a potential method for sulfur removal though it operates at higher temperatures and pressure and requires hydrogen gas. Oxidative desulfurization has vivid significant attention due to its striking subtle operation conditions, such as lower operating temperature and ambient pressure, and without hydrogen consumption. In this study, the ODS process was performed in the presence of heterogeneous tin–molybdenum mixed metal oxide catalyst and oxidant H_2O_2.

1.4 Research Objectives

1.4.1 General Objective

The main objective of this work is to evaluate the performance of tin–molybdenum mixed metal oxides catalyst for oxidative desulfurization of model diesel.

1.4.2 Specific Objectives

(i) To synthesize and characterize tin–molybdenum mixed metal oxide catalyst materials derived from tin and molybdenum inorganic precursors.

(ii) To evaluate catalyst performance in terms of the activity by varying calcination temperature and mole ratio.

(iii) To establish optimum reaction conditions for desulfurization of model diesel using the proposed tin–molybdenum mixed metal oxide catalyst materials.

1.5 Research Questions

(i) What are the characteristics of tin–molybdenum mixed metal oxide catalyst?

(ii) How do calcination temperature and mole ratio affect catalyst activity?

(iii) What are the optimal conditions which influence the performance of the prepared tin–molybdenum mixed oxide catalyst materials for the desulfurization of model diesel?

1.6 Significance of The Study

The sulfur concentration of fuel should be regulated to extend the life of catalytic converters and infrastructure, enhance air quality, and protect human health. The results of this work will contribute to the literature on catalysis and desulfurization, as it is the first time that the use of SnO_2–MoO_3 as one of the sulfur removal catalysts has been documented.

1.7 Delineation of The Study

This study investigates the use of tin–molybdenum mixed metal oxide catalyst for the oxidative desulfurization of model diesel. The characterization of catalysts at different pretreatment conditions is presented. This dissertation is organized into five chapters. Chapter one includes background information, the purpose of the study, objectives, research questions, and the significance of the study. The second chapter provides a detailed assessment of the literature on desulfurization, catalyst, mixed metal oxides, surfactants etc. The third chapter (materials and methods) covers the procedures for oxidative desulfurization, synthesis of tin-molybdenum catalyst, and optimizing catalytic oxidative desulfurization. In the fourth chapter, the results and discussion of the produced catalyst's catalytic activities are presented. The conclusion and recommendations are presented in chapter five. This work was primarily based on a lab scale. As a result, further research into real diesel and piloting is needed.

CHAPTER TWO

LITERATURE REVIEW

2.1 Introduction

Liquid fuels contain many sulfur compounds (thiols, sulfides, disulfides, thiophenes and refractory compounds), which generate SO_2 and airborne particulate emissions during combustion. Therefore, the desulfurization of oil is extremely important in the petroleum-processing industry. To resolve this crisis, several processes have been proposed to deal with the problem of removing these compounds from oil. This chapter highlights desulfurization technologies, oxidants, metal oxides, mixed metal oxides, and preparation methods for mixed metal oxides.

2.2 Sulfur in Transportation Fuel

There exist three primary categories of transportation fuels; gasoline, diesel, and jet fuels. These fuels vary in their composition and characteristics. Diesel fuel is made from petroleum. The aromatic, paraffinic and naphthenic groups of hydrocarbons constitute most of all crude petroleum oils. There is a huge variety of molecular weights in each class. Crude oil can be as thin and transparent as apple cider or as thick and dark as melted tar when it first emerges from the earth. Thin crude oils have high API gravities because of their low densities; hence they are referred to as high-gravity crude oils; in contrast, low-gravity crude oils are thick crude oils with relatively high densities (Owen, 1995).

Figure 1 shows the main organic sulfur compounds present in these fuels, such as thiols (mercaptans), sulfides, disulfides, thiophene, benzothiophene (BT), dibenzothiophene (DBT), naphthothiophene (NT), benzonaphthothiophene (BNT), phenanthrene [4,5-b, c,d]thiophene (PT), and their alkyl-substituted derivates**.** The study by Chen *et al.* (2013) demonstrates that benzothiophene and dibenzothiophene make up 70% of thiophene sulfides, which account for more than 80% of the total sulfur concentration in diesel fuel. Diesel is the primary focus of this study because it has an extremely high energy content and density compared to most other fossil fuels due to its large, long-chain hydrocarbon composition (Ethan, 2021). Alkyl benzothiophenes and alkyl dibenzothiophenes are sulfur compounds found in commercial diesel fuel. These main sulfur compounds are known as refractory sulfur with alkyl groups at the 4- or/and 6-positions, which are challenging to remove by the traditional hydrodesulfurization procedure (Song & Ma, 2004).

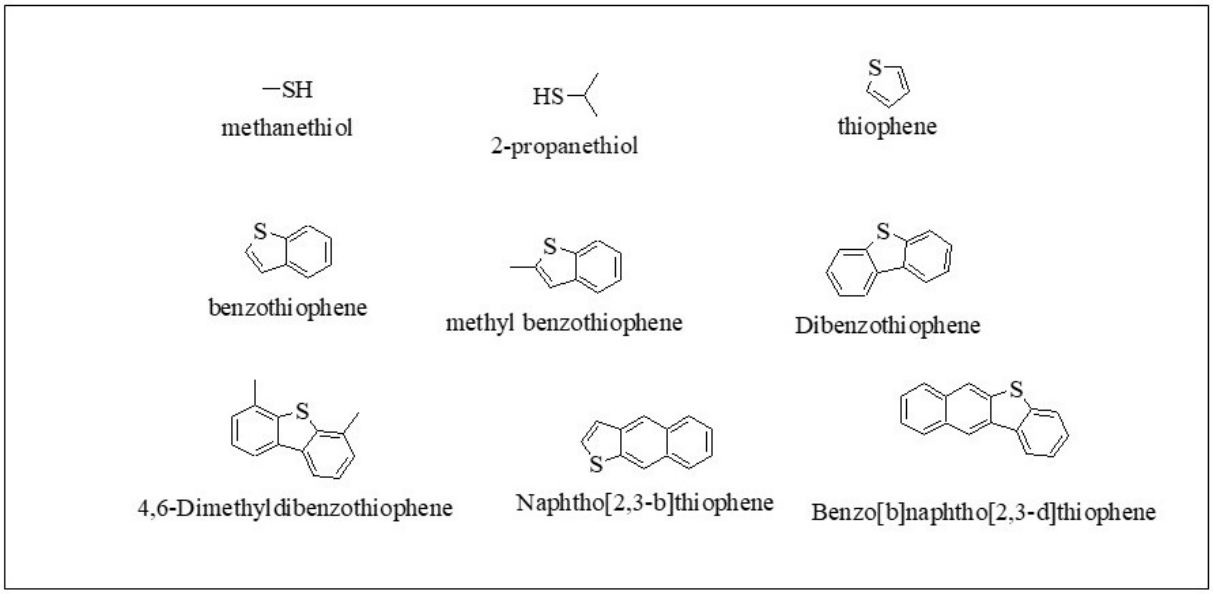

Figure 1: Examples of sulfur compounds present in diesel

The process of turning crude oil into very valuable products is called refining. Most important crude oil products are diesel, jet fuel, and gasoline. Liquefied petroleum gas (LPG), heating fuel, lubricating oil, wax, and asphalt are notable products after refining. High-gravity crude oils are simpler to process because they include lighter products, like gasoline, and are frequently lower in sulfur and nitrogen. However, modern refining techniques may turn low-density crude oils into highly valuable products. Low-density crude oils require more energy, additional processing steps, and complex, expensive equipment, which raises the cost of refining them; hence this difference reflects variation in refining price (Owen, 1995). Separation, upgrading, and conversion are the three types of refining processes. Distillation is a typical separation technique in which the feed is divided into two or more components depending on a physical characteristic, typically boiling point. The feedstock is unaltered by these procedures. Hydrotreating is an upgrading procedure that raises the quality of the material by using chemical reactions to eliminate molecules that give a material an undesirable property at tiny levels. By "cracking" large molecules into smaller ones, conversion processes often change the chemical structure of the feedstock; examples of this include catalytic cracking and hydrocracking.

Sulfur should be eliminated from petroleum fractions for several important reasons, such as the poisoning of catalysts, improved fuel performance and stability, decreased fuel smoke production, reduced or limited corrosion during handling, refining, and product use, and the creation of compounds with tolerable odours. This study focuses on upgrading the process by using oxidative desulfurization as a desulfurization technology.

2.3 Desulfurization Technologies

Deep desulfurization and ultradeep desulfurization refer to the processes of removing sulfur that exists in current gasoline and diesel fuel to below 15 and 30 ppm for diesel fuel and gasoline, respectively, for environmental regulations and removing sulfur in liquid hydrocarbon fuels to below 1 ppm for fuel cell applications (Song & Ma, 2004).

There is currently no comprehensive method for classifying desulfurization processes. However, these processes can be classified based on various factors, such as the resulting state of the organosulfur compound, the involvement of hydrogen, or the specific chemical and physical methods employed in the process (Khodadadi *et al.*, 2012)**.** Various methods are required to achieve desulfurization to produce environmentally friendly fuels. These methods include hydrodesulfurization, oxidative desulfurization, bio-desulfurization, reactive adsorption, non-destructive adsorption, N-adsorption, extraction, and other miscellaneous processes.

2.3.1 Hydrodesulfurization

Hydrodesulfurization (HDS) is a process that involves heating light oil, mixing it with hydrogen, and feeding it to a reactor packed with a pelleted catalyst such as $CoMo/AlO_3$ or $NiMo/AlO_3$. The reactor's temperature typically ranges between 300 and 380 °C. The reactor can be configured so that hydrogen gas flows downward through it, passing around and through the particulate catalyst, or hydrogen flows upward from the bottom of the reactor (Spivey *et al.*, 2002). This is the conventional process for reducing organosulfur in diesel and other intermediate distillates. It is a technique that is effective for removing thiols, sulfides and disulfides, but it is limited to removing some refractory sulfur compounds such as thiophene, benzothiophene, 4,6-dimethyl dibenzothiophene and their alkylated derivatives due to lower hydrogenation activity or steric hindrance (Egorova & Prins, 2004; Grønborg *et al.*, 2016; Qi *et al.*, 2022). For the thiophene compounds, in which the lone pairs on the S atom conjugate with the p-electrons on the ring, including thiophenes, BTs, DBTs, PTs, and BNTs, HDS over the commercial catalysts usually proceeds through two pathways, one is a hydrogenolysis pathway where sulfur is removed through C-S bond breaking (Dumon *et al.*, 2021; Wang & Prins, 2008). The other is via the hydrogenation desulfurization pathway, in which aromatic rings of DBT compounds are preferentially hydrogenated to 4H-or 6H-DBT intermediates and are subsequently desulfurized, as shown in Scheme 1 (Zheng *et al.*, 2017). The two routes can occur parallel and utilize various active sites on the catalyst surface. The selectivity depends

on the reaction conditions, the nature of the sulfur compounds and the catalyst used (Shafi & Hutchings, 2000).

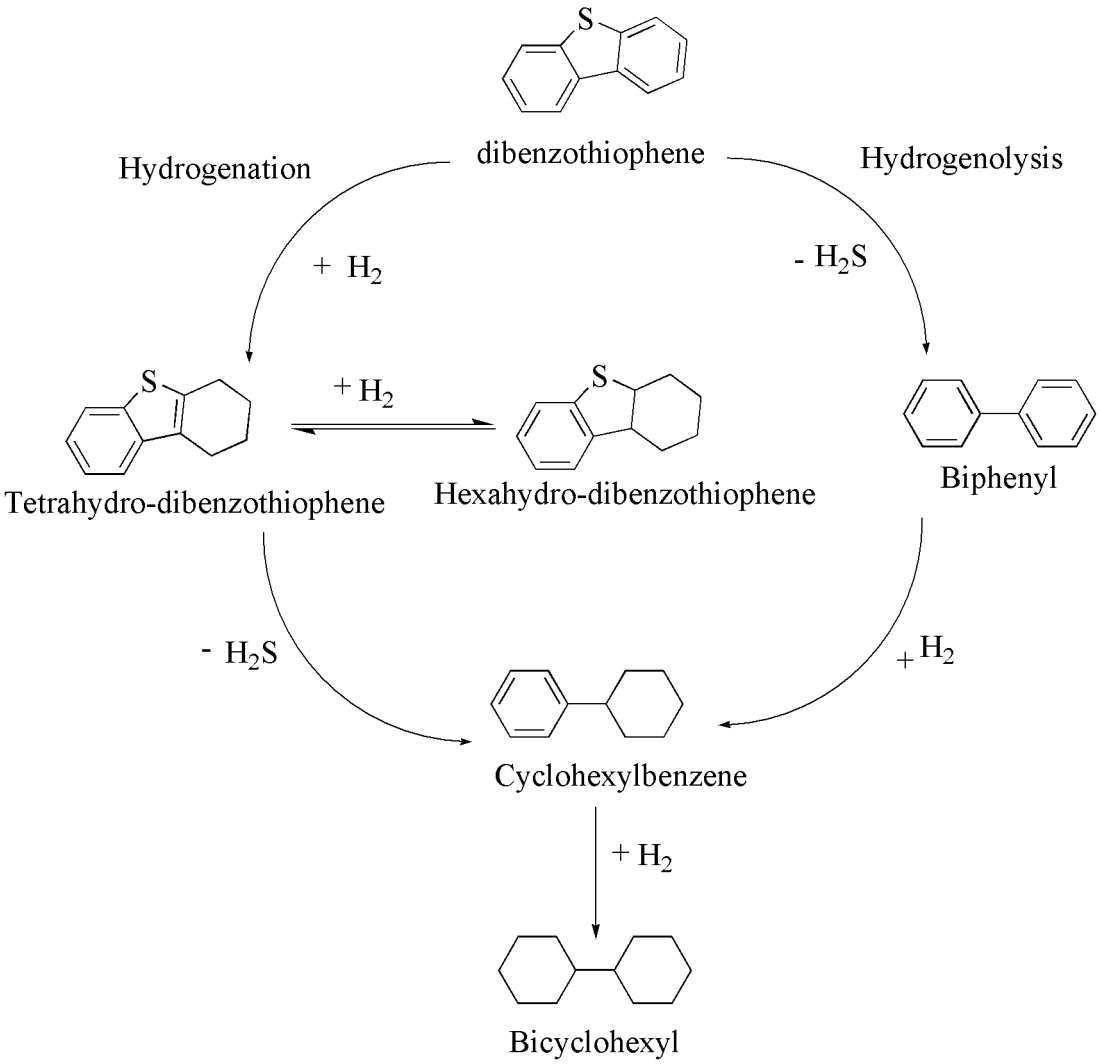

Scheme 1: Hydrodesulfurization route (Al-Hammadi *et al.*, 2018)

The shortcoming of this method is the high cost, which requires high pressure and temperature, and the lack of selective catalysts that lead to a more complex catalytic process, such as the hydrogenation of aromatic compounds (Vedachalam *et al.*, 2022). Some of the gases resulting from cracking are harmful to the environment and cannot be reused, resulting in environmental problems (Blumberg, 2003; Saha *et al.*, 2021). High capital costs to build a thick wall reactor to suit the high-pressure conditions (Optenhostert *et al.*, 2021). The cetane number is reduced due to hydrogenation side reactions, and it is less effective in removing refractory sulfur compounds such as benzothiophene and dibenzothiophene (Tran *et al.*, 2018). An alternate method that can complement the HDS process under moderate conditions to produce ultra-low sulfur fuels is crucial, and oxidative desulfurization satisfies this requirement.

2.3.2 Biodesulfurization

Biodesulfurization is a process that removes sulfur from fossil fuels using a series of enzyme-catalyzed reactions (Boniek *et al.*, 2015). In this, the oxidation chemistry of sulfur species is carried out by a biological system at ambient pressure and temperature; the reaction occurs in water (Mohebali & Ball, 2016). Several bacteria that use the sulfur-selective oxidative desulfurization pathway have been isolated. It involves sequential oxidation of the sulfur moiety and cleavage of the carbon-sulfur bonds (Boniek *et al.,* 2015). This system consists of two monooxygenases, Dez and DszC, which sequentially oxidize DBT to DBT sulfone and 2-hydroxyphenyl-2-sulfinic acid. An NADH-flavin mononucleotide oxidoreductase (DszD) supplies the two monooxygenases with reduced flavin and a desulfurase (DszB), which converts 2-hydroxyphenyl-2-sulfinic acid to the desulfurized product 2-hydroxyphenyl (Gray *et al.*, 2003).

This particular technique is typically unable to effectively eliminate sulfur to the extent of 10-100 parts per million (ppm). The reason for this limitation could be attributed to increased bacterial activity within the higher concentration range. As a result, the likelihood of attaining a sulfur level as low as 10 ppm through biodesulfurization may not be very high. Additionally, another characteristic of the biological system is the occurrence of competitive reactions caused by other bacteria (Kulkarni & Afonso, 2010). The effectiveness of the BDS method was found to be hindered by several challenges, including the scarcity of enzymes that can remove sulfur atoms from heterocyclic compounds present in liquid fuel without causing a loss of carbon. (Madeira *et al.*, 2008; Soleimani *et al.*, 2007). In addition, the BDS exhibited slow reaction rates during the desulfurization of thiophene molecules; this was due to the poor miscibility of bioactive species in organic solvents and the detrimental effect of organic solvents on the growth of many bio-organisms. Another limiting factor in the BDS process is the transport rate of the sulfur compounds from the oil phase to the bacterial cell membrane. Efficient separation of desulfurized oil fraction, recovery of the biocatalyst, and its return to the bioreactor are also important issues that need attention (Mohebali & Ball, 2008).

2.3.3 Oxidative Desulfurization

The oxidative desulfurization method is used to generate diesel fuel with extremely low levels of sulfur by converting sulfur compounds, such as benzothiophene and dibenzothiophene, into sulphoxides and sulphones. This is in contrast to hydrodesulfurization, where sulfur compounds are reduced, and hydrogen sulphide is formed. The process involves two main steps: the oxidation of sulfur compounds in diesel fuel to form sulphoxides and sulphones and

the subsequent extraction or adsorption of the generated sulphones due to their high polarity (Palaić *et al.*, 2015). Different classifications apply to the ODS system, such as a two-phase liquid system that utilizes water-soluble oxidants (Capel-Sanchez *et al.*, 2010), a one-phase liquid system that utilizes oil-soluble oxidants (Kargar *et al.*, 2021), and a gas-liquid system that utilizes gas-phase oxidants (Bai *et al.*, 2021).

The ODS reactions are generally heterogeneous reactions, i.e., two or more phases in the mixture that are immiscible with each other. The non-polar phase solution, formed by dissolving model sulfur compounds in a non-polar solvent such as hexane, heptane, or toluene, has been referred to as denotations such as model fuel, model diesel, model liquid fuel, or model sulfur solution. The polar phase consists of an oxidant and a catalyst (Scheme 2). In the ODS process, sulfur-containing compounds are oxidized using selective oxidants such as nitric acid (Gürü, 2007; Tam *et al.*, 1990), nitrogen oxides (Pouladi *et al.*, 2019), organic hydroperoxides (Wang *et al.*, 2003; Zhang *et al.*, 2018), peroxy acids, hydrogen peroxide (Li *et al.*, 2018; Yang *et al.*, 2017) and ozone (Ma *et al.*, 2015) in the presence of a catalyst to produce sulfone compounds that can be preferentially extracted due to their increased relative polarity. For oxidation to occur, the oxidant needs to be in contact with fuel oils under optimum conditions, and the oxidant donates oxygen atoms to the sulfur in benzothiophenes, dibenzothiophenes, and its derivatives to form sulfoxides or sulfones.

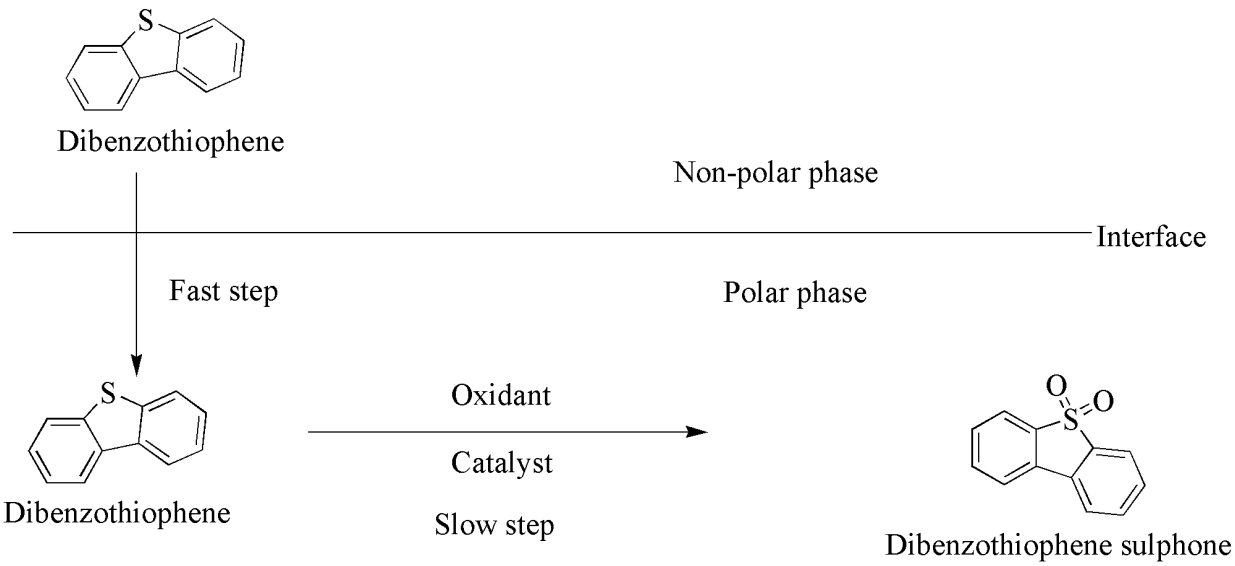

Scheme 2: The mechanistic route for oxidative desulfurization

The reactivity of model sulfur compounds has been assessed in numerous studies, and researchers have identified the ideal conditions for maximizing desulfurization. These conditions include determining the appropriate oxidant/sulfur ratio, temperature, catalyst quantity, volume ratio of the organic phase to the aqueous phase, and time required for optimal

desulfurization. Subsequently, these optimized conditions have been implemented on actual fuel samples to achieve effective desulfurization.

The technology shows great promise for removing sulfur at relatively low temperatures, typically ranging from 20 to 60 °C, and under atmospheric pressure. The significant aspect of this method is its selective oxidation approach, which enhances the polarity of sulfur compounds, followed by their targeted extraction. This selective extraction process holds significant importance in effectively removing sulfur compounds (Srivastava, 2012). When selecting an oxidant, catalyst, and operating conditions for the ODS process, reaction selectivity, safety in the handling of sulfone compounds' waste, and cost are crucial considerations (Ali *et al.*, 2006; Srivastava, 2012). Hence this work uses oxidative desulfurization with a SnO_2-MoO_3 catalyst and oxidant for sulfur removal.

2.4 Oxidants

An oxidizing agent or oxidant is a substance that can oxidize other substances or accept their electrons; it can be solid, liquid, or gas. For example, oxidants can convert organic sulfur compounds (OSCs) to much more polar oxidized species. Figure 2 shows examples of oxidants that are used in the reaction. Oxidants can be solid like sodium bromate (Shaabani *et al.*, 2009), oxone (KHSO5) (Xu *et al.*, 2017), potassium permanganate (Gokel *et al.*, 1980), superoxide (Chan *et al.*, 2008), potassium dichromate (Pandey & Srivastava, 2018), sodium hypochlorite (Subhan *et al.*, 2019), and sodium chlorite (Hao *et al.*, 2017); these oxidants are said to be cheaper, more stable and less corrosive. Other oxidizers such as t-butyl hydroperoxide (Mokhtar *et al.*, 2015), cyclohexanone peroxide (Wei *et al.*, 2017) and cumene hydroperoxide (Safa *et al.*, 2019) can all dissolve in the organic phase and directly oxidise sulfur compounds. Hydrogen peroxide is highly reactive, nonpolluting, and the best results are achieved in conjunction with heterogeneous catalysts (Li *et al.,* 2018; Yu *et al.*, 2018). Furthermore, oxygen (Lü *et al.*, 2010; Zhang *et al.*, 2019), nitrogen dioxide (Tam *et al.,* 1990) and ozone (Ma *et al.,* 2015) are gaseous oxidants. Generally, gases tend to exhibit greater solubility in non-polar solvents compared to water.

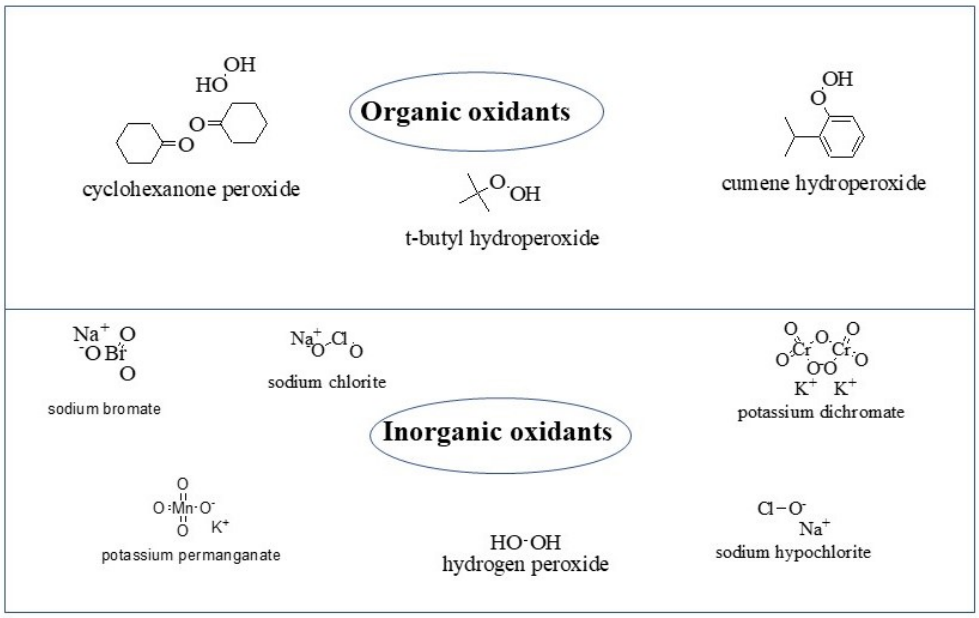

Figure 2: Types of oxidants for oxidative desulfurization

To select the optimum oxidant for research purposes, oxidants must have the following considerations: Active oxygen content, selective ability in its application, a by-product of the reaction, and price. Table 1 indicates that hydrogen peroxide (H_2O_2) gives the highest percentage of active oxygen. The proportion of active oxygen is determined by dividing the weight of oxygen that may be transferred to a suitable substrate by the molecular weight of the oxidant (Strukul, 1992). This work uses H_2O_2 as an oxidant.

Table 1: Single oxygen atoms donor

Donor	Active oxygen (wt%)	By –product
H_2O_2	47.0	H_2O
O_3	33.3	O_2
N_2O	36.4	N_2
$NaClO_2$	35.4	NaCl
NaClO	21.6	NaCl
NaBrO	13.4	NaBr
HNO_3	25.4	NOx
t-BuOOH	17.8	t-BuOH
$KHSO_5$	10.5	$KHSO_4$
$NaIO_4$	7.2	$NaIO_3$
PhIO	7.3	PhI
$C_5H_{11}NO_2$	17.3	$C_5H_{11}NO$

Brégeault (2003) and Strukul (1992)

2.5 Surfactant

Surfactants are amphiphilic compounds with a propensity for surface and interface adsorption. They contain a dual chemical structure: a lyophilic, hydrophilic part (polar group) and a lyophobic, hydrophobic part, often a hydrocarbon chain (Fig. 3A). Lyophilic and lyophobic

classification depend on dispersing medium, a polar group can be lyophilic or lyophobic (Shchukin *et al.*, 2001). The hydrophobic component of a surfactant can solubilize organic species, whilst the hydrophilic component interacts with charged inorganic precursors to guide the development of the inorganic framework (Pal & Bhaumik, 2013).

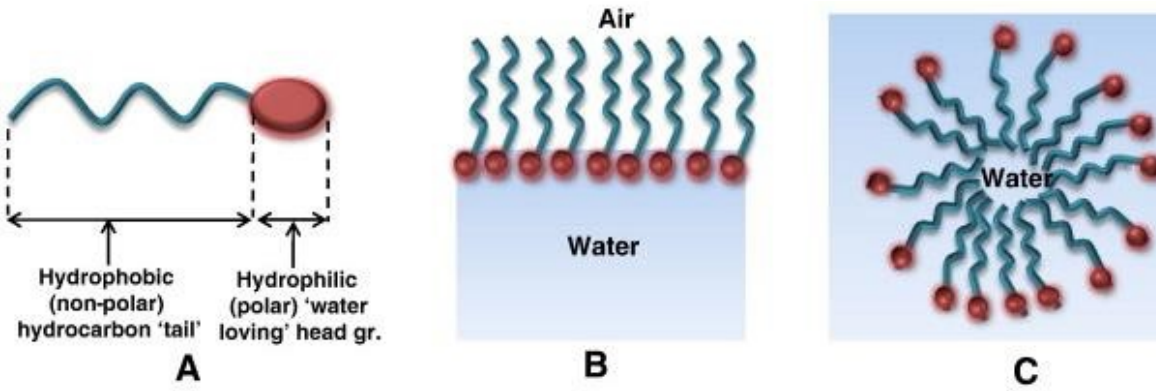

Figure 3: Surfactant molecule and its behaviour in aqueous media (Pal & Bhaumik, 2013)

Surfactants are responsible for concentrating at interfaces, and they do so to decrease the phase boundary's free energy. A surfactant's hydrophobicity and hydrophilicity properties made it behave differently in non-polar and polar solvents. In aqueous media, the hydrophilic part of the molecule interacts with water, while the hydrophobic part stays away from the water molecules (Fig. 3B) (Pal & Bhaumik, 2013). Molecules can form aggregates in which the hydrophobic portions are oriented within the cluster, and the hydrophilic portions are exposed to the solvent (Svensson *et al.*, 1998); such aggregates are called micelles Fig. 3C as reported by Evans (1988) and Pal (2013).

The surfactant concentration above which micelles form is the critical micelle concentration (CMC) and is an essential property of all surfactants (Perinelli *et al.*, 2020). Surfactants generate micelle in oil or aqueous-based solutions to reduce the system's energy.When oil is the dispersing medium,surfactants form reverse micelles. The CMC of a surfactant is determined by the surfactant's chemical structure. According to a study by Shi *et al.* (2019), the longer carbon chains surfactants join with less binding energy, resulting in a more stable system and hence low CMC. Surfactant structure and nature significantly impact the final mesostructured pore sizes and surface areas of materials (Yang *et al.*, 2009). According to the nature of the polar group, surfactants can be classified into nonionic and ionic; anionic, cationic, amphoteric or zwitterionic (Pletnev, 2001; Shi *et al.,* 2019) as shown in Fig. 4.

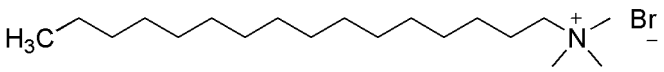

Cetyltrimethylammonium bromide (CTAB)

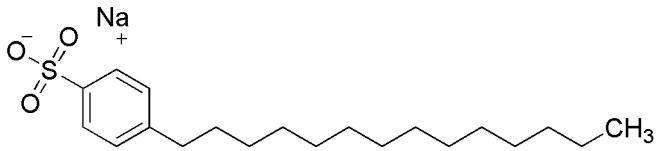

Sodium dodecylbenzene sulphonate

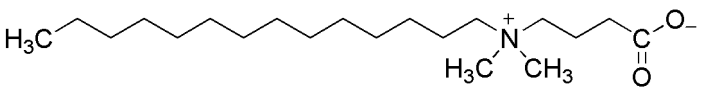

Lauryl betaine

Figure 4: Chemical structure for different types of surfactants

2.5.1 Cationic Surfactants

Cationic surfactants have a positive charge on their hydrophilic end. The positive charge makes them useful in anti-static products, like fabric softeners. Cationic surfactants can also serve as antimicrobial agents, often used in disinfectants. Cationic surfactants cannot be used with anionic surfactants. If positively charged cationic surfactants are mixed with negatively charged anionic surfactants, they will fall out of the solution and no longer be effective. Cationic and nonionic surfactants, however, are compatible. The $C_nH_{2n+1}N(CH_3)_3Br$ (n = 8-22) is a quaternary cationic surfactant that is generally effective in creating ordered mesoporous materials. The CTAB (cetyltrimethylammonium bromide), a commercially accessible compound, is frequently utilized. Gemini surfactants, bolaform surfactants, multi-head group surfactants, and recently discovered cationic fluorinated surfactants could be used as templates to build diverse mesostructures. Cationic surfactants have high CMT values and great solubility, making them suitable for usage in both acidic and basic conditions. However, they are both hazardous and costly. The rational management of organic-inorganic interactions and cooperative assembly of silicate species and surfactants impact the resultant mesostructures.

2.5.2 Anionic Surfactants

Anionic surfactants possess a negatively charged hydrophilic end, which aids in the process of lifting and dispersing soils by forming micelles. Due to their ability to effectively target a wide

range of sols, anionic surfactants are commonly utilized in the production of soaps and detergents. Mixing anionic surfactants results in the formation of significant amounts of foam. While anionic surfactants excel in lifting and suspending particulate soils, their capacity to emulsify oily sols is comparatively less efficient. Examples of anionic surfactants include sulfates, sulfonates, and gluconates.

2.5.3 Amphoteric Surfactants

Positive and negative charges exist on the hydrophilic end of amphoteric surfactants. Dual charges nullify each other, resulting in a zero net charge, a property known as zwitterionic. The pH of a solution will determine the reaction of amphoteric surfactants. Amphoteric surfactants become positively charged in acidic conditions and behave similarly to cationic surfactants. Like anionic surfactants, they acquire a negative charge in alkaline liquids. Amphoteric surfactants are often used in personal care products such as shampoos and cosmetics. Some frequently used amphoteric surfactants are dodecyl betaines, lauryl betaines and amino oxides.

2.5.4 Nonionic Surfactant

Nonionic surfactants are available in a wide variety of different chemical structures. They are widely used in industry for their attractive characteristics, like low cost, nontoxicity, aggregation properties and biodegradability (Zhao & Wan, 2007). Nonionic surfactants have rich phase behaviours, and high CMT values compared to ionic surfactants and are becoming increasingly popular and powerful in synthesizing mesoporous solids (Rapp, 2017). The templating agents are crucial to creating mesoporous materials because they impart pore-directing features. In the case of mesoporous oxides, the templating relies on supramolecular arrays: micellar systems formed by surfactants or block copolymers, which consist of hydrophilic poly(ethylene oxide) (PEO) and hydrophobic poly(propylene oxide) (PPO), arranged in an A-B-A triblock structure, thus giving PEO-PPO-PEO (Batrakova & Kabanov, 2008; Poyraz & Dag, 2009; Zhao & Wan, 2007). The study by Chuenchom *et al.* (2012) and Yang *et al.* (1999) utilized amphiphilic poly (alkylene oxide) block copolymers as structure-directing agents to organize the network-forming mesoporous metal oxide species (Ruel-Gariépy & Leroux, 2004). All the Pluronic copolymers are shown in Fig. 5; they exist as liquids, pastes, and solids at ambient conditions. The name of the pluronic copolymer starts with a capital letter to define its physical form at ambient conditions; (L = liquid, P = paste, F = flake) with the following 2 ~ 3-digit numbers. The first 1 or 2 numbers indicate the molecular weight of the poly (propylene oxide) block, and the last number indicates the weight fraction of the poly (ethylene oxide) block (Pitto-Barry & Barry, 2014).

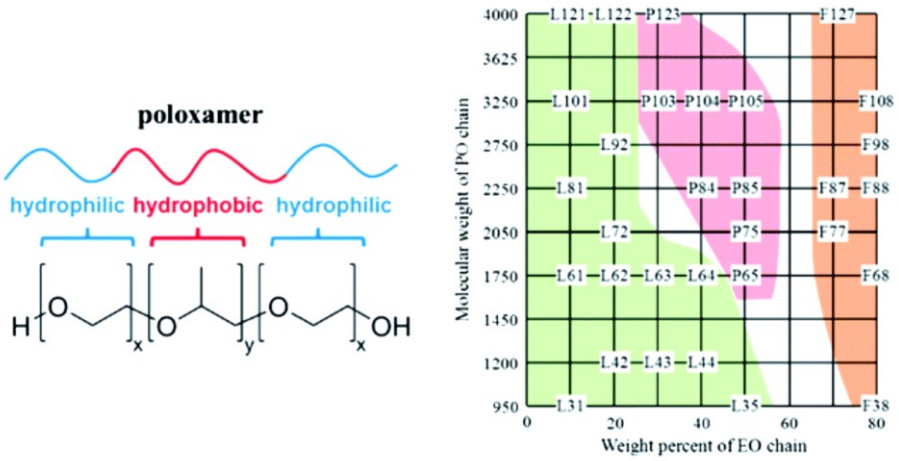

Figure 5: **Molecular structure of a Pluronic® triblock copolymer (left) and the Pluronic® grid (right) copied from (Pitto-Barry & Barry, 2014); colour code: physical state of copolymers under ambient conditions: green = liquid; red= paste; orange =flake)**

Due to their amphiphilic qualities (existence of both hydrophobic and hydrophilic components), pluronic have surfactant properties that enable them to interact with hydrophobic surfaces and biological membranes (Batrakova & Kabanov, 2008). Furthermore, individual block copolymers, also known as unimers, can combine and form micelles in aqueous solutions. When the concentration of the block copolymers falls below the critical micelle concentration (CMC), the unimers persist in water as molecular solutions. However, once the concentration of the block copolymer exceeds the CMC, the unimers will self-assemble and form micelles, which can have spherical, rod-shaped, or lamellar geometries (Fig. 6).

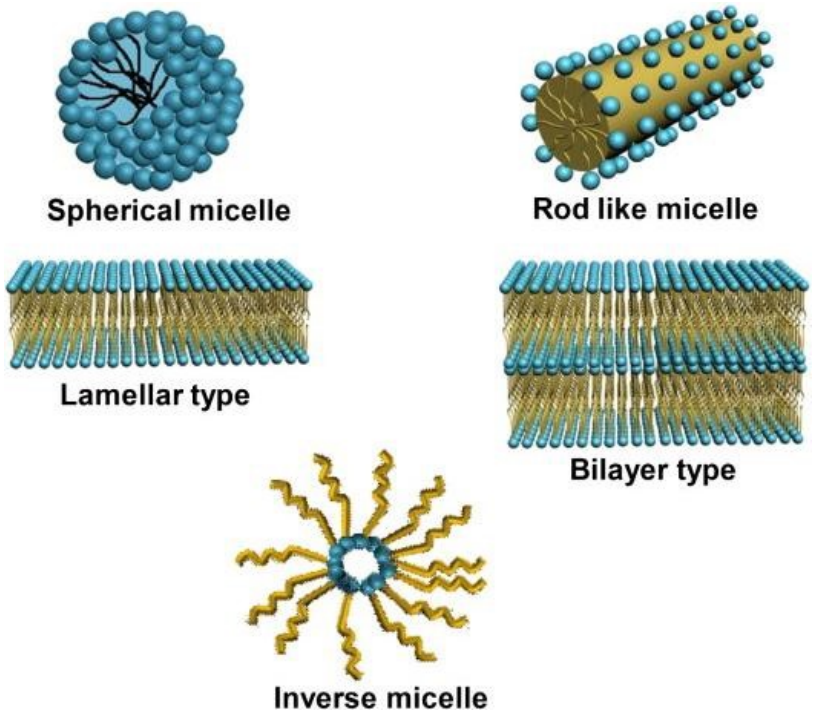

Figure 6: **Different types of surfactant micelle structures (Pal & Bhaumik, 2013)**

Their shapes are determined by the block copolymers' length, concentration, and temperature (Vinogradov *et al.*, 2002). Micelles typically consist of a hydrophobic core, the PO chains in this instance, and a hydrophilic shell, the EO chains. This work uses F108, a flake PEO-PPO-PEO block copolymer with molecular weight PO chain 3250 and PEO chain 80%.

2.6 Surfactant Removal

The elimination of surfactants is a crucial step in creating mesoporous materials. Calcination and solvent extraction is the most common method for removing surfactants (Li *et al.*, 2010; Ren *et al.*, 2012). In this work, surfactant was removed from the produced mesoporous materials through washing and calcination.

2.7 Nanomaterials

Nanotechnology is a recent field of study that focuses on the synthesis, characterisation, modification, and use of nanomaterials for their wide range of applications in industries including pharmaceutics, food, cosmetics, textiles, medicine, optics, electronics, energy science, and electrochemical (Frewer *et al.*, 2014; Hussein, 2016). Nanotechnology studies the relationship between physical qualities or phenomena and material dimensions and the design, manufacturing, and application of nanostructures or nanomaterials (Rao *et al.*, 2006). Materials with one dimension and a size range of 1–100 nm are known as nanomaterials. Compared to their bulk materials, these materials may exhibit entirely new or improved electrical, optical, magnetic, catalytic, and antibacterial capabilities due to their exceptionally high surface area-to-volume ratio, extremely small size, and high packing densities (Charinpanitkul *et al.*, 2008; Granmayeh *et al.*, 2011; Jeevanandam *et al.*, 2018; Purkayastha & Manhar, 2016; Rosi & Mirkin, 2005). Nanostructural materials are composed of two primary components: grain, which includes nano crystallite, nanocluster assemblages, nano amorphous grains, and a matrix as an interface component formed by many interfaces and surfaces. Because the properties of nanomaterials are largely dictated by their size, shape, phase and chemical composition, the synthesis of metastable nanocrystals with controlled form and size has long been an interesting problem (Tjong, 2013). The materials possessing porous morphology with porous features comparable to 100 nm are termed nanoporous materials (Ameen, 2019; Mishra, 2019). The porosity and surface area of nanoporous materials and the arrangement of atoms within the crystal determine their properties. These materials can interact with their surroundings more successfully because they have many voids with adjustable dimensions at atomic, molecular, or nanometer sizes (Polarz & Smarsly, 2019). Nanoporous materials are classified into three groups by the International Union of Pure and Applied Chemistry (IUPAC); microporous (pore

size < 2 nm), mesoporous (pore size 2–50 nm) and macroporous (pore size >50 nm) (Wu *et al.*, 2020). Because of desirable characteristics such as high surface area, large pore volume, chemically stable, biocompatibility, low toxicity, tunable mesoporous materials with well-defined pore-size distribution, controllable wall composition, and modifiable surface properties, they have been extensively researched for use as catalysts, catalyst supports, and adsorbents in technical applications (Zhao *et al.*, 2012).

2.8 Catalyst

A catalyst is a substance that, throughout its lifespan, participates in a series of simple processes that transform reactants into products or a substance at a minimal amount that alters the reaction rate but keeps it unaltered at the end. After each cycle, the catalyst is restored to its initial state. Typically, a catalyst changes the rate of a reaction by promoting a different chemical pathway ("mechanism") (Fogler, 2020). However, Wolkenstein (2012) states that ideally, a catalyst should be regenerated at the end of the reaction, but in practice, it progressively degrades throughout the operation and eventually fails after a prolonged time of operation. A catalyst accelerates the reaction rate; it does not affect thermodynamics (Králik, 2014). Positive catalysis refers to the initiation of a reaction by a catalyst when the reaction velocity is accelerated. Autocatalysis is the process that occurs when the reaction itself generates compounds that accelerate the reaction. Negative catalysis (or retardation) is the opposite of positive catalysis. Poison falls within the category of negative catalysis. Catalytic poisons are chemicals that inhibit solid catalyst action. The catalyst activity depends upon the nature and complexity of the reactions involved. These activities in catalysis are conversion and selectivity. A fractional increase in reaction rate is called the activity of the catalyst, while the ability of a catalyst to control the direction of a reaction is known as its selectivity. The activity of a catalyst always increases with temperature; the activity and selectivity of a catalyst can be controlled by introducing minute quantities of impurity. Apart from activity, selectivity and stability, the catalyst should be regenerated, reproducible, mechanically and thermally stable, original, cost-effective, and have the right morphological features (Wang & Astruc, 2014). The catalyst is classified as either homogeneous or heterogeneous.

2.9 Homogeneous Catalysts

Homogeneous catalysts have the advantage that they are well-defined on a molecular level and readily soluble in the reaction medium. Such single-site catalysts are highly accessible to the substrates and often show high catalytic activity and selectivity, even under mild conditions.

However, removing them from the reaction mixture to avoid product contamination requires expensive and tedious purification steps (Shylesh *et al.*, 2010).

2.9.1 Heterogeneous Catalysts

The ability to produce valuable chemicals and fuels from raw materials efficiently, cost-effectively, and environmentally friendly made heterogeneous catalysis crucial to the global economy. They have a wide range of commercial uses in the pharmaceutical, food, chemical, petrochemical and automotive industries (Dumesic, 2008). Heterogeneous catalysis is also finding new applications in cutting-edge sectors, including fuel cells (Ghouri *et al.*, 2015; Huang *et al.*, 2012; Qin *et al.*, 2019), green chemistry (Ghashang *et al.*, 2016; Hosseini *et al.*, 2016; Yadav & Pujari, 1999), nanotechnology (Kazemi *et al.*, 2018; Kirkham *et al.*, 2007) and biorefining (Leal *et al.*, 2019; Wilson & Lee, 2016).

Heterogeneous catalysts are materials in different phases than the reactant because of their ease of separation from the reaction medium, hence outperforming homogeneous catalysts, and in the most extreme conditions, the stability of heterogeneous catalysts is remarkable. In heterogeneous, catalyst surface area is a critical parameter because; a catalyst works in three ways, it adsorbs the reactants and cleaves the required bonds, then it holds the reactants in proximity so that they can react, and finally, the surface lets the products desorb back into the surrounding phase (Nilsson, 2011). In ODS processes, heterogeneous catalysis is favourable because it reduces active species leaching and allows the catalyst to be recovered and reused for subsequent reactions (Liu *et al.,* 2019) .

This work uses tin–molybdenum mixed metal oxide catalyst, a heterogenous catalyst in sulfur removal reaction. Table 2 shows a comparison between the homogenous and heterogenous catalysts.

Table 2: Difference between homogenous and heterogeneous catalyst

Homogenous catalyst	Heterogenous catalyst
Low thermal stability	Thermally stable
Difficulty in identifying the structure	Well defined structure
Diffusion limits are practically absent	Diffusion controlled
Difficult to separate	Simple separation and reusability
Limited process applicability	Diverse process applicability
Use of toxic and expensive reagents	
Generation of large amounts of wastes	

2.9.2 Stages in a Heterogenous Catalytic Reaction

The reactants and products can go through several processes over the catalyst in a catalytic reaction which includes: (a) Reactants diffusion through a boundary layer enclosing a catalyst particle, (b) Reactants diffusion into catalyst pores and the active sites via intraparticle diffusion, (c) Adsorption of the reactants onto active sites, (d) Surface diffusion processes, (e) Product desorption from catalyst sites, (f) Product intraparticle diffusion through the catalyst pores, and (g) Diffusion of the products from the boundary layer surrounding the catalyst particle to allow recycling to step1 (Dizaji *et al.*, 2019; Dumesic, 2008; Fan *et al.*, 2015). This work carried out the following processes: initial physical adsorption, surface diffusion of the adsorbed species, chemisorption processes (bond breaking), a chemical reaction between the adsorbed species, and product desorption.

2.9.3 Surface Acidity

The surface acidity of a catalyst is an important feature that frequently dictates surface chemistry (Weiss & Ranke, 2002). Numerous techniques for measuring its presence and concentration have been developed. Spectroscopic examination of adsorbed probe molecules is the most prevalent technique (Gross *et al.*, 2010; Lavalley, 1996). This strategy may be the most practical for conducting experiments. With today's vastly better spectroscopic tools, it is possible to determine surface acid sites' existence rapidly. The second method is determining the isoelectric point, and the third is titration using indicators. This work uses the titration method to calculate the acidity properties of the prepared catalysts, as reported by Noh and Schwarz (1990) and Gong *et al.* (2017).

2.10 Metal Oxides

A metal oxide is a chemical species composed of repeated metal-oxygen bonds. Metal oxides are significant and widely used solid catalysts, active phases or supports (Kung, 1989). Metal oxides are used in heterogeneous catalysis for acid-base and redox properties (Kung, 1989). According to the position of the metal in the periodic table, they are classed as either metal oxides from the main group or transitional metal oxides. The number of distinct metals present determines classification. Transition and noble group metal catalysts are commonly utilized, and their activity is due to their outer electron configuration. Isotropic, anisotropic, amorphous, and local coordination are single metal oxide crystallization (Fahlman, 2007). All-metal oxides crystallize at ambient temperature, but many phases may remain amorphous at low calcination temperatures (Lermusiaux *et al.*, 2022). The majority of one-component metal oxides

crystallize with anisotropic morphology, and the surface may terminate with M–OH, M–O–M, M=O or M-() functionalities where M-() represents an oxygen vacancy (Jolivet *et al.*, 2010). Transition metals are the most popular metal oxide catalysts because of their inexpensive cost of manufacture, ease of regeneration, and selective activity. They're utilized in oxidation, reduction, dehydration, dehydrogenation, and isomerization, among other organic reactions. The partially filled d-shells of the metal ions and the influence of the oxide ligand field on this partially filled d-shell are responsible for their catalytic activity (Gawande *et al.*, 2012).

2.9.1 Molybdenum Oxide

Molybdenum is a transition metal oxide with an electronic configuration of $[Kr]4d^5 5s^1$; all six valency electrons are available for forming chemical bonds. It belongs to group VI of the periodic table. About nine molybdenum oxides have been reported, but the monoclinic dioxide MoO_2 and orthorhombic trioxide MoO_3 are the most common and stable (Green, 1994). The others, with formulae between MoO_2 and MoO_3, are metastable mixed valency oxides with intense colour and metallic lustre formed from one or both stable oxides. Molybdenum trioxide (MoO_3), an n-type semiconductor with a 2.8–3.6 eV bandgap, is one of the most interesting transition metal oxides. This is a vital material with broad applications in many fields, such as electronics, catalysis, sensors, energy-storage units, field emission devices, lubricants, superconductors, thermal materials, biosystems, chromogenic and electrochromic systems (Inmanee *et al.*, 2017; Jin *et al.*, 2012; Jittiarporn *et al.*, 2015; Reddy *et al.*, 2019). They are found in various stoichiometries, ranging from full stoichiometric MoO_3, which features a wide bandgap (>2.7 eV), to more conducting reduced oxides in the form of MoO_{3-x} ($2 < x < 3$) and eventually semi-metallic MoO_2 with a significantly reduced bandgap. Inducing oxygen defects, Mo^{6+} ions can be reduced to Mo^{5+} and, finally, Mo^{4+} (MoO_2). These variations in the oxidation states allow the handling of the crystal structure, morphology, oxygen vacancies, and dopants to control and engineer electronic states (Castro *et al.*, 2017; Thangasamy *et al.*, 2017).

The oxide MoO_3 has three common crystal structures; the well-known thermodynamically stable orthorhombic MoO_3. Figure 7 is a highly anisotropic layered structure along the direction formed by stacking bilayer sheets of MoO_6 octahedral with van der Waals forces, all the MoO_3 components share edges and corners (Hu *et al.*, 2015).

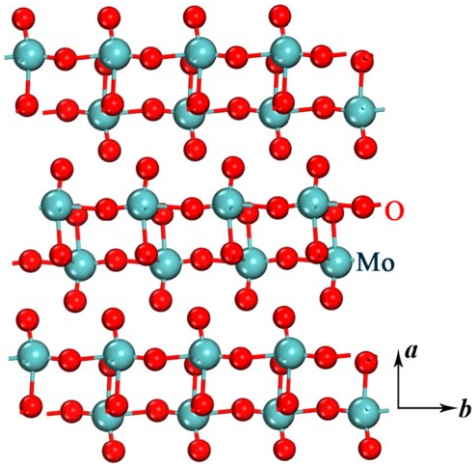

Figure 7: Crystal unit cell for α-MoO_3 (Wang *et al.*, 2020)

The metastable monoclinic MoO_3 (β-MoO_3) has the MoO_6 octahedral unit with shared corners resulting in a distorted cube (Fig. 8).

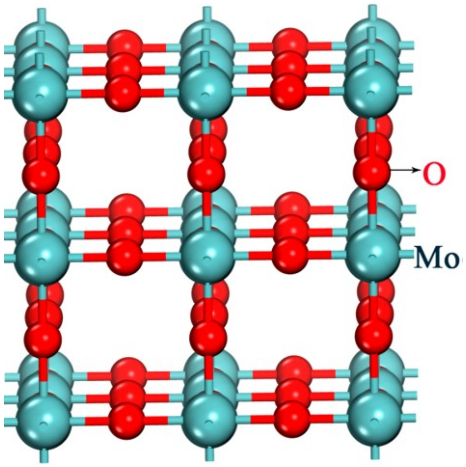

Figure 8: Crystal unit cell for β-MoO_3 (Wang *et al.*, 2020)

Lastly, the metastable hexagonal MoO_3 (h-MoO_3) (Fig. 9) is also constructed of zigzag chains of MoO_6 octahedra connected at cis-positions, one-dimensional tunnels in [001] direction (Zhou *et al.*, 2015).

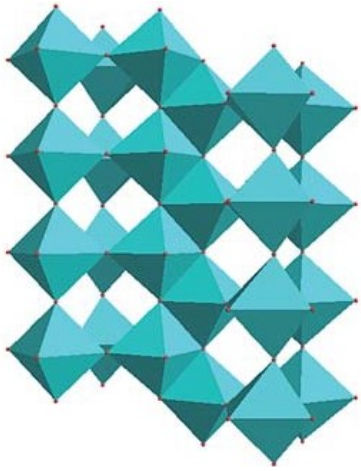

Figure 9: Crystal unit cell for h-MoO_3 (Zhou *et al.*, 2015)

Metastable structures often provide new and improved properties relative to thermodynamically stable structures (Castro *et al.,* 2017; Thangasamy *et al.*, 2017). The oxides have been formed into various structures, including nanorods, quantum dots, nanobelts, two-dimensional sheets, nanopores, and other nano morphologies. Various methods to fabricate MoO_3 include hydrothermal (Chen *et al.*, 2010; Zheng *et al.*, 2009; Zhou *et al.,* 2015), ultrasonic-assisted chemical method (Hu *et al.,* 2015), sol-gel (Bharate, 2021), atomic layer deposition (Dai *et al.*, 2018), spray pyrolysis (Afify *et al.*, 2017), chemical vapour deposition (Chen *et al.*, 2015; Wang *et al.*, 2016), precipitation (Pradeesh *et al.*, 2018; Wang & Ueda, 2009), and thermal evaporation (Siciliano *et al.*, 2009).

2.9.2 Tin Oxide

Tin has an electronic configuration of [Kr] $4d^{10}5s^25p^2$ and belongs to Group 14 of the periodic table. Its principal valence state is Sn (IV) and Sn (II). Tin has 10 stable isotopes, the largest number for any element, and results in very characteristic mass spectra.

The SnO_2 crystallizes as the tetragonal rutile structure with a point group D_{4h}^{14} and space group $P4_2/mnm$ and lattice constants a = b = 4.7374 and c = 3.1864 is regarded as an oxygen-deficient n-type semiconductor in the field of materials science (Diéguez *et al.*, 2001). Figure 10 shows a unit cell which consists of four three-fold coordinated oxygen atoms and two six-fold coordinated tin atoms (Jarzebski & Marton, 1976). The ionic radii for O_2^{2-} and Sn^{4+} are 1.40 and 0.71 Å, respectively (Jarzebski & Marton, 1976). Tin oxides (SnO_x) are generally available in two oxidation states, divalent and tetravalent and are termed p-type and n-type semiconductors, respectively (Liu *et al.*, 2010; Xu *et al.*, 2013). The Sn^{3+} valence is missing due to Sn's inert pair effect (Baidya *et al.*, 2009). Furthermore, the divalent oxide is stable in maintaining structure and electronic properties because of the high density of delocalized $5s^2$ and $5p^2$ states in the valence and conduction bands, respectively (Granato *et al.*, 2013).

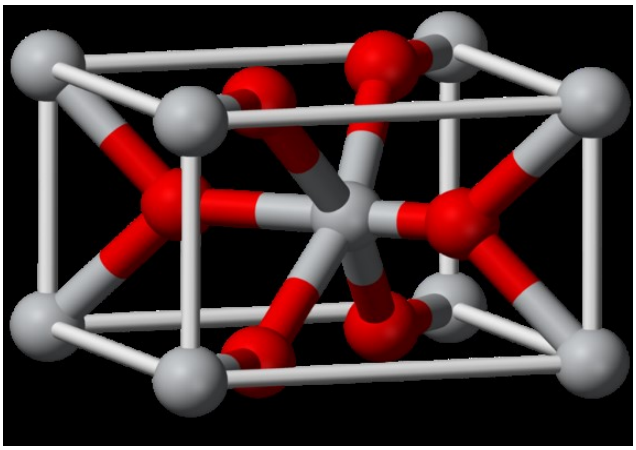

Figure 10: Unit cell for the SnO_2 crystal structure. Red balls indicate oxygen atoms, and the grey balls indicate tin atoms (Jarzebski & Marton, 1976)

The SnO_2 is a promising candidate for potential use because of its wide energy gap (3.6 to 3.8 eV), high carrier density, strong thermal stability (up to 500°C), high degree of transparency in the visible spectrum, and strong chemical and physical interactions with the adsorbed species (Das & Jayaraman, 2014). Since the presence of dopants or impurities can alter its n-type carrier capacity, it is a valuable semiconductor material for tailoring in a variety of applications at the nanometer scale, as opposed to bulk materials, to name a few; solid-state sensors (Li *et al.*, 2002; Shehzad *et al.*, 2018), transparent conductor (Agashe *et al.*, 2009), the catalyst for organic reactions (Manjunathan *et al.*, 2018), biomedicine (Sagadevan *et al.*, 2021). The properties of SnO_2 nanomaterials are largely determined by their composition and microstructures porosity, presence of defects, and particle size, which are controlled by the preparation method (Dammala *et al.*, 2019; Li *et al.*, 2020; Xu *et al.*, 2014).

There are different methods to synthesize tin dioxide nanomaterials, such as solid-state reaction (Li *et al.,* 2002), co-precipitation (Sangeetha *et al.*, 2011; Tazikeh *et al.*, 2014), hydrothermal (Haneda *et al.*, 2016), template free/assisted (Manjunathan *et al.,* 2018), carbothermal reduction (Shehzad *et al.,* 2018) and sol-gel method (Al-Saadi *et al.*, 2019; Priya *et al.*, 2016).

2.11 Mixed Metal Oxides Nanomaterials

Mixed metal oxides are oxygen-containing combinations of two or more different types of metal cations in proportions that may vary or be defined by strict stoichiometry. Oxides can be binary, ternary, or quaternary, depending on the number of distinct metal cations present. They are further classified according to their crystallinity or amorphousness. If the oxides are crystalline, their crystal structure can determine their composition. Combining two metals in an oxide matrix can result in materials having novel physical and chemical properties, resulting in improved stability or alteration of the chemical properties of the component oxides (Romanelli *et al.*, 2004). Frequently, mixed oxides have a surface acid strength that is significantly greater than the acid strength of the constituent oxides (Tanabe *et al.*, 1976). By incorporating a minor oxide component, the thermal stability of the main oxide component can be improved, allowing it to operate at greater operating temperatures. The main properties of the mixed oxides which are involved in the catalytic process are as follows: redox properties, Lewis acidity, Bronsted acidity, basic properties, surface coordination (unsaturated coordination of transition elements), surface topology: types of neighbours near the transition element, lattice oxygen mobility, and presence of defects which can activate molecular oxygen (Trifirò, 1998). These metals can function independently and impart intrinsic properties to the system or be modified through metal-metal or metal-oxygen-metal interactions leading to

substantial changes in the electronic and chemical properties of the cations (Rodriguez, 2003). Doping and mixing metal oxides with organic and inorganic materials to modify their structural, physical, and chemical properties have been the subject of numerous investigations. For example, ODS was successfully performed using W-doped TS-1 zeolite, which had better Lewis acid active sites and a high surface area (Lv *et al.*, 2019). For the selective oxidation of hydrogen sulfide to sulfur, iron-antimony and iron-tin mixed-metal oxide catalysts were studied; the mixed metal oxides exhibit significantly better catalytic activity than individual oxides (Li *et al.*, 1997). Tin-based sensors mixed with vanadium and magnesium oxides perform better than individual sensors for SO_2 gas detection, according to Lee *et al.* (2011). Fe-doped γ-Al_2O3 performed better in ODS due to oxygen vacancies and Lewis acid sites (Zhao *et al.*, 2018). A synergistic effect between Na (or Ce) and Mo was reported by Tu *et al.* (2019) that improves the activity and stability of catalysts for ODS. According to Li *et al.* (2011), the presence of oxygen vacancies allowed tin-copper mixed metal oxide nanowire sensors to be more sensitive than pure tin and copper oxide nanowire sensors.

2.12 Mixed Metal Oxides Preparation Method

In general, multi-component oxides are prepared using various methods. The ideal method produces a solid with a reasonable surface area, the desired stoichiometry, the desired number of phases, and, most importantly, the desired spatial distribution of these phases. The latter is critical in catalytic reactions where molecule diffusion is required for selectivity. There is no universally preferred preparation method for all oxides (Harold, 1989). The preparation method enormously affects the catalyst activity for any reaction/conversion. Qiu *et al.* (2015) prepared mesoporous $H_3PMo_{12}O_{40}/SiO_2$ by precipitation method, which affects pore structure with a high surface area that controls catalytic activity on ODS. The catalytic performance of mesoporous phosphotungstic acid/SiO_2 (HPW/SiO_2) synthesized by amino-functionalized (AF) and evaporation-induced self-assembly (EISA) methods for deep oxidative desulfurization of diesel was investigated. The results show that the EISA method had higher catalytic activities than AF due to the high BET surface area and Keggin structure maintenance of HPW molecules (Lei *et al.*, 2013). Our work uses the sol-gel method to prepare the materials over another method, such as the precipitation or incipient wetness impregnation method, because the sol-gel method is well suited for synthesizing highly crystalline metal oxide materials with small particle size, increased surface area, and tunable acidic properties (Abdul-Kadhim *et al.*, 2017).

2.11.1 Precipitation Method

This method is widely preferred due to its simplicity and cost-effectiveness. Generally, precipitation involves adding a specific solution to a desired pH level to precipitate substances from a solution. This process results in the formation of either lyophobic crystalline precipitates or lyophilic precipitates in the form of amorphous or weakly crystalline gels. Nucleation, the formation of solid seed crystals in the original solution, can occur through either homogeneous or heterogeneous mechanisms. In the case of homogeneous nucleation, the formation of seed crystals takes place within a pure solution as a result of interactions between ions or molecules. These interactions initiate an irreversible process of crystallization, leading to the formation of agglomerates under conditions of supersaturation. This process continues until the solution reaches a state of simple saturation. On the other hand, heterogeneous nucleation, which is more commonly observed, involves the formation of seed crystals through contact with any solid surface capable of reducing the energy barrier for their formation. This solid surface can be an impurity, the walls of the equipment, or intentionally added seed crystals. The growth of these seed crystals occurs at the solid-solution interface, and the rate of growth depends on the degree of supersaturation. The size of the resulting crystals is determined by the ratio of the nucleation rate to the crystal growth rate. The greater this ratio is, the smaller the crystallites will be and vice versa (Hutchings, 2004). Examples of mixed oxides synthesized by this method are the work by Tang *et al.* (2006), who prepared MnOx-CeO_2 mixed oxide for oxidation of formaldehyde, as well as Shan *et al.* (2011), who synthesized novel Ce-W mixed metal oxide for catalytic reduction of NOx with NH_3. The disadvantage of this method is that you need to control the factors that affect the catalyst properties, such as pH; as distinct cations precipitate at various pHs, it is crucial to choose a pH where the chosen base precipitates both cations. The anions found in metal salt solutions have the potential to poison catalysts. For example, chlorine works as a reversible poison for Cu catalysts. In the context of precipitation, various factors play a crucial role, including the choice of precipitating agent, solvent, sequence of mixing, temperature, additives, duration of aging, and composition of the solution. (Hutchings, 2004).

2.11.2 Sol-Gel Method

The sol-gel process can be defined as a preparation of sol, gelation of sol and removal of solvent. The sol can be produced from inorganic or organic precursors (nitrates or alkoxide) and may consist of dense oxide particles or polymeric clusters (Brinker, 2013). There are two

types of sol-gel chemistry, i.e., aqueous sol-gel chemistry (hydrolytic) and non-aqueous sol-gel chemistry (non-hydrolytic).

The aqueous sol-gel process changes a precursor solution into an inorganic solid through inorganic polymerization reactions induced by water. Generally, the starting compound is either an inorganic metal salt such as nitrate, chloride, sulfate or a metal-organic compound such as an alkoxide. Metal alkoxides are the most widely used precursors because they react readily with water and are known for many metals.

Overall, the sol-gel process involves the subsequent stages shown in Fig. 11 as reported by Niederberger (2009): (a) the formation of homogeneous solution from inorganic salts dissolved in water or metal-organic precursors in an organic solvent which is miscible with water, (b) sol formation, (c) aging, (d) shaping, and (e) thermal treatment/sintering.

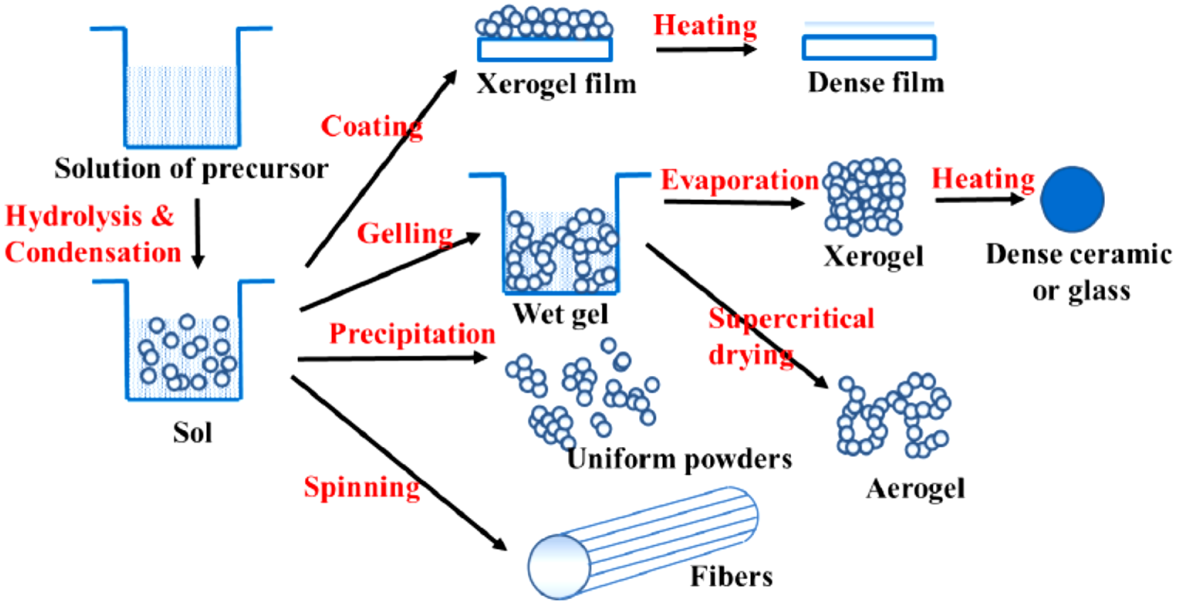

Figure 11: Various steps in the sol-gel process to control the final morphology of the product (Niederberger, 2009; Zha & Roggendorf, 1991)

Hydrolysis and condensation reactions are the first steps in a sol-gel reaction whereby an inorganic polymer is formed. Hydrolysis leads to a dispersion of colloidal particles in a liquid, and condensation results in an interconnected, rigid, and porous inorganic network enclosing a continuous liquid phase. This transformation is called the sol-gel transition. The gels can be dried using hypercritical conditions to form aerogels and ambient conditions to form a xerogel. The ability to shape the material into any desired form, such as monoliths, films, fibers, and monosized powders, and then to turn it into a ceramic material by heat treatment, is one of the very desirable aspects of the sol-gel method (Zha & Roggendorf, 1991). The higher reactivity

with the metal oxide precursors for water and the dual function of water as ligand and solvent makes the aqueous sol-gel chemistry complex.

The conventional sol-gel routes to metal oxides frequently present material stoichiometry and homogeneity control challenges. Homogeneity is determined by the ratio of homocondensation (i.e., the formation of M-O-M and M-O-M′) to hetero-condensation, which is particularly difficult to control under hydrolytic conditions due to the different reactivities of the various precursors toward hydrolysis and condensation (Cristoni *et al.*, 2001). Moreover, due to the numerous reaction parameters that must be strictly controlled (hydrolysis and condensation rate of the metal oxide precursors, pH, temperature, method of mixing, rate of oxidation, nature and concentration of anions), the hydrolytic sol-gel chemistry becomes complicated (Livage *et al.*, 1988). Another fundamental problem of aqueous sol-gel chemistry is that the as-synthesized precipitates are generally amorphous. The required post-synthetic annealing step to induce the crystallization process prevents any subtle control over crystal size and shape.

In nonaqueous sol-gel chemistry (non-hydrolytic), the precursor is dissolved into an organic solvent without water. The list of precursors includes metal acetates and metal acetylacetonates, in addition to inorganic metal salts and alkoxides. Inorganic precursors are used as the starting material. An alcoholic solvent is used instead of water because of its lower surface tension, so the gel structure could be retained from collapsing during drying (Kung, 1989). One advantage of using inorganic salts as precursors is that the rates associated with precursor hydrolysis, condensation of metal species, and precipitation of mesostructured oxides can be controlled (Vioux, 1997; Yang *et al.,* 1999). These nonhydrolytic routes involve the cleavage of the carbon-oxygen bond rather than the metal-oxygen bond and generally tend to retard the crystallization of metal oxides (Vioux, 2016).

Furthermore, the nonhydrolytic process favours the formation of homogeneous binary oxides from various metal precursors due to the reduced differences in hydrolysis and condensation rates for various inorganic sources in nonaqueous media. These nonhydrolytic conditions were critical in mesoporous mixed oxide synthesis (Yang *et al.,* 1999). Amphiphilic surfactant molecules can form regular micelle in polar solvent or inverse micelles in non-polar (Malliaris *et al.*, 1985; Zhu *et al.*, 1992). Generally, the sol-gel-based inverse micelle method includes the solution, the sol-gel transition, and the post-synthesis step as shown in Fig. 12.

The inorganic precursor solution is created during the solution stage. Different features of mesoporous materials can be tuned using the type of inorganic precursors, dopant quantity, surfactant qualities (such as size, type, and mixing ratio), and other small molecules. In the sol-

gel transition stage, the solvent evaporates, and the micelles assemble. The inorganic precursors transform into oxide, and the oxide network when the liquid dries.

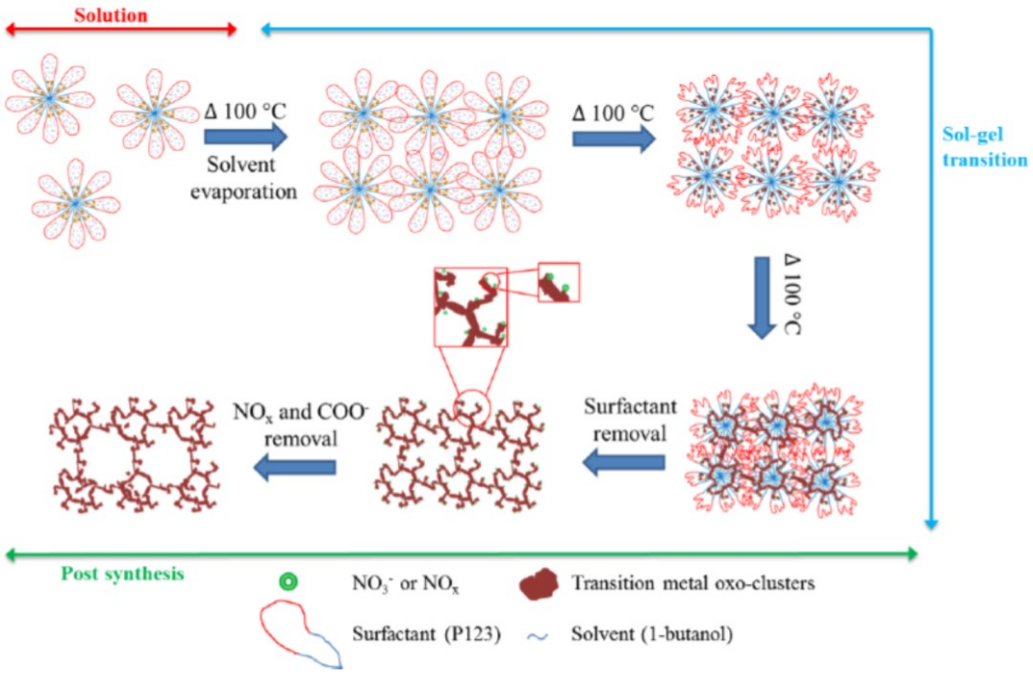

Figure 12: General procedure of sol-gel-based inverse micelle method (Poyraz *et al.*, 2013)

Key elements in this process that impact the properties of mesoporous materials are reaction temperature, reaction duration, and the solvent. In the post-synthesis phase, the solvent first removes the surfactant. Then, calcination at 150°C eliminates the by-products created during the sol-gel transition stage, such as NOx and carboxyl groups. Mesoporous materials' characteristics can be tuned by modifying the calcination temperature, heating rate, and environment during post-synthesis (Poyraz *et al.,* 2013).

This work uses the non-hydrolytic sol-gel method, where the inorganic precursors and surfactant are combined, resulting in a wet gel in the solvent. The inorganic precursor is then converted into a mesoporous network. The surfactant is then removed using solvent washing and calcination.

CHAPTER THREE

MATERIALS AND METHODS

3.1 Overview

This Chapter describes the materials, equipment, and methods used to prepare and characterize the mesoporous tin–molybdenum mixed metal oxides catalyst. It further presents the desulfurization performance of the prepared catalyst.

3.2 Materials and Equipements

3.2.1 Chemicals

The chemicals used in the experimental work are listed in Table 3.

Table 3: Chemicals used in catalyst preparation and ODS reactions

Chemical used	Formula	Function	Purity	Company
Sodium molybdate	Na_2MoO_4	Source of Molybdenum	98%	Sigma-Aldrich
Tin (II) chloride	$SnCl_2$	Source of Tin	98%	Sigma-Aldrich
1-Butanol, ACS	$C_4H_{10}O$	Reaction solvent	99.4%	Sigma-Aldrich
Nitric acid	HNO_3	pH control	67%	Sigma-Aldrich
F-108	PEO-PPO-PEO	Structure directing		Sigma-Aldrich
n-heptane	C_7H_{16}	Nonpolar solvent	99%	Sigma-Aldrich
acetonitrile anhy	C_2H_3N	Polar solvent	99.8%	Sigma-Aldrich
Benzothiophene	C_8H_6S	Sulfur source	98%	Sigma-Aldrich
Dibenzothiophene	$C_{12}H_8S$	Sulfur source	98%	Sigma-Aldrich
Hydrogen peroxide	H_2O_2	Oxidant	30%w/v	Merck

3.2.2 Equipment

The equipment used for catalyst preparation and ODS reaction are listed in Table 4.

Table 4: Specifications of the equipment

Apparatus	Specification	Function
Citizen scale (CY204)	Min weight 2mg, max weight 220 g	Measuring weight
Stirrer SB-161-3	Rotation speed (40-2000) rpm	For mixing
Electrical oven	Max temperature 300°C	For heating
Lindberg/Blue M	Max temperature 1200°C	For calcination
Intelligent stirring oil & water bath	Max temperature 300°C,	Desulfurization unit

3.3 Synthesis of the tin– Molybdenum Mixed Metal Oxide Catalyst

The catalyst was synthesized using the sol-gel method (Poyraz *et al.,* 2013). The preparation conditions greatly influenced the material's catalytic activity. The catalyst was prepared by varying two conditions, calcination temperature and Sn/Mo mole ratio (Fig. 13).

3.3.1 Different Calcination Temperatures

Synthesis was done following the work by Poyraz *et al.* (2013). In a typical synthesis, an equimolar amount of tin chloride and sodium molybdate were dissolved in a beaker containing 0.016 mol nitric acid, 0.11 mmol F-108 surfactant and 0.047 mol of 1-butanol with magnetic mixing at room temperature (RT). The synthesized mixture was oven kept at 100°C for 4 h, after which it was washed with ethanol and oven-dried overnight. After drying, the samples were heated at 150, 250, 350, 450 and 550°C at a 2°C/min ramp in a muffle furnace.

3.3.2 Different Sn/Mo Mole Ratio

The following amount of 0.01 mol Na_2MoO_4 and 0.01 mol $SnCl_2$ was dissolved in a Pyrex beaker which contains butanol as solvent, pluronic surfactant (F108) and the pH of the mixture was approximately 1 measured by pH meter after adding 2 mL HNO_3 acid at ambient conditions which were stirred for 3h to make a catalyst with Sn/Mo mole ratio of (1:1). For mole ratio of (1:2); 0.01 mol Na_2MoO_4 and 0.005 mol $SnCl_2$ was used while for (2:1) mole ratio; 0.01 mol $SnCl_2$ and 0.005 mol Na_2MoO_4 was used. The obtained suspension was then placed in the oven at 100°C and aged for 4 h. The precipitate was filtered and washed with

ethanol. Following that, the powder was dried in an oven at 150°C for 12 h to remove carboxylate ion (COO^{-1}) from the surfactant and 250°C for 4 h to remove nitrogen gas (NOx) from nitric acid decomposition and finally to 450°C for 6 h at the ramp rate of 5°C/min in the muffle furnace. The tin–molybdenum mixed metal oxide catalysts with the mole ratio of 2 :1 is represented hereafter as Sn/Mo (2:1). The other two catalyst samples are expressed as Sn/Mo (1:1) for 1:1 mole ratio and Sn/Mo (1:2) for a mole ratio of 1:2; pure Sn and Mo oxides have also been synthesized.

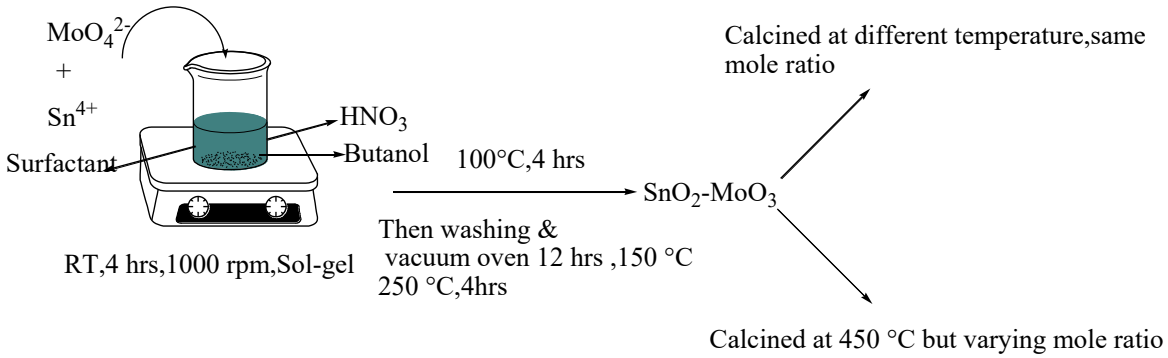

Figure 13: Schematic diagrams for the preparation of tin–molybdenum mixed metal oxide catalyst

3.4 Catalyst characterization

The catalyst's physicochemical properties were investigated using a variety of analytical techniques.

3.4.1 Nitrogen Physisorption Studies

Adsorption is the attachment of atoms or molecules to the surface of a substance through chemisorption or physisorption. This is a non-destructive technique for assessing porous materials. By generating an adsorption-desorption isotherm over various partial pressures, this method is utilized to evaluate the pore size distribution, specific surface area, and pore volume of the materials. The catalyst was calcined at different temperatures and mole ratios and analyzed for its textural properties. The textural properties of the materials, specific surface area (SSA) and pore size distribution (PSD) analysis of the samples were performed by using a Discrete Fourier transform (DFT) model via the aid of a Quantachrome (NOVAtouch NT 2LX-1, Volts 220, USA) operated with the Quantachrome TouchWin Software Version: 1.22, following standard analytical procedures.

3.4.2 Thermogravimetric Analysis

Thermogravimetric analysis (TGA) is an analytical technique in which changes in the chemical and physical properties of the sample are determined as a function of increasing temperature or time. It is used to characterize materials that exhibit either mass loss or gain due to decomposition, oxidation, or loss of any volatile materials. In such materials, analysis is performed by measuring the weight change as a function of temperature or time under a controlled atmosphere. Thermogravimetry analysis of the synthesized mesoporous tin–molybdenum mixed metal oxide was done on a synchronous thermal analyzer (PerkinElmer, STA8000). Samples were prepared by weighing 40 mg and putting them into the clean sample holders. A pre-weighed dry solid sample was allowed to heat under an air atmosphere with a purge rate of 20 mL/minute from room temperature to 950°C at a heating rate of 5°C/minute.

3.4.3 X-ray Diffraction Analysis

X-ray diffraction (XRD) is a technique for analyzing the quality and quantity of crystalline material. It provides information regarding the kind of crystalline phase, the structural composition of the phases, the degree of crystallinity, crystallite sizes, and orientation. Samples were packed into the sample container and smoothed using a microscope slide during the XRD analysis. To compare peak intensities, samples were not weighed, but efforts were made to ensure that the quantity measured was equal. X-ray diffraction (Bruker BV with 2D Phaser Benchtop, reflection geometry), $2\theta = 5–90°$, requisition time: 5.240 s per step, radiation source: Fe filtered Co Kα1 ($\lambda = 0.1789$ nm), operates at 30 mA and 50 kV was used.

3.4.4 Scanning Electron Microscopy

Scanning electron microscopy (SEM) is an electron microscopic technique that creates a high-resolution sample picture by scanning the sample with a focused stream of electrons. These electrons (with an energy of up to 40 keV) directed at a specimen interact with atoms in the sample to generate numerous signals that carry information on the surface topography (texture), chemical composition, crystalline structure, and orientation of materials of the sample. Therefore, it is mostly utilized to examine solid materials' surface topography and morphology. During the examination, solid powdered samples were placed on a conductive carbon tape mounted on an aluminium stub and coated with carbon. A scanning electron microscope (SEM-EDX) model JSM-7600F was utilized for morphological and elemental composition studies.

3.4.5 Fourier Transform Infrared Technique

Fourier transforms infrared (FT-IR) spectroscopy is used to analyze the functional groups of materials. The IR radiation is passed through the sample, some infrared light is absorbed, and some are transferred through the sample (transmitted). The resulting spectrum indicates molecular absorption and transmission, establishing a molecular fingerprint of the material. Like a fingerprint, no two distinct molecule configurations yield identical infrared spectra. As a result, infrared spectroscopy can be utilized for various analyses. The FT-IR spectrometer (Bruker Tensor-27) with a resolution of 2 cm^{-1} was used.

3.4.6 Raman Spectroscopy Analysis

Raman spectroscopy is based on the inelastic light scattering in a substance where the incident light transfers energy to molecular vibrations. The scattered light can be detected by a Raman spectrometer and represents a chemical fingerprint of the substance. Based on such spectral information, a material can be identified or characterized.

Raman spectroscopy and Fourier transform infrared differ in that they depend on changes in a molecule's polarizability, while IR spectroscopy depends on changes in the dipole moment. In contrast to IR spectroscopy, which measures the absolute frequencies at which a sample absorbs light, Raman spectroscopy measures the relative frequencies at which a sample scatters light. The following specifications for the Confocal Raman Microscope were used in this study. The chemical bonding investigation was conducted using the following model: WITec alpha 300 R Germany, Laser wavelength: 532 nm, Laser power: 10 mW, and spectral acquisition, 120 s.

3.4.7 Acid Site Density Calculation

Strong and weak/moderate acid site densities were computed using the neutralization ion exchange method adapted from (Benak *et al.*, 2002; Gong *et al.,* 2017; Thalgaspitiya *et al.*, 2020). The catalyst (0.05 g) was mixed with 0.5 M NaCl (50 mL) for six hours to determine the strong acid site density. A 25 mL sample of the supernatant was separated, and 0.05 M NaOH was titrated with HCl in the presence of a phenolphthalein indicator. The catalyst (0.05 g) was combined with 0.025 M NaOH and agitated for six hours to calculate the density of weak/ moderate acid sites. With phenolphthalein indicator present, a 25 mL portion of the resulting supernatant was back titrated with 0.05 M HCl. For the strong acidic group, Equation (1) was used.

$$\text{Normalized loading capacity} = \frac{\text{The volume of NaOH} \times \text{Normality of NaOH}}{\text{Mass of catalyst (g)}} \quad (1)$$

The combined acid site density of the strong and weak acidic group was calculated using Equation (2)

$$\text{Normalized loading capacity} = \frac{\text{mmol of NaOH-mmol of HCl used}}{\text{Mass of catalyst (g)}} \quad (2)$$

3.5 Catalytic Activity Evaluation

Catalyst activity is evaluated in terms of conversion and selectivity. A fractional increase in reaction rate is called the activity of the catalyst, while the ability of a catalyst to control the direction of a reaction is known as its selectivity. The activity and selectivity of a catalyst can be controlled by introducing minutes of quantities of impurity.

Before performing a catalytic activity, screening was done to obtain the optimal calcination temperature, and after that, optimal reaction parameters were evaluated. Furthermore, the optimal Sn/Mo mole ratio was determined by using optimal reaction parameters.

Model diesel treatment with ODS requires both an oxidant and a solid catalyst. Model diesel is formed by dissolving model sulfur compounds such as DBT or DMDBT in a non-polar solvent such as hexane, heptane, or toluene. The tin–molybdenum mixed metal oxide was used as the catalyst, and H_2O_2 was chosen as the oxidant because of its eco-friendliness and green nature. The generated sulfones were separated using polar acetonitrile as an extraction agent during the ODS procedure. To accomplish the oxidation and separation of organosulfur compounds in a model diesel with a single reaction unit, a biphasic catalytic oxidation/extraction system incorporating a solid catalyst, a green oxidant, and an extraction solvent was developed (Fig. 14).

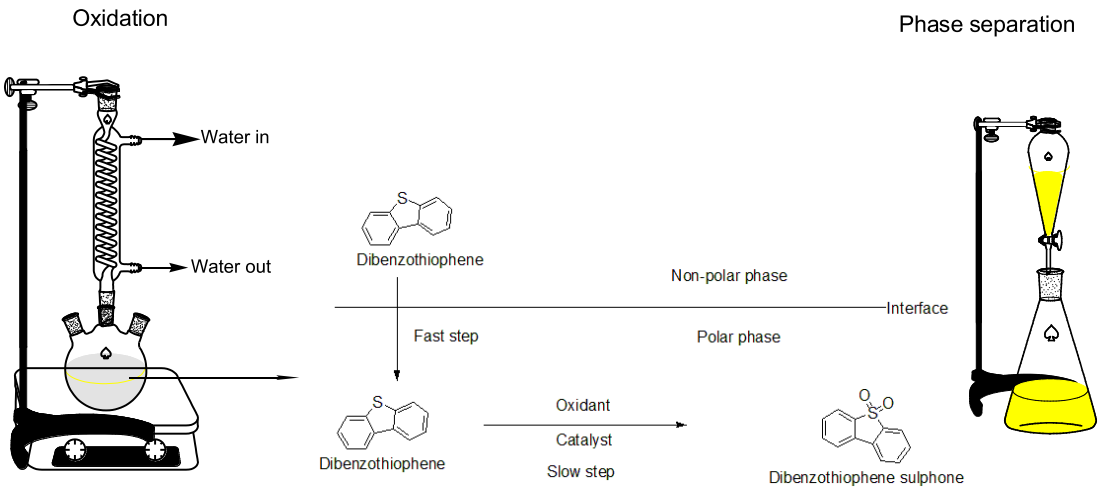

Figure 14: Experimental setups for ODS biphasic system

3.5.1 Effect of Calcination Temperature on ODS Reaction

In a typical experiment, an oil bath was initially heated and stabilized at the required reaction temperature in each run. The experiments were carried out in a two-necked 250 mL glass reactor fitted with a condenser and thermometer. The model diesel comprised 250 ppm DBT, obtained by dissolving 0.125 g of DBT in 500 ml of n-heptane. The 20 mL of model oil, a specified amount of catalyst (mg) calcined at different temperatures, i.e., 250, 350, 450,550, 650 and 750°C and peroxide were added to 20 mL of acetonitrile and stirred with a magnetic stir. The mixture was vigorously stirred at 1000 rpm for 30 minutes at atmospheric pressure to avoid external mass transfer resistance (Jose *et al.*, 2011).

The oil phase was withdrawn, and the DBT content was assessed utilising an ultraviolet-visible spectrophotometer (UV-vis 2800 spectrophotometer, SHIMADZU, Japan) at 200 to 300 nm wavelength. The DBT showed a strong peak at the maximum absorption wavelength (λmax), 284 nm (Arellano *et al.,* 2014). A working solution of 5–100 ppm was prepared to draw a calibration curve (Fig. 15), of Absorbance versus the DBT concentration, with an accuracy of linear approximation of R^2=0.9996. The DBT conversion (η) calculation versus reaction time was done according to Equation (3).

$$\eta = \left(\frac{C_o - C_t}{C_o}\right) \times 100\% \qquad (3)$$

Whereby, Co and Ct represent the initial DBT concentration at time zero and the final DBT concentration at time t.

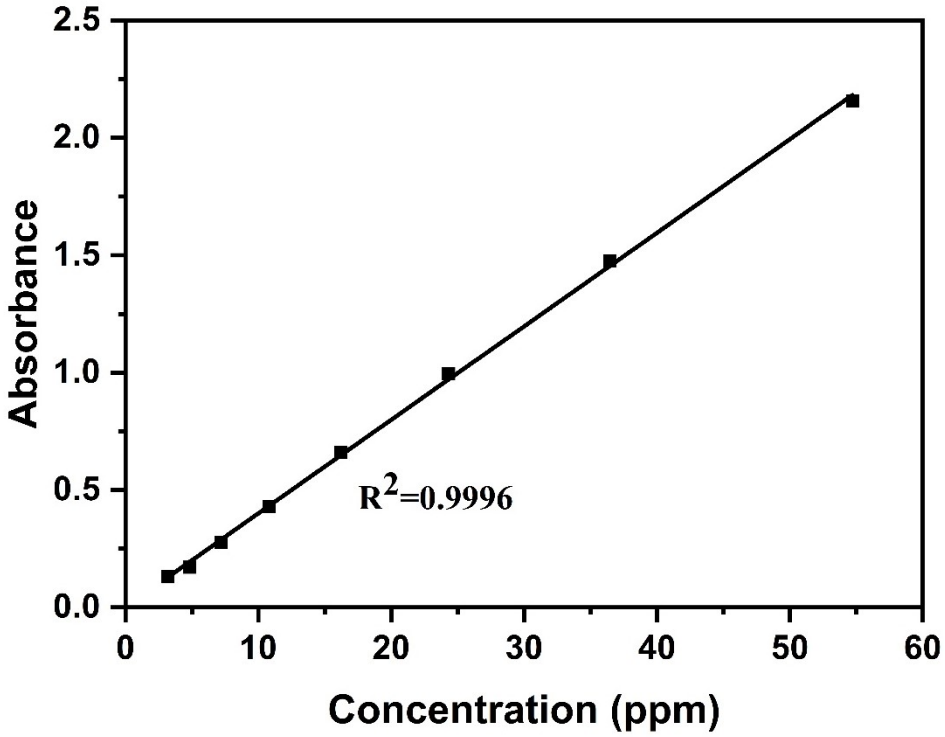

Figure 15: Calibration graph of absorbance against the concentration of DBT

3.5.2 Other Factors Influencing Catalytic Performance on ODS Reaction

After obtaining optimal calcination temperature for catalyst performance, other reaction parameters such as temperature, reaction time, catalyst load, and oxidant/sulfur ratio were varied. In a typical experiment, an oil bath was initially heated and stabilized at the required reaction temperature in each run. The experiments were carried out in a two-necked 250 mL glass reactor fitted with a condenser and thermometer. The model diesel comprised 250 ppm DBT, obtained by dissolving 0.125 g of DBT in 500 ml of n-heptane. The 20 mL of model oil, a specified amount of catalyst (mg) calcined at 450°C while keeping other reaction parameters constant such as temperature, oxidant/sulfur ratio and reaction time and peroxide were added to 20 mL of acetonitrile and stirred with a magnetic stirrer. The mixture was vigorously stirred at 1000 rpm for 30 minutes at atmospheric pressure to avoid external mass transfer resistance (Jose *et al.,* 2011).

The oil phase was withdrawn, and the DBT content was assessed utilising an ultraviolet-visible spectrophotometer (UV-vis 2800 spectrophotometer, SHIMADZU, Japan) at 200 to 300 nm wavelength. The DBT showed a strong peak at the maximum absorption wavelength (λmax), 284 nm (Arellano *et al.,* 2014). The concentration of the DBT remained in the sample after the ODS reaction was determined and calculated, as reported in section 3.4.1. A series of experiments on different temperatures, time, and oxidant/sulfur ratios were conducted with the same experimental procedure.

3.5.3 Effect of Sn/Mo Mole Ratio On ODS Reaction

The DBT sulfur model compound was dissolved into heptane to make a stock solution with a sulfur content of approximately 250 ppm. The prepared catalyst sample with different Sn/Mo mole ratio was subjected to ODS reactions in Erlenmeyer flasks (250 mL) equipped with a magnetic stirrer. The oil phase was withdrawn, and the DBT content was assessed utilizing an ultraviolet-visible spectrophotometer (UV-vis 2800 spectrophotometer, SHIMADZU, Japan) at 200 to 300 nm wavelength. The concentration of the DBT remained in the sample after the ODS reaction was determined and calculated, as reported in section 3.4.1.

3.5.4 Characterization of The Oxidized Product

The white residual obtained at the end of the ODS reaction was filtered and dried in the fume hood overnight to evaporate trapped solvents within the solid and sent for analysis using FT-IR to determine the final product.

3.5.5 Catalyst Reusability

In industrial applications, the ability to reuse catalysts is of great importance. Therefore, tests were conducted to examine the reusability of a catalyst made of a mixed metal oxide of tin and molybdenum under optimal conditions. Following the initial reaction run, the catalyst was subjected to a series of steps, including centrifugation, two rounds of ethanol washing, and drying at 80°C for 5 hours. Subsequently, the catalyst was utilized in another experiment, thereby assessing its suitability for multiple cycles of use.

CHAPTER FOUR

RESULTS AND DISCUSSION

4.1 Structural Characterization

The crystal structure, orientation, and particle size of SnO_2-MoO_3 catalysts calcinated at different temperatures were determined using X-ray diffraction.

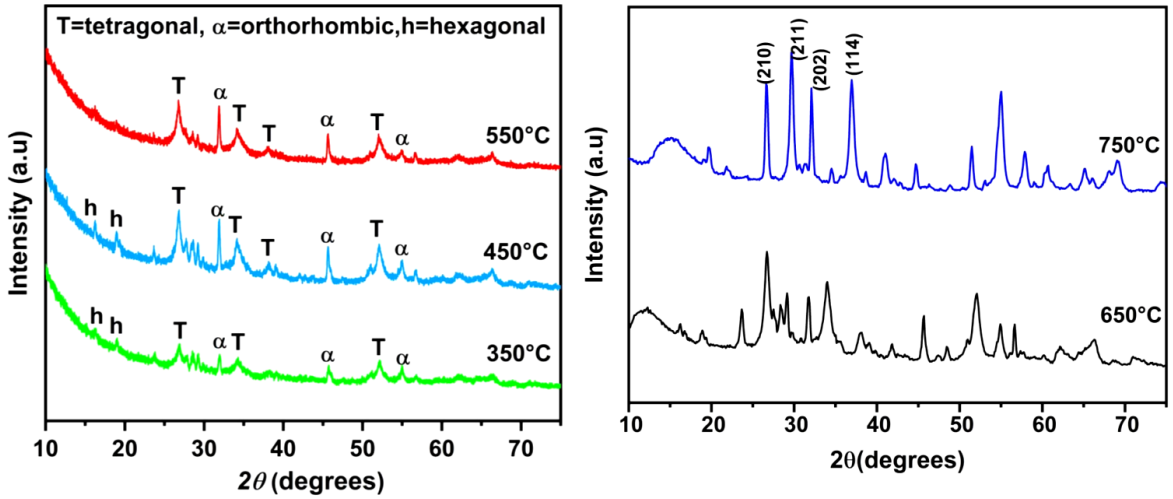

Figure 16: The XRD patterns of the SnO_2-MoO_3 catalyst materials calcinated at different temperatures

Figure 16, the impact of calcination temperature on the phase transformation of the SnO_2-MoO_3 catalyst materials is depicted. All three samples exhibited diffraction peaks at angles of 26.5°, 33.9°, 37.9°, and 51.9°, which corresponded to the lattice planes (110), (101), (202), and (211), respectively. These peaks could be attributed to the tetragonal structure of tin oxide, with lattice parameters a = 4.72 Å, b = 4.72 Å, and c = 3.17 Å, per JCPDS card no 01-0657. Furthermore, the X-ray diffraction (XRD) patterns of all the samples revealed the presence of two phases of MoO3: hexagonal MoO_3 (JCPDS card No. 21-0569) and orthorhombic MoO_3 (JCPDS card No. 35-0609). With an increase in temperature from 350 to 450 °C, the hexagonal phase gradually transformed into α-MoO_3, accompanied by a weight loss of 27.6%, which was attributed to the polymorphic transition from h-MoO_3 to α-MoO_3. At a calcination temperature of 550°C, almost all of the h-MoO_3 phase converted to α-MoO_3, as indicated by the disappearance of XRD peaks at 18° and 20°, corresponding to the (110) and (200) lattice planes of the hexagonal structure. Both the hexagonal and tetragonal phases were found to be responsible for the catalytic activity observed in the study being presented. At higher temperatures, the formation of the $Sn(MoO_4)_2$ phase is supported by the presence of distinct diffraction peaks, particularly (210) and (211); this observation aligns with previous reports on the subject (Il'in *et al.*, 2017).

In general, as the temperature rises, the diffraction peaks tend to become more narrow and sharp while their intensity increases. These changes suggest an enhancement in the crystallinity of the material and an increase in particle size (Choodamani *et al.*, 2014; Sengupta *et al.*, 2011; Sui *et al.*, 2003). The Scherrer formula (4) was applied to calculate the average crystallite size:

$$D = \frac{K\lambda}{\beta cos\theta} \quad (4)$$

Whereby, β stand for line broadening at the half-maximum intensity, θ is the Bragg angle, K stands for the shape factor ≅ 0.9, D denotes the crystallite size in nanometers, and λ denotes X-ray wavelength (0.15406 nm). The crystallite sizes were 24, 29, 32 and 38 nm for the sample prepared at 350, 450, 550 and 650°C, respectively. As previously stated, the increase in crystallite size observed with increasing temperatures between 350 and 650°C can be attributed to the Oswald ripening phenomenon. Oswald ripening is a diffusion-driven process in which larger particles grow at the expense of smaller particles, resulting in an overall increase in crystallite size (Choodamani *et al.,* 2014; Madras & McCoy, 2004; Sengupta *et al.,* 2011). The XRD patterns of all the as-prepared samples, including pure Mo, Sn oxide and SnO_2–MoO_3 mixed metal oxides with different Sn/Mo mole ratios, are shown in Fig. 17. The peaks at 12.7, 23.3, 25.7, 27.3, 33.8, 39.0 and 48° corresponding to (020), (110), (021), (101), (060), (002) reflections attribute to the distinctive diffraction peak of orthorhombic MoO_3 (JCPDS card No.00-005-0506), while the peaks at 26.6, 33.9, 37.9, 51,7° correspond to (110), (101), (200) and (211) characteristic diffraction peaks of tetragonal SnO_2 (JCPDS card No.01-077-0451). The Sn/Mo (1:2) oxide's diffraction peaks are less pronounced than those of pure MoO_3, indicating that Mo is doped into a substitutional position of the SnO_2 lattice. The diffraction peaks of the Sn/Mo (2:1) oxide shifted slightly to a higher 2θ angle compared to those of the tetragonal rutile SnO_2 phase because the crystal structure of MoO_3 is considerably disturbed by the mutual contact with Sn oxide to form amorphous Mo oxide in the boundary (Mallesham *et al.*, 2020; Okamoto *et al.,* 1981)

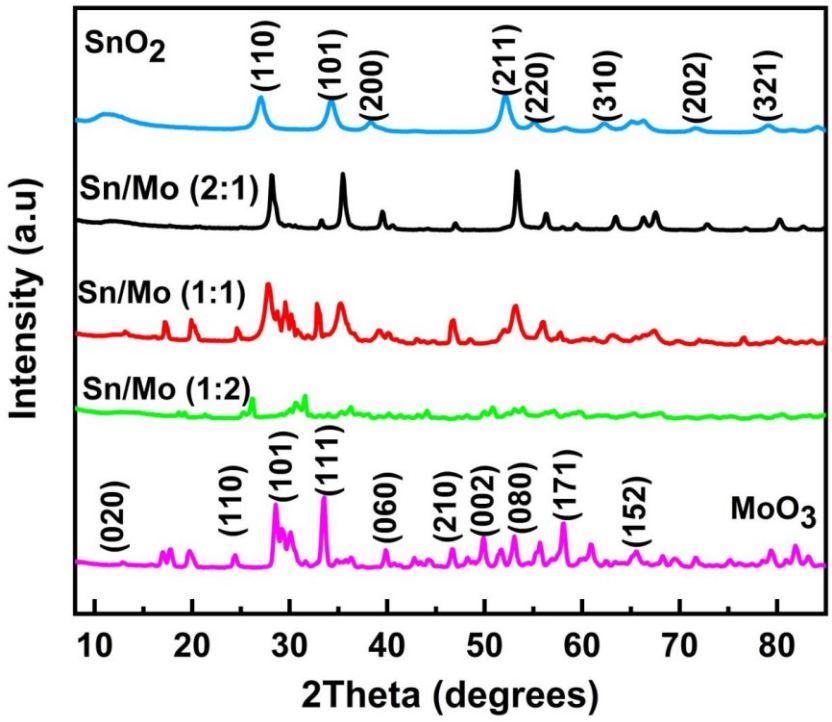

Figure 17: The XRD patterns for SnO_2–MoO_3 catalysts with varying mole ratios calcined at 450°C

When the mole ratio of Sn/Mo is (1:1), the main diffraction peaks observed at 2θ = 28.9◦, 33.22◦, and 52.8 are assigned to the (021), (111) and (211) planes of hexagonal MoO_3 and tetragonal SnO_2 oxides. Furthermore, the diffraction peaks for tetragonal tin oxides are much broader, indicating the presence of smaller MoO_3 domains, which agrees well with the specific surface area obtained from BET analysis**.** The broad diffraction peak at 35.1° resembles the highest intensity peak for tetragonal SnO_2 oxide. Furthermore, the Scherrer formula (4) was used to calculate the crystal size of the SnO_2-MoO_3 catalyst prepared at different Sn/Mo mole ratios. The crystal size for SnO_2 oxide was 47.5 nm, while for MoO_3 was 34.5 nm. For the SnO_2-MoO_3 catalyst materials with different mole ratios Sn/Mo (2:1), (1:1) and (1:2), the crystal size was 42.4, 31.9 and 29.9 nm, respectively. The presence of MoO_3 oxide in SnO_2-MoO_3 catalyst materials causes a decrease in crystal size for SnO_2. All these observable characteristics may have the following causes. First, applying a powerful oxidant during synthesis verifies the presence of Mo^{6+} ions in the SnO_2 framework. Second, the shorter ionic radius of Mo^{6+} (0.62 A) compared to Sn^{4+} (0.72 A) and its higher valence state cause the cell to contract and, most likely, the development of cation vacancies to preserve the lattice's electroneutrality (Bai *et al.*, 2014; Cao *et al.*, 2019).

4.2 Morphological Studies

The SEM was used to examine the materials' morphological properties. Figure: 18 shows SEM images for pure MoO_3 with a flake-like structure, while the SnO_2 presents a sphere-like structure that agglomerated.

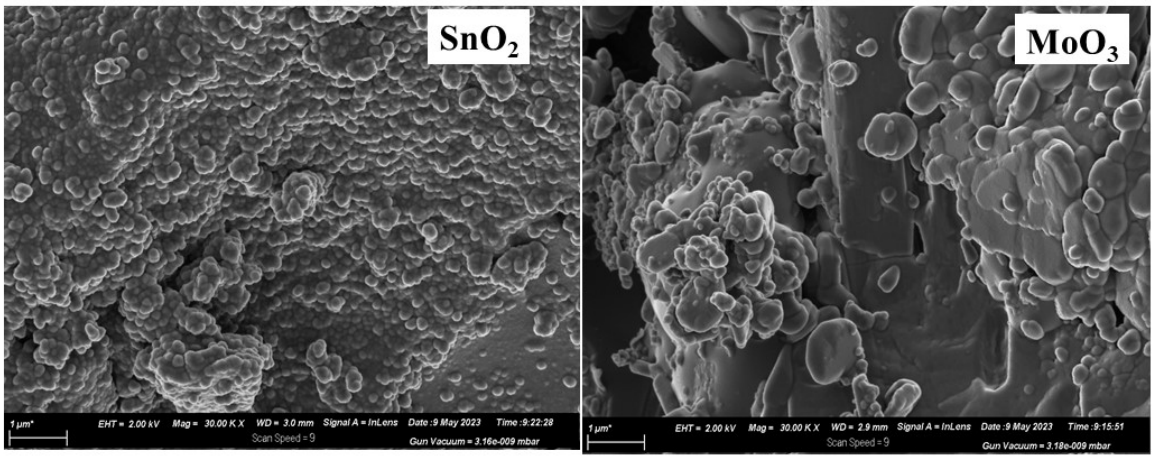

Figure 18: The SEM images of SnO_2, MoO_3

The morphology of the SnO_2-MoO_3 materials was found to be influenced by the calcination temperature. Lower calcination temperatures resulted in a rough surface, whereas at 450°C, a nanobelt structure was observed. This specific morphology has been identified as the key factor responsible for the catalytic performance of the materials. The energy-dispersive X-ray (EDX) analysis confirmed the presence of tin, molybdenum, and oxygen in the synthesized mixed metal oxide SnO_2-MoO_3 catalysts, as shown in Fig. 19.

The surface morphology of the SnO_2-MoO_3 catalysts synthesized at different mole ratios is shown in Fig. 20. Fused particles were observed when the amount of Mo oxide was higher than that of Sn. A cauliflower morphology is formed when the amount of Mo and Sn oxides are equal. When Sn was higher than Mo, the cauliflower morphology was destroyed, and materials with relatively smaller agglomerated particles were formed. These relatively smaller agglomerated particles have a higher surface area, which could explain their superior catalytic activity compared to the other materials.

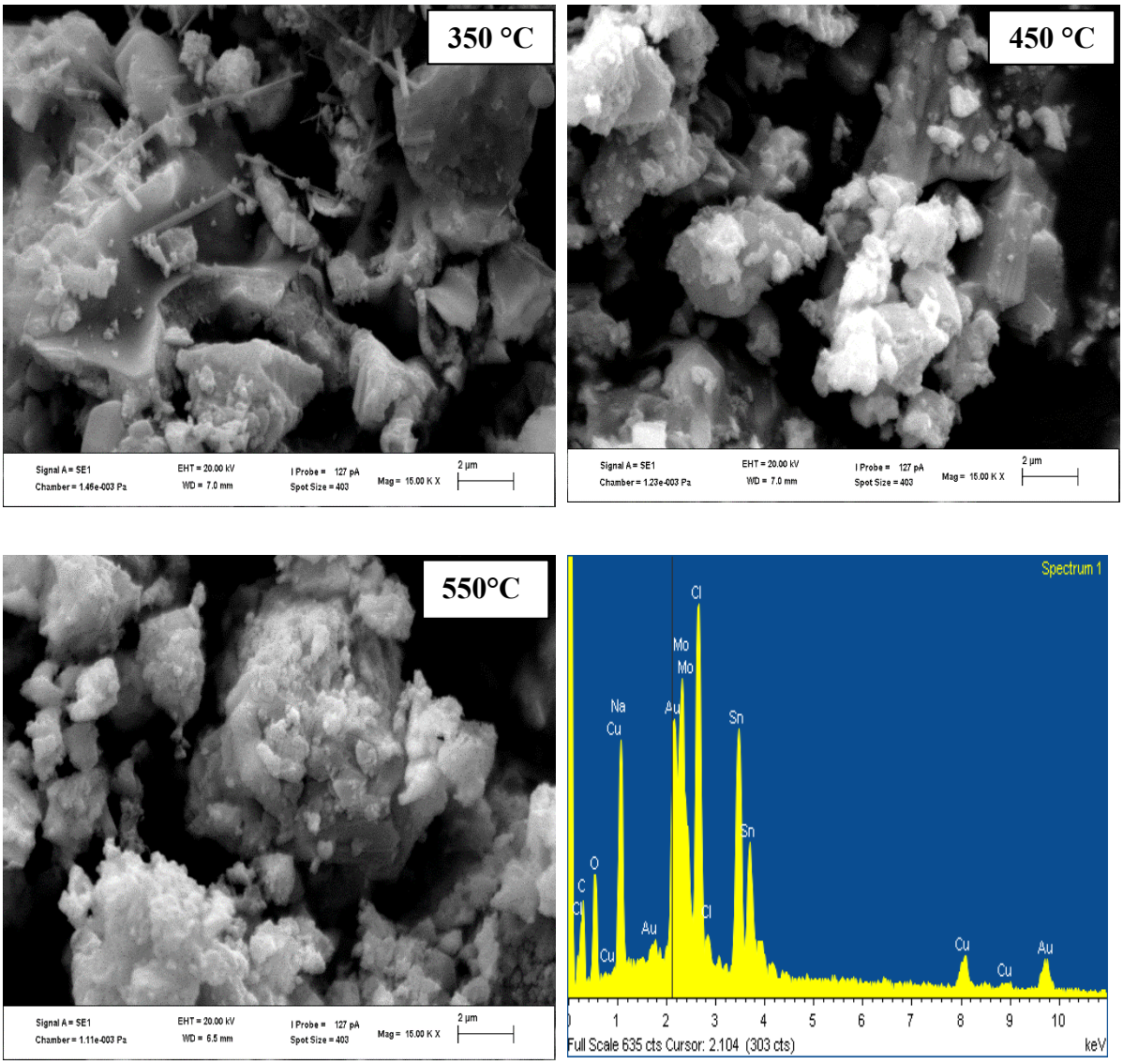

Figure 19: The SEM images showing the morphology of the SnO_2-MoO_3 catalyst material calcinated at different temperatures and EDX profile

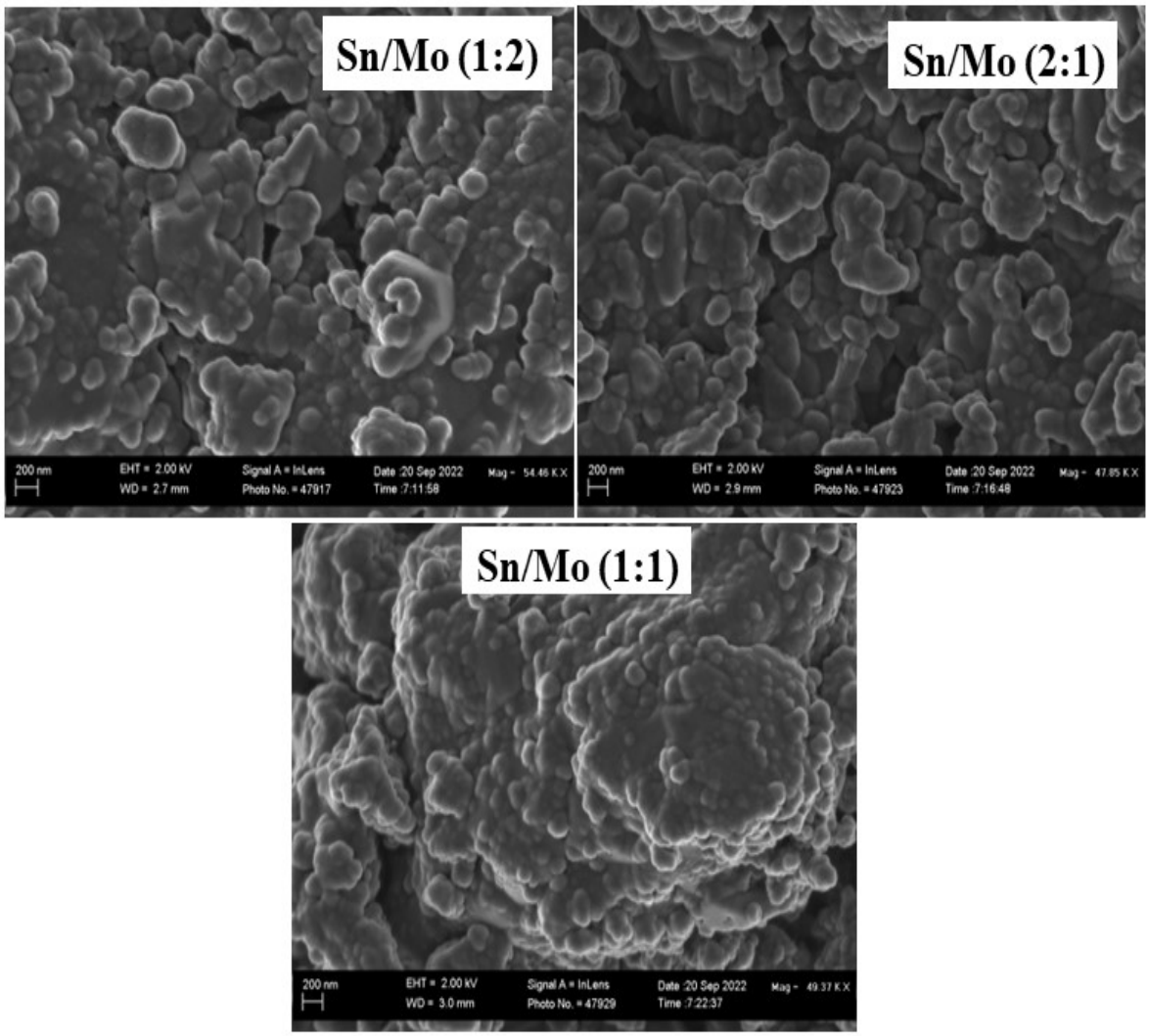

Figure 20: The SEM images of SnO_2-MoO_3 catalyst materials at different mole ratios: Sn/Mo (1:2), Sn/Mo (1:1) and Sn/Mo (2:1) calcined at 450°C

4.3 Nitrogen Adsorption-Desorption Isotherms Analysis

The impact of calcination temperature on the textural properties of the SnO_2-MoO_3 catalyst was examined. Figure 21 displays the N_2 adsorption-desorption isotherms of the catalyst. Based on the IUPAC classification, these isotherms exhibit characteristics of type IV, indicating the presence of mesoporous materials. The hysteresis observed in the isotherms is classified as H3, further confirming the mesoporous nature of the catalyst (Sing, 1985; Zhang *et al.*, 2021; Zhang *et al.*, 2017). In addition, we realized a decrease in the BET surface area as the volume of nitrogen adsorbed diminishes with increasing calcination temperature.

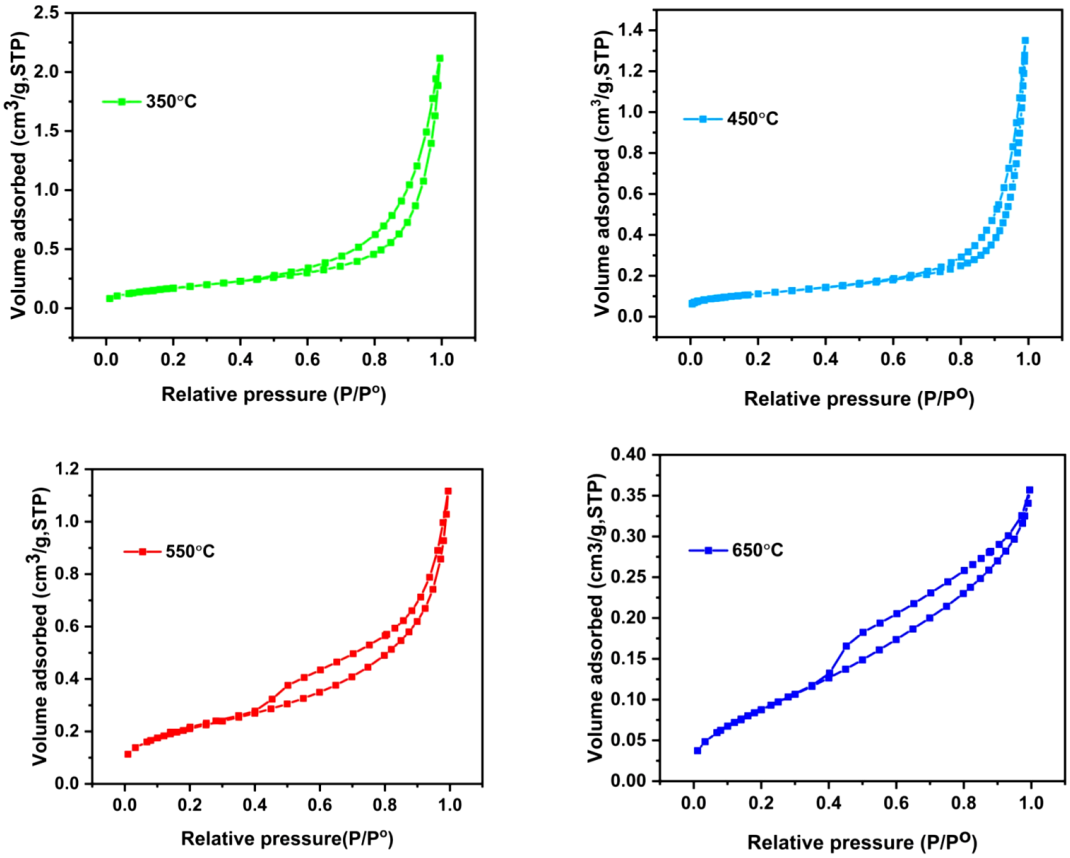

Figure 21: The adsorption-desorption nitrogen isotherms of the SnO_2-MoO_3 catalyst calcined at different temperatures

Table 5 presents a summary of the pore volume, BET surface area, and pore diameter of the SnO_2-MoO_3 samples that underwent calcination at different temperatures. As the calcination temperature increased from 350 to 450°C, the BET surface area and pore volume exhibited a rise, reaching values of 9.0 to 17.7 m^2 g^{-1} and 0.027 to 0.041 cm^3 g^{-1}, respectively. This increase can be attributed to the removal of organic matter in the samples, which was confirmed through XRD, TGA, and FTIR analysis. However, when the temperature was further increased beyond 450°C, both the surface area and pore volume decreased significantly, measuring 17.7 to 7.8 m^2 g^{-1} and 0.041 to 0.011 cm^3 g^{-1}, respectively. This decline was attributed to particle sintering and microstructure coarsening at higher temperatures, and a similar observation was reported elsewhere (Liu *et al.,* 2019).

Table 5: Textural properties of SnO_2-MoO_3 catalysts at different calcination temperatures

Calcination temperature (°C)	Pore size (nm)	Pore volume (cm^3g^{-1})	Surface area (m^2g^{-1})
350	2.1	0.027	9.0
450	3.2	0.041	17.7
550	3.1	0.034	10.2
650	4.5	0.011	7.8

To determine the pore size distribution within the catalyst and evaluate the accessibility of active sites to reactants, pore analysis was conducted. The pore distribution of the SnO_2-MoO_3 catalyst calcined at different temperatures was calculated using the BJH (Barrett-Joyner-Halenda) method. The results were then plotted in the corresponding (Fig. 22). The materials presented a mesopore width distribution between 2–4.5 nm.

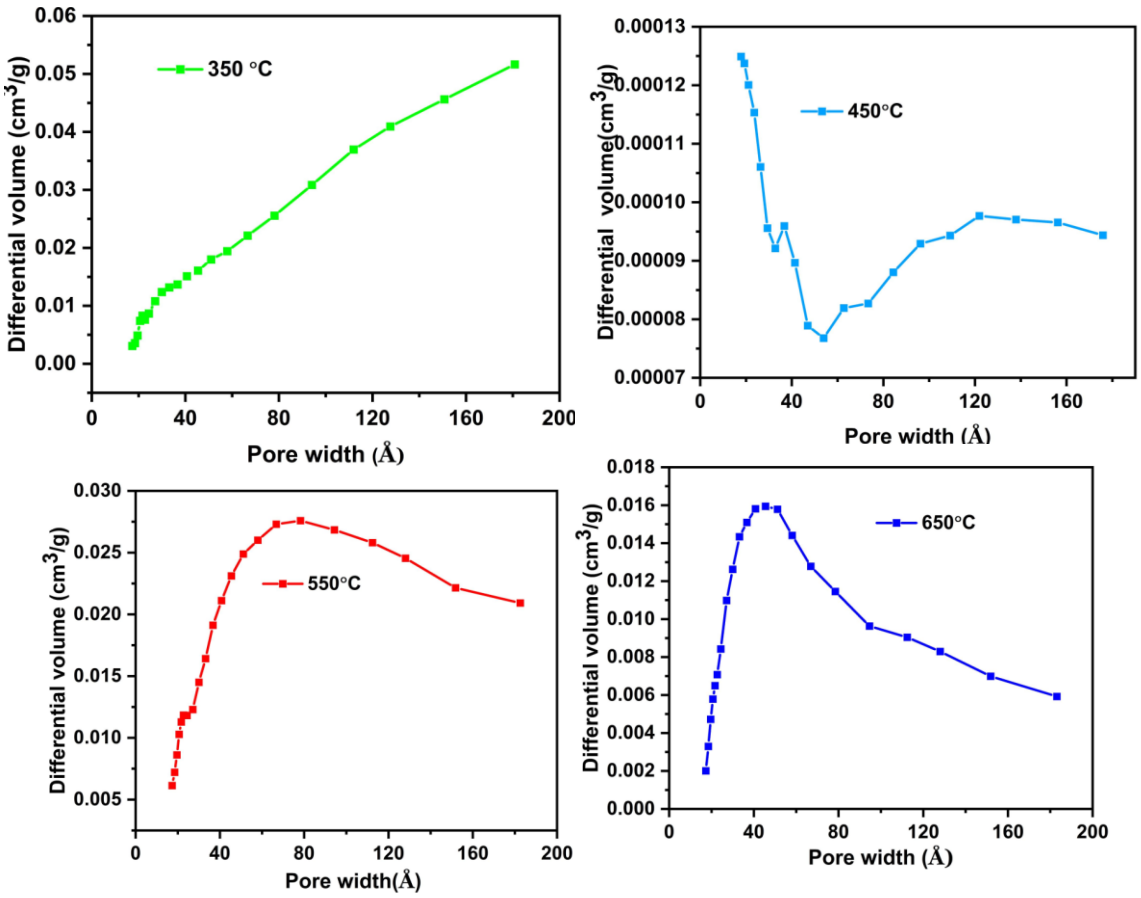

Figure 22: Pore size distribution of SnO_2-MoO_3 catalyst calcined at different temperatures

In addition, to investigate the impact of varying mole ratios, Nitrogen adsorption experiments were done on the synthesized materials to evaluate their textural properties. Figure 23 illustrates the isotherm observed for MoO_3 and SnO_2 oxides. The isotherm of MoO_3 oxide

exhibits a type IV pattern accompanied by a type H3 hysteresis loop, indicating the presence of mesopores and micropores, which is in agreement with previously reported observations in scientific literature (Sing, 1982), while the isotherm of SnO_2 oxide demonstrates type IV behavior with H3-type hysteresis loops, indicating the existence of narrow slit-like mesopores that possess a consistent size and shape, this aligns with previous reports in the literature (Liu *et al*., 2019).

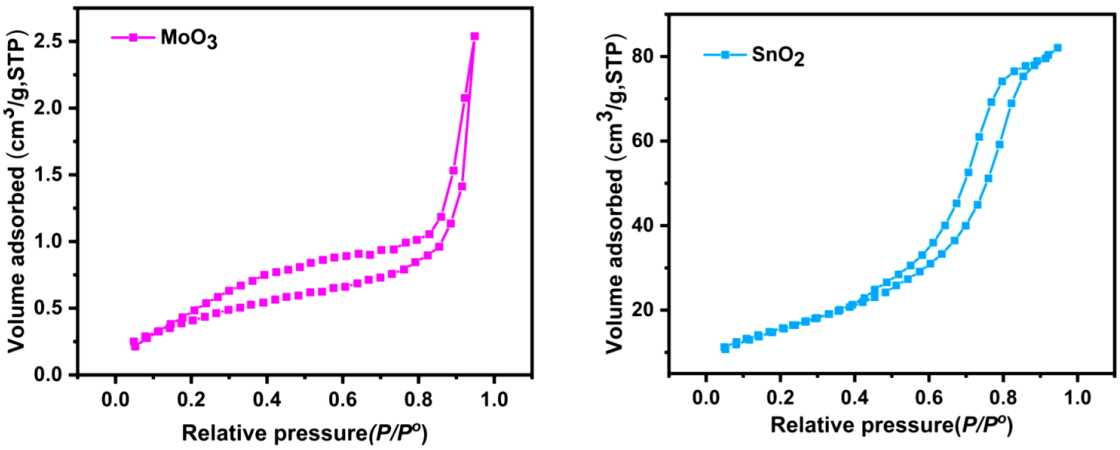

Figure 23: Nitrogen isotherm for MoO_3 and SnO_2 catalyst calcined at 450°C

For the SnO_2-MoO_3 catalyst materials synthesized at different mole ratios, the nitrogen adsorption-desorption isotherms are shown in Fig. 24. Sn/Mo (1:2) and Sn/Mo (1:1) samples exhibited type IV, H3 hysteresis loops characteristic of capillaries in laminate form. On the other hand, Sn/Mo (2:1) samples showed a sharp slope at a relative pressure of around 0.4, then a linear increase to approximately 0.9 in both the adsorption and desorption branches. The increase in slope at around 0.4 corresponds to capillary condensation, which is characteristic of mesoporous materials. The additional increase in relative pressures suggests significant interparticle porosity with homogeneous pore networks. Furthermore, the capillary condensation step for Sn/Mo (2:1) catalyst materials is not pronounced; the isotherm shape is type IV with an H4 hysteresis loop according to Sing (1985).

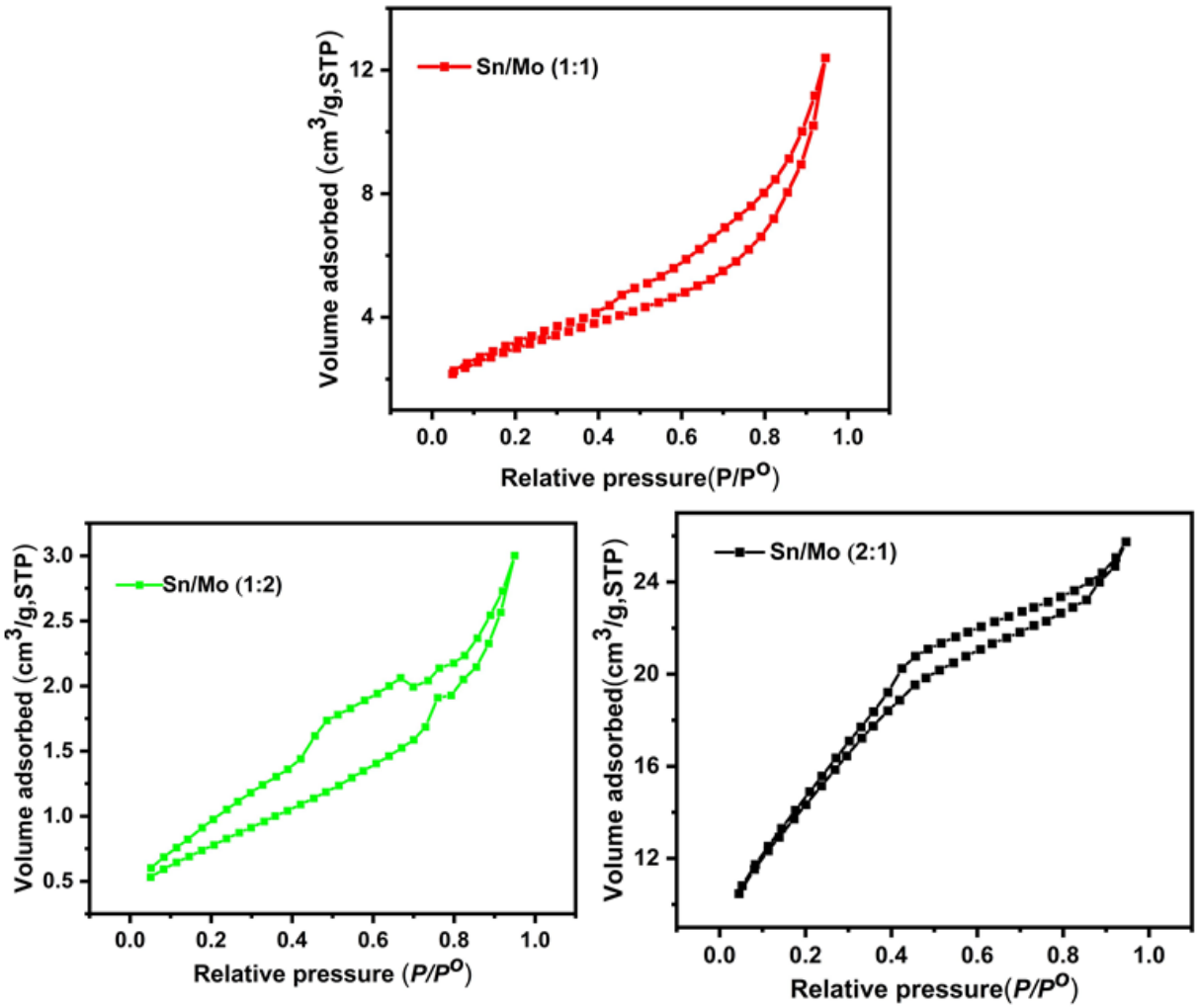

Figure 24: Nitrogen isotherms for SnO_2-MoO_3 catalyst materials at different Sn/Mo mole ratios Sn/Mo (1:2), Sn/Mo (1:1) and Sn/Mo (2:1) calcined at 450 °C

Figure 25 shows the pore size distribution for MoO_3, SnO_2 oxides and SnO_2-MoO_3 catalytic materials at different mole ratios. The MoO_3 shows a broad BJH pore diameter with multimodal distribution in the mesopore and macropore size region. The SnO_2 oxide shows a bimodal distribution. It can be observed that differential volume increases with the increase in tin content. The BJH pore size distribution curves were bimodal, and the average pore sizes of all materials were 3.5 nm confirming mesoporous materials as per IUPAC classification: Ultra-micropores (size <0.7 nm), micropores (size <2 nm), mesopores (2 nm <size<50 nm), macropores (size >50 nm) (Leofanti *et al.*, 1998).

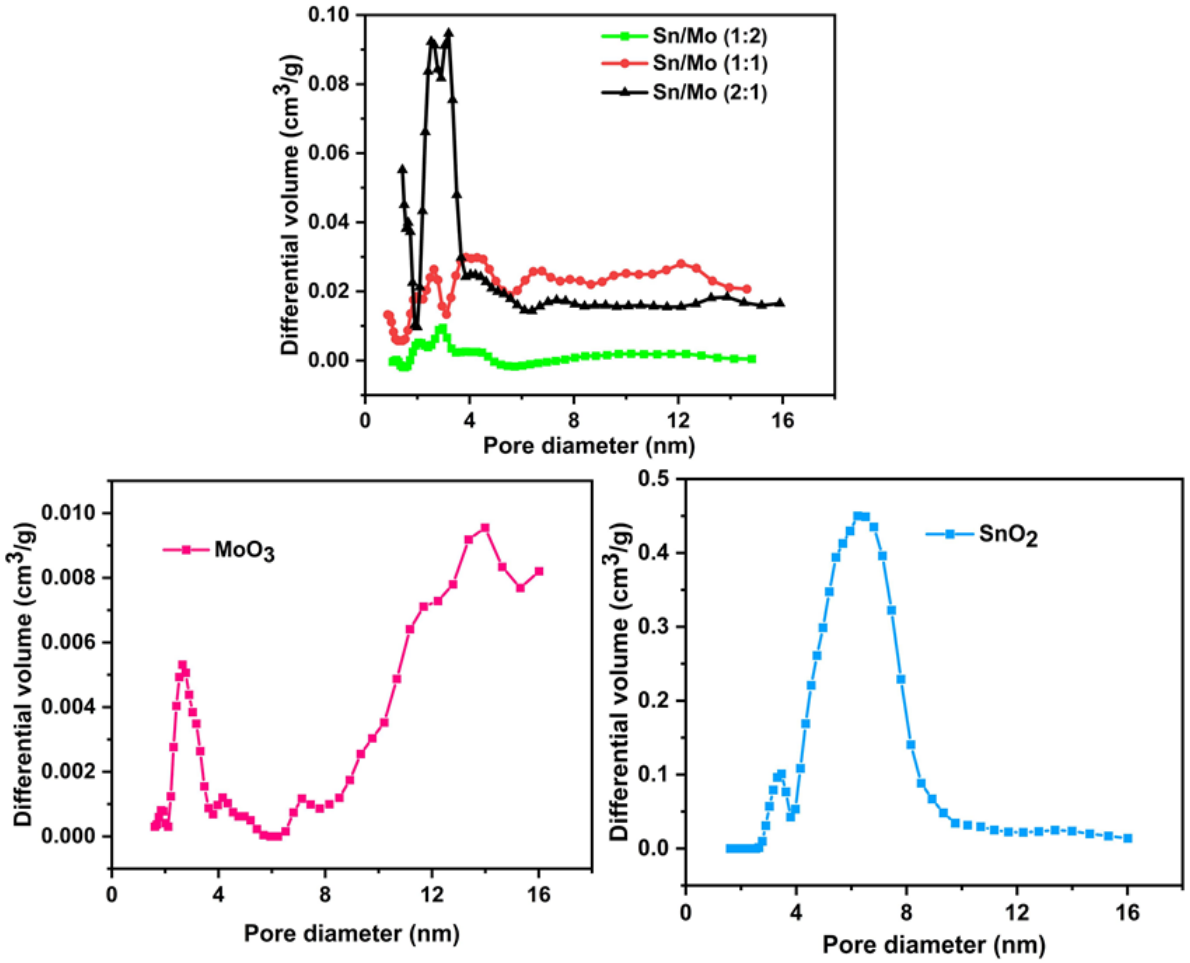

Figure 25: Pore size distributions of the SnO_2-MoO_3 catalyst prepared at different mole ratio calcined at 450°C

The specific surface areas of mesoporous SnO_2–MoO_3, estimated from the BET method (Table 6), increase with the increasing tin content. The lowest value (2.3 m^2 g^{-1}) for the catalyst with the Sn/Mo (1:2) content was comparable to the pure MoO_3 (1.5 m^2 g^{-1}). The successive addition of tin proportionally increased the catalysts' surface areas up to (50.4 m^2 g^{-1}) for the material containing Sn/Mo (2:1) mole ratio while for pure SnO_2 is (42.2 m^2g^{-1}), confirming the molybdenum's promotion effect.

Table 6: Textural properties of the MoO_3, SnO_2 and SnO_2–MoO_3 catalyst at different mole ratios calcined at 450°C

Sample	Surface area (m^2g^{-1})	Pore volume (cm^3g^{-1})	Pore size (nm)
SnO_2	42.2	0.120	6
MoO_3	1.5	0.003	3 and 14
Sn/Mo (1:2)	2.3	0.004	3.5
Sn/Mo (1:1)	10.7	0.016	3.5
Sn/Mo (2:1)	50.4	0.036	3.5

4.4 Thermal Gravimetric Analysis

To assess the thermal stability of the SnO_2-MoO_3 catalysts, thermal gravimetric analysis (TGA) was conducted. Figure 26 exhibits the TGA/DTG profiles of the as-synthesized SnO_2-MoO_3 catalysts, subjected to heating from room temperature to 950°C at a rate of 5°C per minute in the presence of air. The profiles reveal three distinct regions that correspond to varying degrees of weight loss. In the low-temperature range, spanning from 100 to 156°C, a weight loss of 3.4% is observed. This can be attributed to the removal of physically adsorbed water molecules within the sample, as well as the decomposition of carboxylate ions (COO^-); this finding aligns with previous reports in the literature regarding similar phenomena Elhi *et al.* (2020). The middle-temperature region from 156 to 532°C with a 27.6 % weight loss, is attributed to NO emissions, SnO_2 crystallization, and polymorphic transition of *h*-MoO_3 to α -MoO_3 (Il'in *et al.,* 2017; Poyraz *et al.,* 2013). Within this temperature range, specifically around 450 °C, the active phase of the catalyst was obtained. Above 532°C, a weight loss of 8.2% was observed, which can be attributed to the formation of crystalline tin molybdate $Sn(MoO_4)_2$. This is further confirmed by X-ray diffraction (XRD) analysis, as shown in Fig. 16. However, although this phase is thermodynamically stable, it exhibits reduced catalytic activity due to its decreased surface area (Il'in *et al.,* 2017).

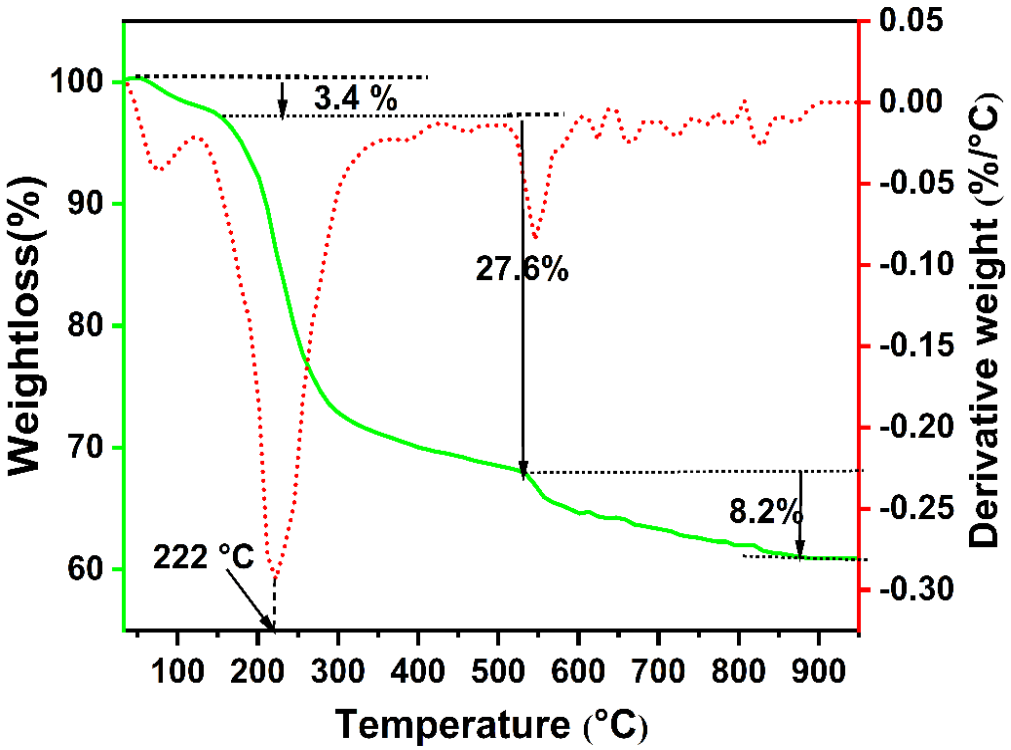

Figure 26: TGA/DTG curve of SnO_2-MoO_3 catalyst before calcination

4.5 The FT-IR analysis

The catalysts were analyzed using FT-IR studies within the wavenumber range of 400 to 3500 cm^{-1} to identify the specific functional groups present (Fig. 27). The presence of a wide vibrational peak at 2881 cm^{-1} in the uncalcined sample can be attributed to the stretching of O–H bonds, which indicates the presence of water molecules associated with the powder (Mamatha *et al.*, 2022; Zakharova *et al.*, 2007). The sharp vibrational peak observed at 1653 cm^{-1} was identified as the result of bending vibrations of the hydrogen-bonded–OH group found in water molecules adsorbed on the surface of the sample; this is also reported by Sen *et al.* (2019) and Zakharova *et al.* (2007)). As the calcination temperature increased, there was a noticeable and significant increase in absorption bands attributed to interatomic vibrations. This phenomenon provides strong evidence of the formation of metal oxides (Madhu *et al.*, 2010). The peaks at 649 and 837 cm^{-1} match the bridging Sn-O-Sn and Mo-O-Mo modes, respectively, while the peak at 938 cm^{-1} matches Mo-O stretching with double-bond character according to Martos *et al.* (2000) while the peak at 649-499 cm^{-1} is due to Sn-O bonds. The absorption peaks at 1523, 1344, and 1084 cm^{-1} confirm the presence of C=O and C–O from surfactant, which disappears due to an increase in calcination temperature, which is also documented by Yang *et al.* (2012).

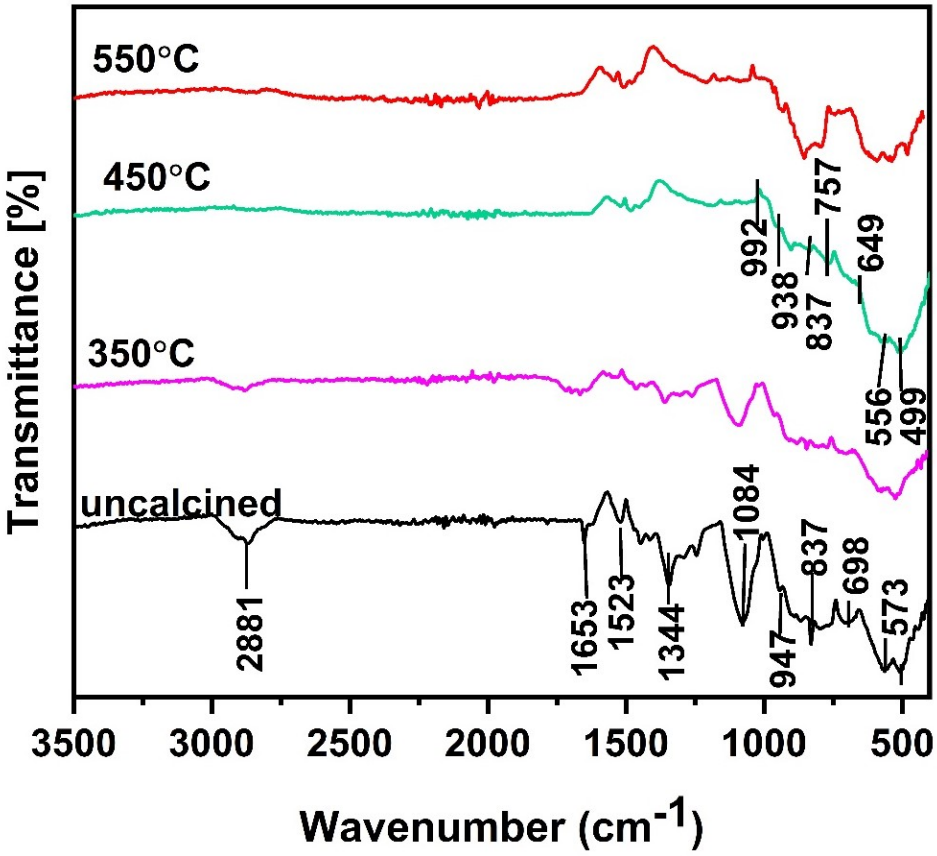

Figure 27: The FTIR spectra for SnO_2-MoO_3 catalyst materials calcined at different temperatures

4.6 Raman Studies

Raman spectroscopy is an invaluable tool for examining the molecular arrangement and surface properties of metals. The physical characteristics of materials are influenced by the vibration modes of oxides and the associated functional groups or bonds they possess. The phases of the oxides and the structural imperfections in the produced catalysts were determined by Raman spectroscopy studies. Figure 28 shows the Raman spectra of pure MoO_3 and SnO_2 oxides. The Raman modes for the MoO_3 crystal can be written as follows:

$$\Gamma = 8A_g+8B_{1g}+4B_{2g}+4B_{3g}+4A_u+3B_{1u}+7B_{2u}+7B_{3u} \quad (5)$$

Whereby, A_g, B_{1g}, B_{2g}, and B_{3g} are Raman active, A_u is inactive, and others are infrared-active modes (Seguin *et al.*, 1995). The modes between 1000 and 600 cm^{-1} belong to MoO_6 octahedral stretching vibrations, while the modes between 400 and 200 cm^{-1} and below 200 cm^{-1} correspond to MoO_6 octahedral bending vibrations (Atuchin *et al.*, 2011; Lupan *et al.*, 2014). The apparent Raman signal at 198 cm^{-1} (A_g, B_{1g}) is due to the translation of the stiff chains. The peak at 348 cm^{-1} (B_{2g}, B_{3g}) is a doublet consisting of the oscillating modes of the terminal oxygen atoms.

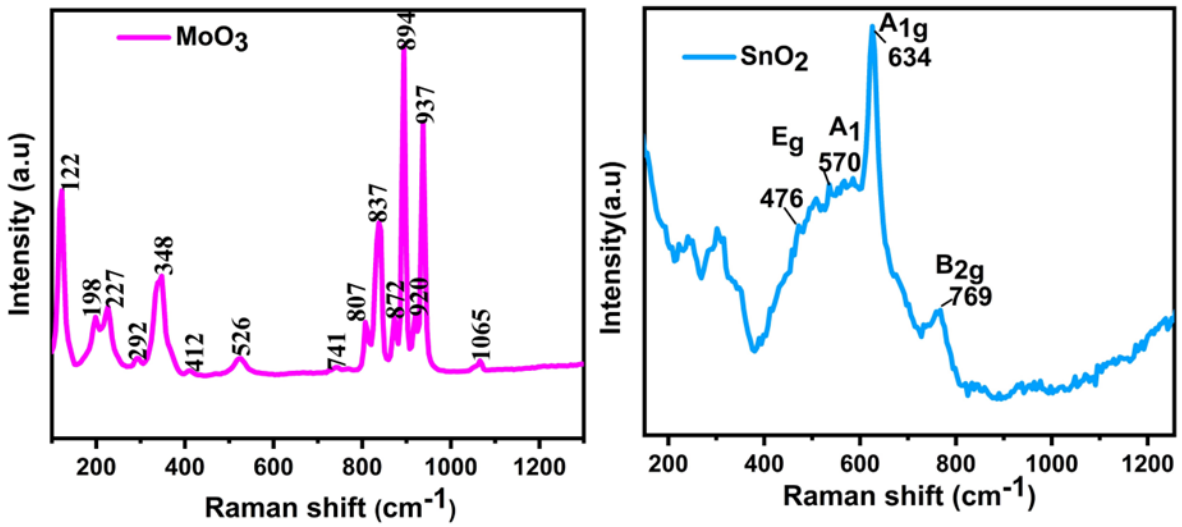

Figure 28: Raman spectra for MoO_3 and SnO_2 pure oxides calcined at 450°C

On the other hand, the two predominant Raman bands at 894 cm^{-1} are stretching modes of Mo-O-Mo in two MoO_6 octahedrons sharing corner oxygen atom, while the 937 cm^{-1} correspond to the Mo=O asymmetric stretching modes of the terminal (unshared) oxygen. These peak assignments agree with the spectra obtained by Gong and Haur (2017), Siciliano *et al.* (2009) and Sivan *et al.* (2019).

The lattice vibration modes of SnO_2 at the Γ point of the Brillouin zone are given as:

$$\Gamma=1A_{1g}+1A_{2g}+2A_{2u}+1B_{1g}+1B_{2g}+2B_{1u}+1E_g+4E_u \quad (6)$$

whereby A_{1g}, B_{2g}, and E_g are Raman active, while A_{2u}, A_{2g}, B_{1g} and B_{1u} are inactive (Guan *et al.*, 2019). The three distinctive peaks of SnO_2, 477 (E_g), 634 (A_{1g}), and 769 (B_{2g}) cm^{-1}, confirm the tetragonal rutile phase structure (D_{4h} point group) as follows (Rajendran *et al.*, 2021): The A_{1g} (634 cm^{-1}) and B_{2g} (769 cm^{-1}) are associated with the expansion and contraction vibration modes of Sn-O bonds, respectively, while the A_1 band at 570 cm^{-1} is said to be connected to the SnO_2 surface oxygen vacancies, whose quantity can affect the development of surface-active oxygen sites (Diéguez *et al.,* 2001; Liu *et al.*, 2012; Rao *et al.*, 2018). In contrast, E_g is associated with the vibration of in-plane oxygen vacancy (Yu *et al.*, 1997). The Raman spectra for SnO_2–MoO_3 catalyst synthesized at different Sn/Mo mole ratio shows the characteristic mode of the SnO_2 catalyst (Fig. 29). The Raman shift of (A_g) and (B_{1g}) is attributed to the stretching vibration of the Mo=O bond and the vibration of the bridging oxygen in the Mo–O–Mo structure of the terminal MoO_3 crystal. The observed changes in the vibration peaks of Mo–O–Mo and Mo=O bonds in the SnO_2–MoO_3 catalysts indicate a significant modification in the interatomic forces between the Mo and O atoms, when compared to the pure MoO_3 crystal. The lower positioning of the Raman band (A1g) in the SnO_2–MoO_3 catalyst, compared

to pure SnO_2, can be attributed to the incorporation of Mo^{6+} cations into the SnO_2 lattice. This doping process results in a contraction of the SnO_2 lattice and an increase in the presence of oxygen vacancies (Mallesham *et al*., 2020). Oxygen vacancy defects, which belong to a category of point defects found in different oxide materials, can have a notable impact on heterogeneous catalysis. Increased SnO_2 concentration in the catalytic system causes a significant interaction between molybdenum oxide and SnO_2, resulting in the transformation of the MoO_3 crystal to an amorphous MoO_3 structure. High SnO_2 concentration in the SnO_2-MoO_3 catalytic materials causes a significant interaction between molybdenum oxide and SnO_2, resulting in the transformation of MoO_3 crystal to an amorphous MoO_3 structure.

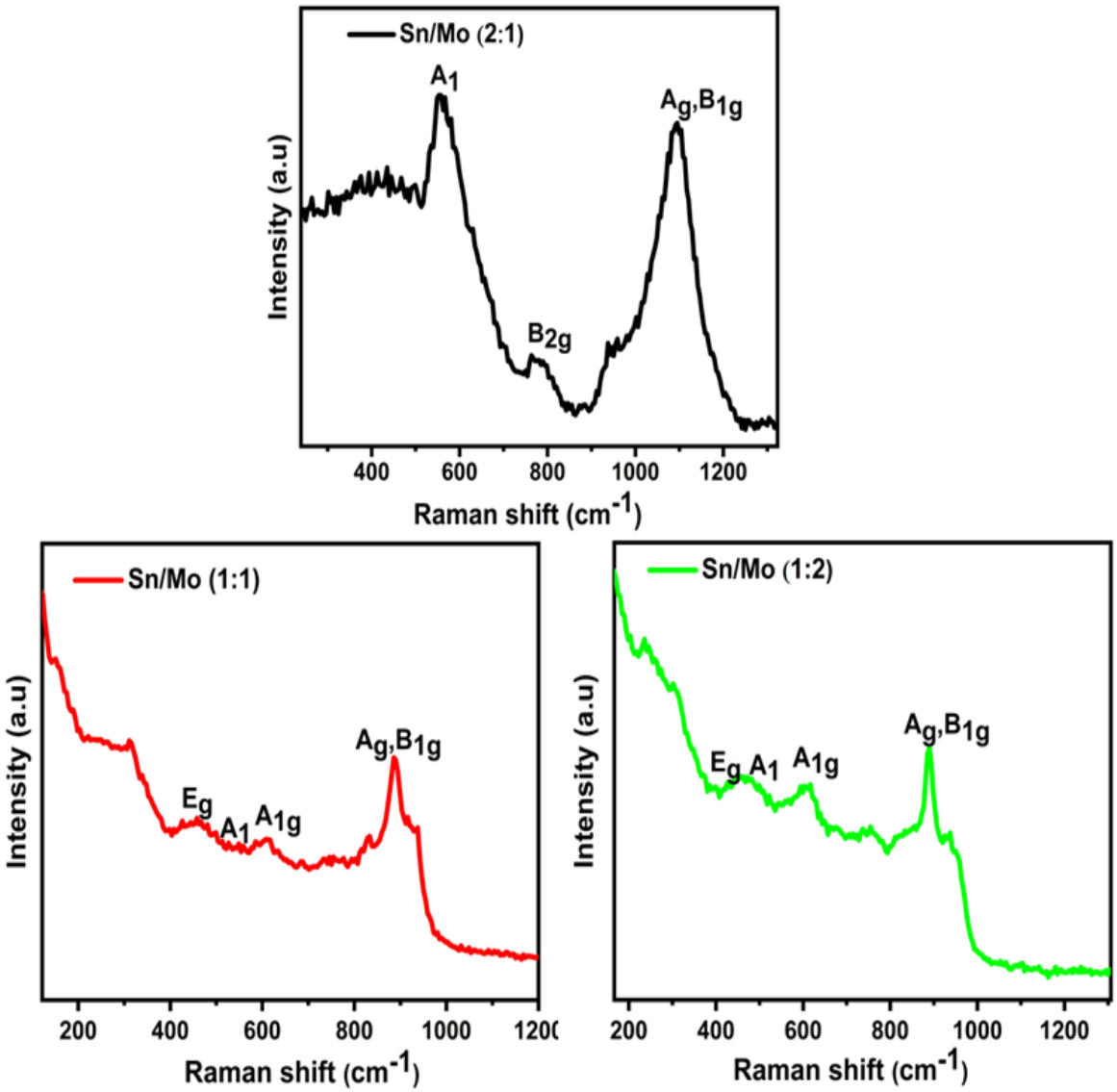

Figure 29: Raman spectra for SnO_2-MoO_3 catalyst materials at different Sn/Mo mole ratios Sn/Mo (1:2), Sn/Mo (1:1) and Sn/Mo (2:1) calcined at 450°C

In conjunction with the XRD results, (Fig. 17) indicates that varying the Sn/Mo mole ratio promotes the transformation of MoO_3 crystal into amorphous MoO_3. The MoO_3 dispersion

improves the reaction performance of the catalyst for DBT oxidation to DBTO2 because the SnO_2 catalyst active sites are widely distributed.

4.7 Acidity Measurement

A solid catalyst's surface acidity and basicity are crucial factors that affect its activity. The surface properties were examined by titration following a displacement reaction in which the adhering free OH and H+ on the solid catalyst were treated with acidic and basic species to neutralize and displace from the surface via protonation. The surface acidity and combined measurement of the strong and weak acidic group were calculated using the formula by Benak *et al.* (2002) and Gong *et al.* (2017). Table 7 displays the acid site densities computed by neutralizing ion-exchange techniques for pure and mixed oxides at different mole ratio. The SnO_2–MoO_3 catalyst with mole ratio Sn/Mo (2:1) exhibited better density acid sites (49.7 mEq g^{-1}) compared to (41.3 $mEqg^{-1}$) for pure MoO_3, (41.5 $mEqg^{-1}$) for pure SnO_2, (46.7 $mEqg^{-1}$) for Sn/Mo (1:1) and (46.7 $mEqg^{-1}$) for Sn/Mo (1:2). The acid sites are related to surface tin cations and decrease rapidly with increasing molybdenum cations.

Table 7: Calculated acid site densities using the titration method

Material calcined at 450 °C	Strong acid site density ($mEqg^{-1}$)	Moderate acid site density ($mEqg^{-1}$)	Total acid site density ($mEqg^{-1}$)
SnO_2	0.1	41.4	41.5
MoO_3	0.9	40.4	41.3
Sn/Mo (1:1)	0.45	46.9	47.4
Sn/Mo (1:2)	0.35	46.3	46.7
Sn/Mo (2:1)	0.15	49.1	49.3

4.8 Catalytic Activity Evaluation

The catalytic activity of the prepared tin –molybdenum mixed metal oxide catalyst was studied in terms of the conversion. The activity was studied by considering the effect of calcination temperature and the mole ratio of the prepared materials**,** as well as other factors such as reaction temperature, oxidant ratio and so on.

4.8.1 Effect of Calcination Temperature on the ODS of DBT

The performance of a catalyst can be understood by examining the level of conversion achieved for a specific reactant. A catalyst's activity for a particular reaction is considered higher when

it attains greater conversion under given conditions. By measuring the contents of DBT (dibenzothiophene) at various reaction conditions, the conversion efficiency η was determined, as explained in the provided description 3.4.1. The pretreatment conditions greatly influenced the materials' catalytic activity, as reported by Wang *et al.* (2021) and Bi *et al.* (2021). The oxidative desulfurization performance of the SnO_2-MoO_3 catalyst materials prepared at different calcination temperatures was examined. The catalytic performance of the SnO_2-MoO_3 was greatly enhanced as the calcination temperature was increased from 250 to 450°C (Fig. 30) and monotonically decreased beyond 450°C. As the calcination temperature increased, the XRD analysis presented in Fig. 16 indicated that the peak intensities of both SnO_2 and MoO_3 exhibited varying patterns of increase and decrease. This implies that the SnO_2–MoO_3 catalyst crystallinity is affected by calcination temperature, as reported by Zhang *et al.* (2022). Moreover, elevated calcination temperatures induce a transformation in the crystalline structure of MoO_3 from hexagonal to orthorhombic, which is unfavourable since the hexagonal phase demonstrates superior catalytic activity. The SEM analysis presented in Figure 18 illustrates the impact of calcination temperature on the morphology of the sample. At lower calcination temperatures, a rough surface is observed, whereas at 450°C, a nanobelt structure is evident. The weak/moderate site of the catalyst, as in Table 7, is responsible for this catalytic activity. The catalysts synthesized at a calcination temperature of 450°C exhibited the highest conversion rate of 96% within a 60-minute timeframe, suggesting that 450°C was the most favorable calcination temperature. Calcination temperatures exceeding 450°C resulted in a reduction in the BET surface area, pore size, and volume of the catalyst, as well as distortions in the surface structure. These changes negatively affected the catalyst's performance (Luo *et al.*, 2019). Consequently, the SnO_2-MoO_3 sample that underwent calcination at 450°C was selected for subsequent experiments.

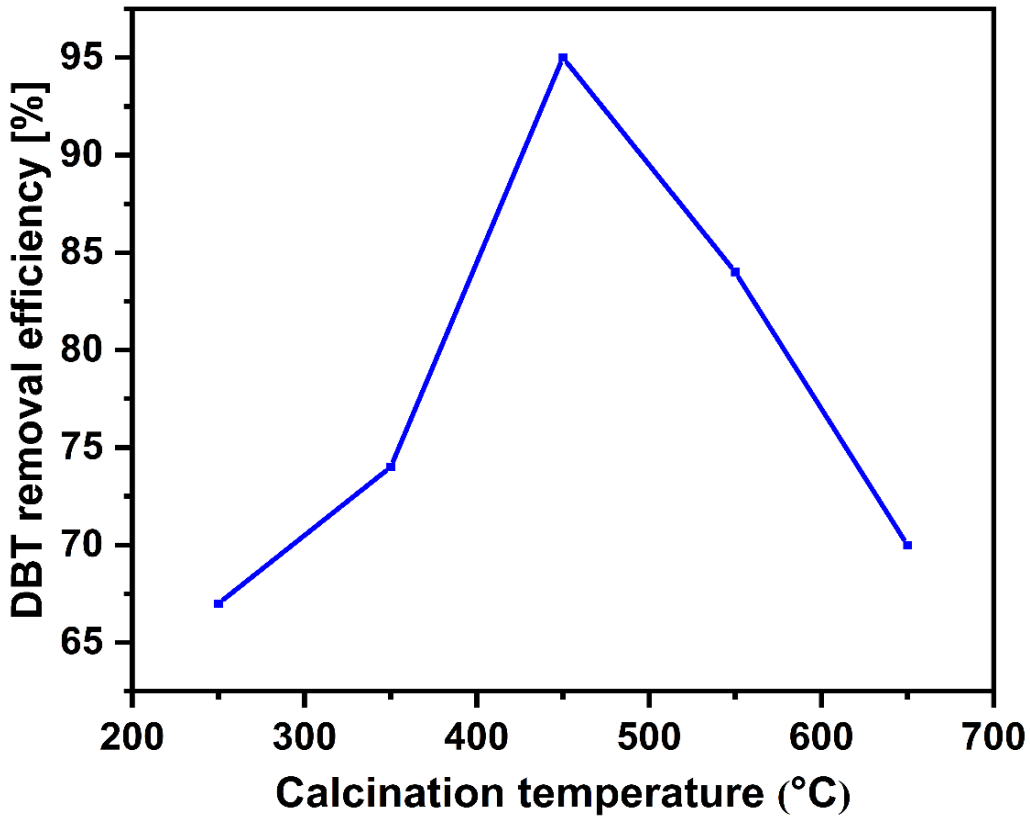

Figure 30: Effect of SnO_2-MoO_3 catalyst calcination temperature on the oxidative DBT removal efficiency η. The ODS reaction conditions: catalyst dosage 100 mg, temperature 50 °C, O/S molar ratio 5; reaction time 60 min

4.8.2 Other Factors Influencing the Catalytic Activity of the SnO_2-MoO_3

In addition to the calcination temperature, the catalytic activity of the SnO_2-MoO_3 catalyst was investigated by evaluating four factors: catalyst loading, reaction time, oxidant/sulfur ratio, and reaction temperature.

Optimization of catalyst loads is an efficient strategy to improve desulfurization efficiency. Figure 31 shows the DBT removal efficiency rose from 81.0 to 99.6% when the dosage increased from 40 to 100 mg and reduced to 95% when the dosage was further increased from 100 mg to 180 mg. The enhancement in removal efficiency, observed with catalyst dosages of up to 100 mg, can be attributed to the increased number of active sites in the reaction system. However, beyond 100 mg, the removal efficiency (η) diminishes, likely due to catalyst aggregation, resulting in a decrease in active sites and surface area and, consequently, reduced interaction between the catalyst and DBT (Cao *et al.*, 2020). Hence, the optimum catalyst dosage was determined to be 100 mg.

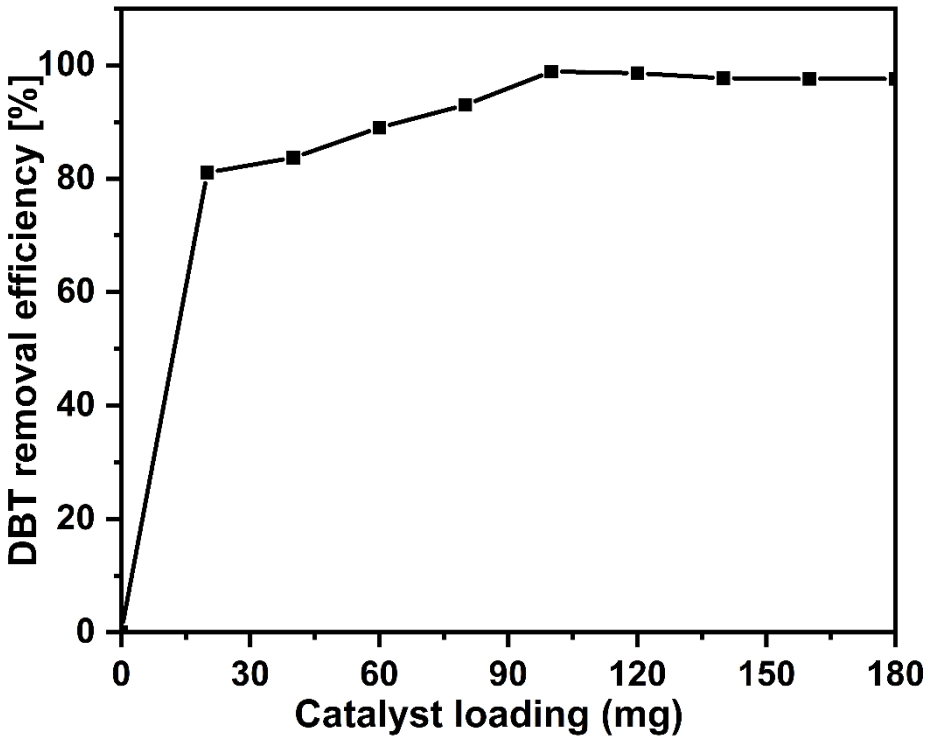

Figure 31: DBT removal efficiency in oxidative desulfurization versus varying catalyst loading: Reaction conditions when fixed: O/S = 5, T =60 °C, t = 60 min

Considering economic considerations, the reaction time is considered a crucial factor in both catalytic and industrial processes. Remarkably, a DBT conversion rate of 83% was achieved within the 30-minute reaction time (Fig. 32). The removal efficiency increased to 99.6% when the time for the reaction increased to 60 min.

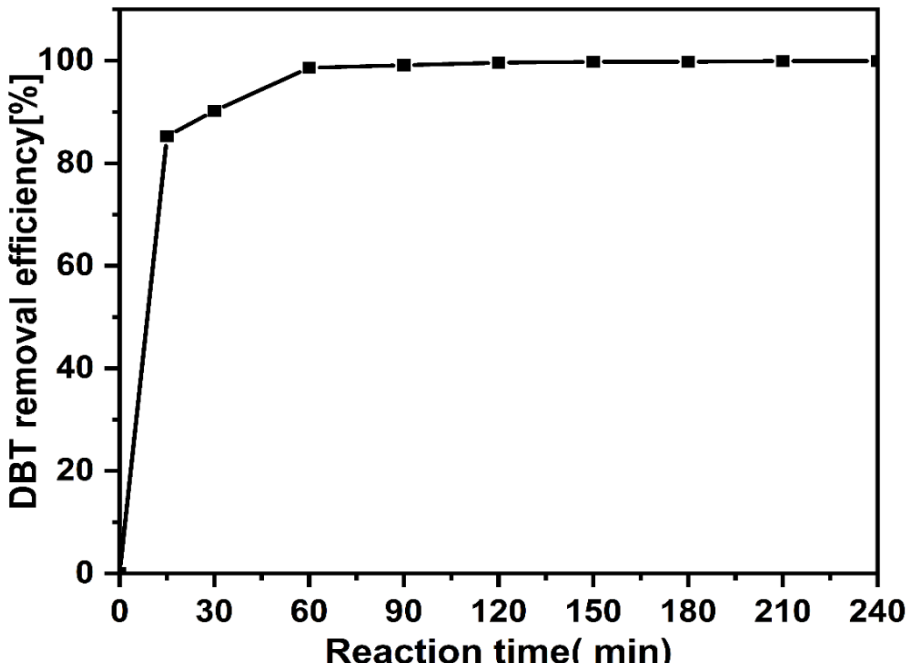

Figure 32: The DBT removal efficiency in oxidative desulfurization at different reaction time: Reaction conditions when fixed: O/S = 5, catalyst load= 100 mg, T= 60°C

The steep incline observed in the graph corresponds to the region where the reaction rate is directly proportional to time. However, when the reaction time surpassed 60 minutes, the DBT conversion reached a plateau, suggesting that the catalyst's active sites became saturated.

The effect of the O/S amount was investigated, as illustrated in (Fig. 33). By altering the O/S molar ratio in the range of 2:1, 3:1, 4:1, and 5:1, the conversion of DBT was influenced. With an O/S ratio of 5:1, the removal efficiency (η) reached 98.6% within a 60-minute timeframe. However, when the O/S ratio exceeded 5:1, the removal efficiency decreased to 94%. The diffusion of H_2O_2 regulates the reaction rate, increasing the quantity of H_2O_2 to speed up the oxidation of DBT (Haw *et al.*, 2010). An excessive amount of oxidant facilitates the oxidation reaction, but it can also lead to the thermal decomposition of the oxidant, resulting in the formation of water, inhibiting the ODS reactions (Caero *et al.,* 2005; Ghubayra *et al.*, 2019; Zhuang *et al.*, 2014). Therefore, the optimal O/S ratio was determined to be 5:1. Furthermore, a control experiment conducted without the catalyst resulted in a DBT elimination efficiency of 15%, indicating that the selectivity of H_2O_2 is low in the absence of a catalyst.

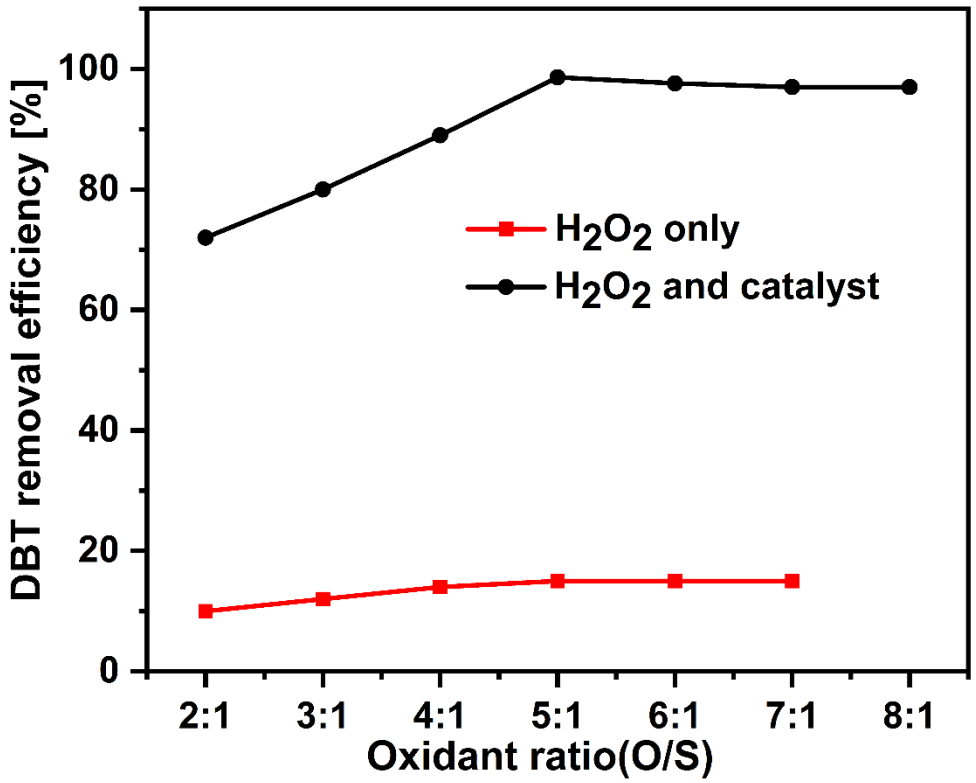

Figure 33: Different oxidant/sulfur ratio (O/S) for DBT removal efficiency in oxidative desulfurization. Reaction conditions when fixed: T = 60 °C, catalyst dosage 100 mg, t = 60 min

The reaction temperature is a vital factor in ODS and other industrial processes. Figure 34 depicts the impact of different temperatures, ranging from 30 to 70°C, on the ODS removal. The reaction time was kept constant at 60 minutes. The removal efficiency *(η)* and kinetic rate

constant (k) depend on temperature. The ODS increased substantially from 72.0 to 99.6% when the temperature increased from 30 to 60°C. Beyond 60°C, there was a notable decrease in DBT removal efficiency. The rise in DBT removal efficiency with increasing temperature can be attributed to the exothermic nature of the desulfurization reaction. This indicates that molecular mobility increases with temperature, leading to a greater number and higher energy collisions between reactants (Zuo *et al.*, 2019). Nevertheless, when the temperature surpasses 60°C, thermal decomposition occurs in peroxide complexes. As a result, the formation of active oxygen species on the catalyst's surface decreases, as reported by González *et al.* (2016) and Huang *et al.* (2020).

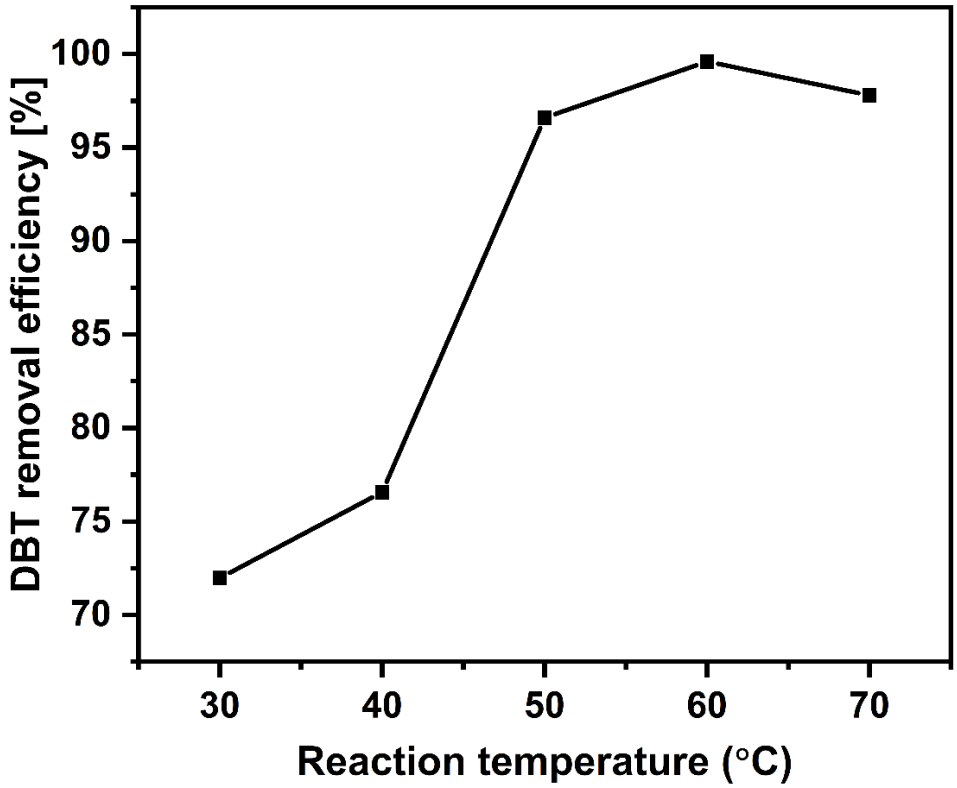

Figure 34: DBT removal efficiency in oxidative desulfurization versus reaction temperature. Reaction conditions when fixed: O/S = 5, catalyst dosage = 100 mg, t = 60 min

4.8.3 Effects of the Mole Ratios of Sn and Mo on ODS

Catalysts with varying mole ratios comprised different active site species, which influenced the acidity distribution on the catalyst surface and improved the synergistic effect, enabling the catalysts to achieve the highest possible efficiency in the reaction. Figure 35 shows the dibenzothiophene conversion using tin molybdenum catalyst with different mole ratio.

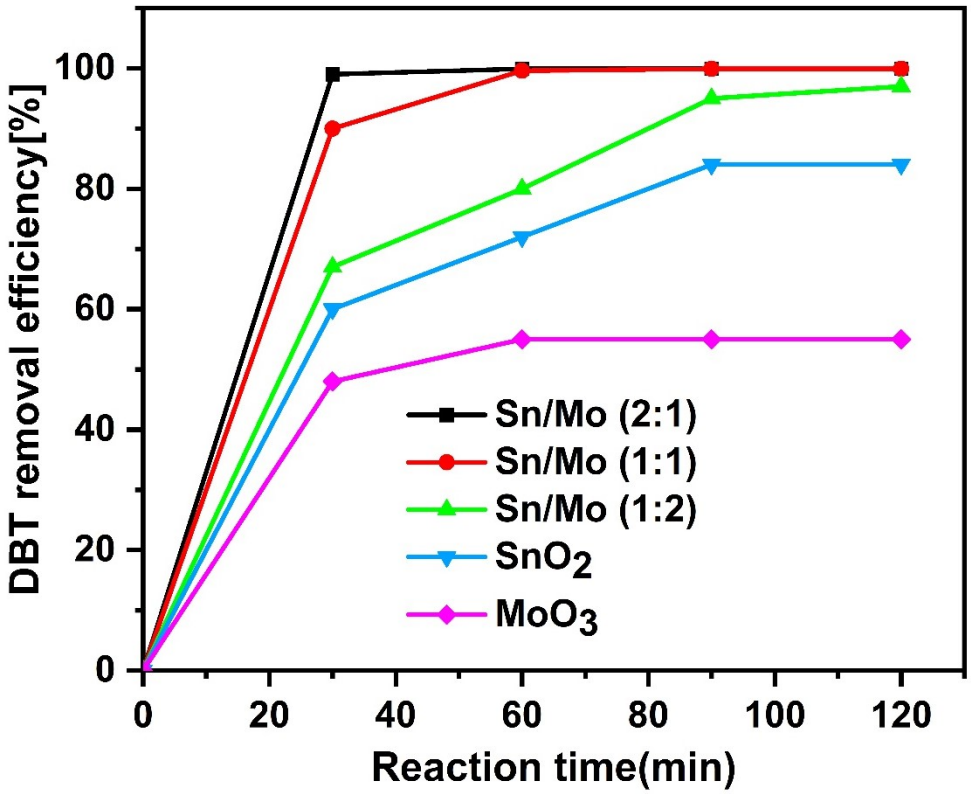

Figure 35: The DBT removal efficiency against reaction time for the SnO_2-MoO_3 catalyst with varying Sn/Mo mole ratios. Reaction conditions; 20 mL model diesel, O/S ratio 5, reaction temperature 60°C, catalyst weight 100 mg

The DBT conversion efficiency η for the catalyst Sn/Mo (2:1) was around 99.8% after 30 minutes of reaction, whereas for Sn/Mo (1:2) and Sn/Mo(1: 1), they approached 100% after 90 and 60 minutes, respectively. Over time, the removal efficiency increased and stayed consistent, demonstrating that all catalysts had ODS catalytic potential. At the same time, the DBT conversion with pure SnO_2 and MoO_3 were approximately 80% and 50 %, respectively, after 120 min.

According to the literature, when the pH of the synthesis condition is in the range of 0.8 < pH <2.0, MoO_3 will acquire a negative charge and react with Sn^{4+} to form Mo–O–Sn. The Sn^{4+} cations occupy part of the Brønsted acid sites, thus increasing Lewis's acid sites (Cao *et al.,* 2019; Gavrilova *et al.,* 2021). The remote-control theory (Delmon & Ruiz, 1987) is an alternative explanation for the synergistic effect of binary metal oxide phases in contact during oxidation processes. The theory states that the catalyst comprises two well-defined oxide phases which are acceptor and donor phases. The acceptor phase is the center for catalytic activation and has poor catalytic activity for the selective oxidation reaction when isolated; while the donor phase has no selective oxidation activity, and its job is to produce large amounts of activated oxygen, which spills over into the acceptor phase and speeds up the catalytic reaction. In our case, SnO_2 is the donor phase, and MoO_3 is the acceptor phase. Due

to its highest activity, the catalyst with composition Sn/Mo (2:1) was used for further reaction testing.

4.8.4 Reaction with other Sulfur Compounds

Dibenzothiophene, benzothiophene and thiophene were organic sulfides used in this work using the same reaction conditions as the one used in DBT. The reactivity of organic sulfide compounds depends on the electron density of the sulfur atom present in the compound. The electron density on the S atom increases in the order Th < BT <DBT, which explains the higher DBT and BT reactivity than Th (Otsuki *et al.*, 2000). Hence the oxidation reactivity increases concerning the electronic density of sulfur (Fig. 36). The same trend has also been observed in homogeneous and other heterogeneous systems (Jiang *et al.*, 2009; Liu *et al.,* 2019; Zhang *et al.*, 2011).

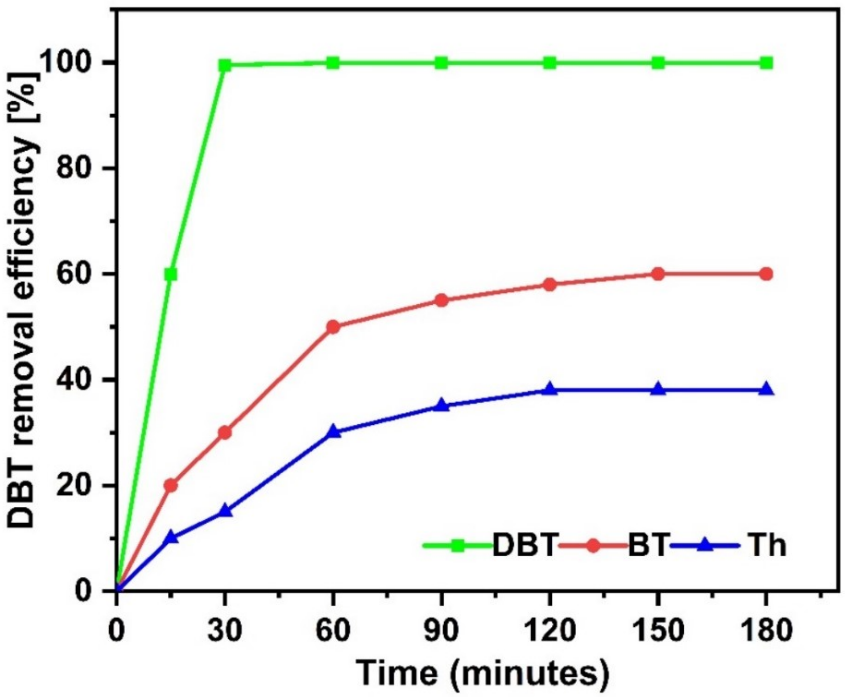

Figure 36: The ODS of different sulfur compounds; Reaction conditions: m(catalyst) = 100 mg; O/(S) = 5; reaction temperature 60°C

4.8.5 Effect of DBT Initial Concentration

Because the sulfur content of fuels varies depending on the region where the crude is mined, it's crucial to investigate the impact of sulfur levels in the treated fuel. Different model fuels were constructed for this purpose, each with different content of DBT, ranging from 250 to 2000 ppm. The amount of oxidant, catalyst (0.1g), and temperature (60°C) were all constant when desulfurizing these model fuels.

Figure 37 shows that increasing initial sulfur content reduces the ODS system's effectiveness. Complete desulfurization was achieved after 30 minutes using model fuel treated with 250 ppm DBT, compared to 15 % using model fuel treated with 2000 ppm DBT. The modest decrease in desulfurization efficiency could be due to the high concentration of sulfone and sulfoxide molecules in the reaction medium, which causes saturation on the solid catalyst surface, blocking easy access to the active sites.

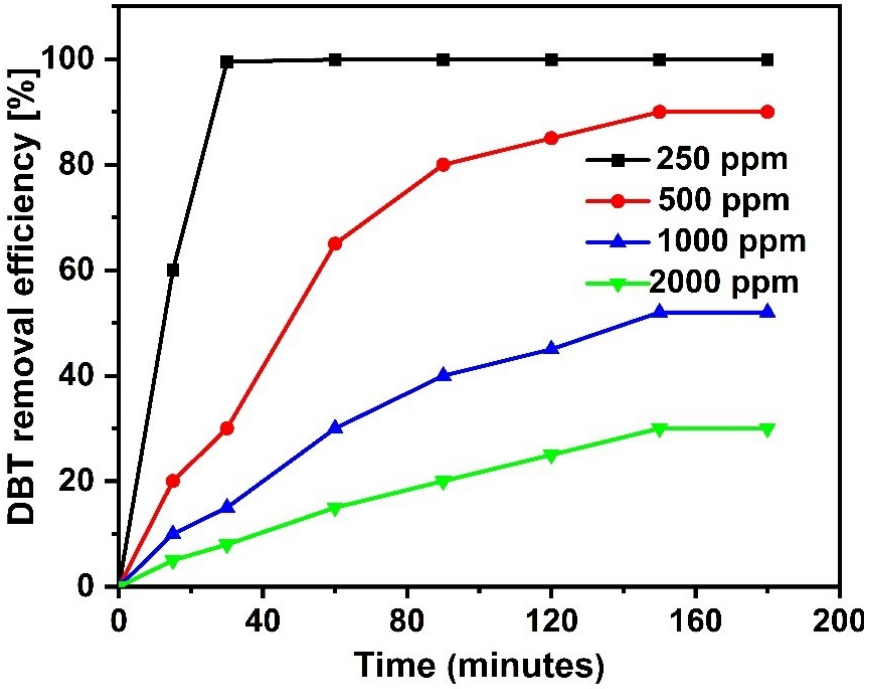

Figure 37: Effect of initial DBT concentration. Reaction conditions: reaction temperature 60 °C, O/S molar ratio 5:1, 100 mg of SnMo–2:1 catalyst, the volume of model diesel 20 mL

4.9 Kinetics of the ODS Reaction

The ODS reaction kinetics allows for the prediction of the ODS rate at various temperatures and reaction times, as depicted in Fig. 38. The rate equation serves to demonstrate the relationship between concentration and reaction time. The kinetics of dibenzothiophene oxidation was investigated at temperatures ranging from 30 to 70°C.

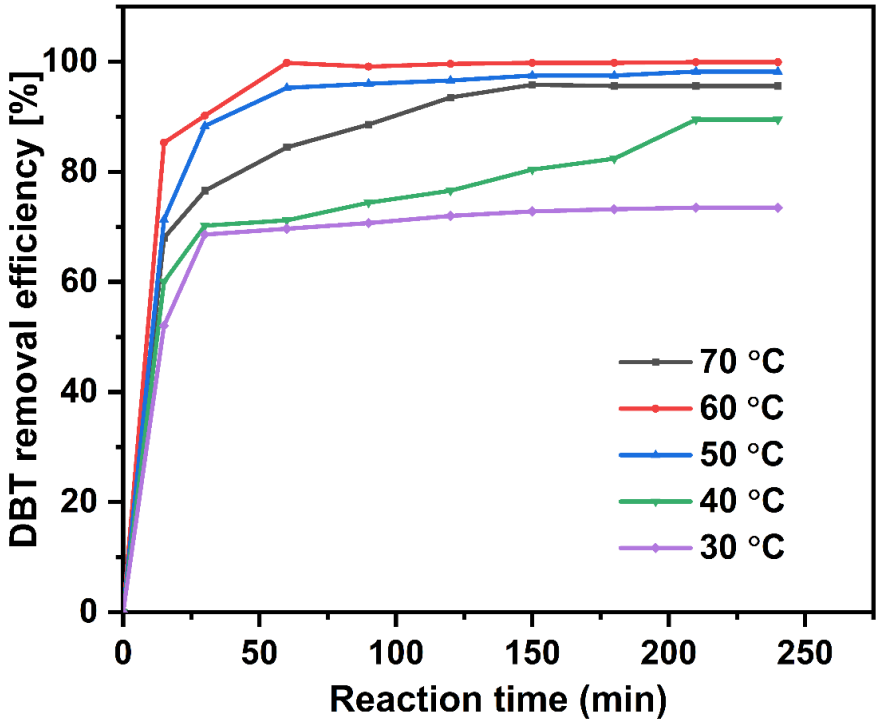

Figure 38: The DBT removal efficiency versus reaction time and temperature. Reaction conditions: 100 mg catalyst, 20 mL of model diesel, O/S molar ratio of 5

Interfacial mass transfer between liquids controls the process for biphasic media, increasing the reaction time and reducing yield (Boltes *et al.*, 2013). The ratio of reagents, stirring speed, surfactant and its content, treatment ratio, and volume ratio of membrane phase to internal phase affect the mass transfer rate (Ma & Shi, 1987). External mass transfer effects are insignificant at stirring speeds of more than 900 rpm because the overall area of mass transfer in the system increases while the size and stability of emulsion globules decrease (Jose *et al.,* 2011; Sengupta *et al.*, 2012). This ODS reaction was kinetically controlled by running it at a stirrer speed (1000 rpm) to reduce the impact of external mass transfer resistance. The Langmuir-Hinshelwood mechanism provide an insight into how the reaction proceeds and allows for the identification/determination of the rate law for a heterogeneous solid catalytic fluid phase reaction (Chamack *et al.*, 2015; Sengupta *et al.,* 2012). The mechanism occurs through adsorption, surface reaction and desorption from the catalyst surface (Fogler, 2020; Olutoye & Hameed, 2016). It includes a liquid phase reaction on a catalyst's surface. The mechanism comprises two critical steps if the catalyst's surface does not absorb the n-heptane solvent. As illustrated in Equation (7), the first step is the equilibrated adsorption of DBT on the catalyst's surface:

$$DBT + * \rightleftharpoons DBT \cdot * \qquad (7)$$

Whereby, * is the active catalyst site.

For adsorbed species, the surface coverage θ_A Is given by the Langmuir adsorption isotherm (Satterfield, 1991):

$$\theta_A = \frac{KC_A}{1 + KC_A} \tag{8}$$

The second stage is the formation of DBTO2 through the reaction of the adsorbed species:

$$\mathrm{DBT}\cdot * + H_2O_2 \longrightarrow \mathrm{DBTO2}\cdot * + H_2O \cdot * \tag{9}$$

Since H_2O_2 is abundant, it is assumed that the reaction is proportional to the amount of adsorbed DBT molecules, θ_A. For a reactor with a volume of V and a catalyst mass of $\boldsymbol{m}_{\mathrm{cat}}$, the reaction rate per unit volume can be expressed as follows:

$$-r_A = \frac{m_{cat}\, k_L\, \theta_A}{V} \tag{10}$$

where $\boldsymbol{k}_{\mathrm{L}}$ has units mol $(\mathrm{mass_{cat}time})^{-1}$. Combining equations (8) and (10)

$$-r_A = -\frac{dC_A}{dt} = \frac{m_{cat}}{V} k_L \frac{KC_A}{1 + KC_A} \tag{11}$$

Equation (11) depicting the Langmuir adsorption isotherm and first-order kinetics of the adsorbed species is called the Langmuir-Hinshelwood kinetic model (Satterfield, 1991). The adsorption coefficient *K* is inversely related to temperature:

$$K = Aexp\left(-\frac{\triangle H_{ads}}{RT}\right) \tag{12}$$

As a result, $\boldsymbol{KC}_{\mathrm{A}}$ becomes less than unity at higher temperatures, and Equation (12) becomes a first-order reaction. When Equation (11) is separated and integrated, it becomes:

$$(C_{Ao} - C_A) + \frac{1}{K} ln\left(\frac{C_{Ao}}{C_A}\right) = \frac{k_L\, m_{cat}}{V} t \tag{13}$$

$\mathrm{DBT} + * \underset{kdes}{\overset{kads}{\longleftrightarrow}} \mathrm{DBT}\square$ ble adsorption) (14)

$\mathrm{DBT}\square \xrightarrow{k2} \mathrm{DBTO2} + *$ (surface reaction - rate determining step) (15)

$$DBT + H_2O_2 \xrightarrow{k} DBTO2 + H_2O \text{ (overall reaction)} \quad (16)$$

where k_{ads}, k_{des}, and k_2 refer to the rate constants for adsorption, desorption, and surface reaction, respectively. It shows that during the reaction, species DBT is reversibly adsorbed onto the solid catalyst to produce species DBT· ∗, which subsequently, in a rate-determining step, leads to product formation from DBT· ∗ species; thus, the reaction rate (r) can be expressed as

$$r = k_2 [DBT \cdot *] \quad (17)$$

and the steady-state approximation:

$$-\frac{d[DBT \cdot *]}{dt} = 0 = k_{ads}[DBT][*] - k_{des}[DBT \cdot *] - k_2[DBT \cdot *] \quad (18)$$

The concentration of reactive intermediate is obtained by solving Equation (18) simultaneously

$$[DBT \cdot *] = \frac{k_{ads}[DBT][*]}{k_{des} + k_2} \quad (19)$$

We can define the apparent rate constant as:

$$k = \frac{k_2 k_{des}[*]}{k_{des} + k_2} \quad (20)$$

Hence Equation (17) can be simplified as follows:

$$r = k[DBT] = k[C] \quad (21)$$

Equation (21) can also be written as

$$-\frac{\boldsymbol{d[C]}}{\boldsymbol{dt}} = \boldsymbol{k[C]} \quad (22)$$

When integrating both sides of Equation (22) becomes;

$$\mathbf{ln}\left(\frac{\mathbf{C_o}}{\mathbf{C_t}}\right) = \mathbf{kt} \quad (23)$$

Therefore, the dibenzothiophene oxidation reaction is assumed to be a pseudo-first-order reaction. Figure 39 displays a plot of ln (Co/Ct) against time, demonstrating straight lines at

different temperatures, confirming the pseudo-first-order reaction kinetics. The relationship between the reaction temperature and the rate constant (k) is direct, suggesting that raising the temperature of the reaction reduces the overall resistance (Dizaji *et al.,* 2019). When reflecting the effect of temperature, the rate constant ***k*** from Equation (21) can be expressed by the Arrhenius formula:

$$k = Ae^{-\frac{E_a}{RT}} \tag{24}$$

Whereby, T= temperature of reaction (K), E_a = Energy of activation (kJ mol^{-1}), R = universal gas constant (Jmol^{-1}K^{-1}), A = frequency factor (min^{-1}).

Introducing natural logarithm on Equation (24), we get:

$$ln\ k = ln\ A - \frac{E_a}{RT} \tag{25}$$

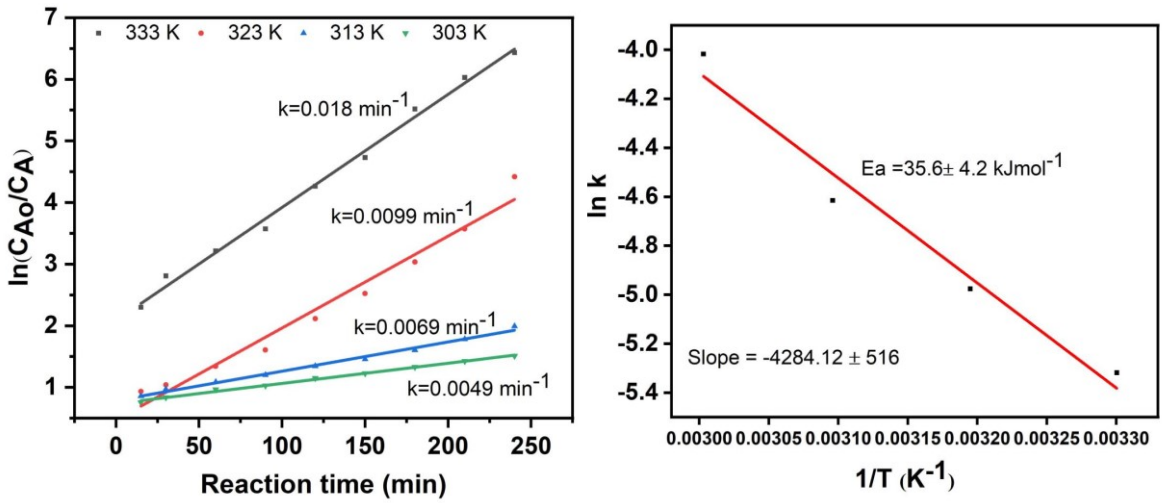

Figure 39: Pseudo-first-order model for the DBT desulfurization and Arrhenius Equation plot

The plot ln*k* against 1/T represents a linear line as presented in Fig. 39, the value of activation energy was established from the slope by Equation (25), and it was found to be 35.6 ± 4.2 kJmol^{-1}. The activation energy provides insight into the level of difficulty involved in a reaction, with higher activation energy indicating a need for higher reaction temperatures for oxidation reactions. In the case of DBT oxidation on the SnO_2-MoO_3 catalyst, the activation energy is moderate, suggesting that the oxidative desulfurization process is relatively easier to carry out. This indicates that the designed SnO_2-MoO_3 catalyst holds potential for industrial

applications. Additionally, the rate constant can be determined by analyzing the relationship between time and concentration in a given process.

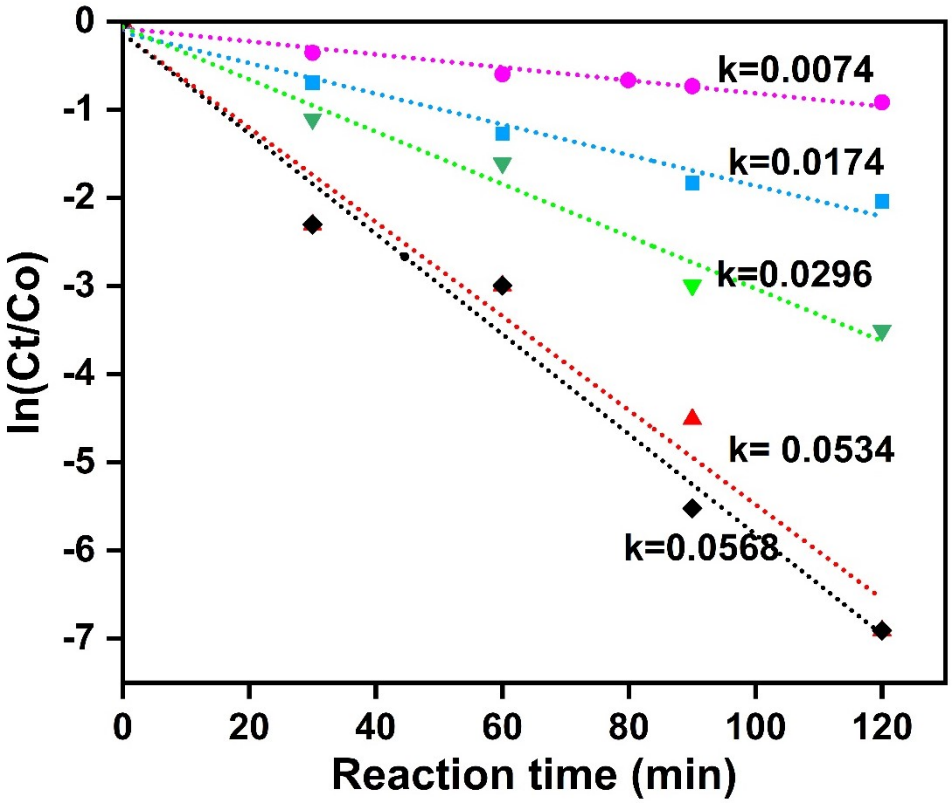

Figure: 40 **A plot of ln (C_t/C_o) against reaction time for the SnO_2-MoO_3 catalysts with varying Sn/Mo mole ratios. Reaction conditions; 20 mL model diesel, O/S ratio 5, reaction temperature 60 °C, catalyst weight 100 mg**

The pseudo-first-order kinetic model calculates rate constants (Teimouri *et al.*, 2018; Zhu *et al.*, 2013). Substituting C_t by $C_o/2$ equation (23) becomes:

$$t_{1/2} = {}^{0.693}/_{k} \qquad (26)$$

The C_o and C_t are concentrations at time zero, t, ***k*** is the rate constant of pseudo-first order (min^{-1}), and $t_{1/2}$ is the half-life of the compounds. Figure 40, demonstrates a linear relationship between ln(Ct/Co) and reaction time (t) derived from various Sn/Mo catalyst mole ratio. The ODS reaction is consistent with the pseudo-first-order model, which displays the ***k*** values for various catalysts. The ***k*** values diminish in the order of Sn/Mo (2:1), > Sn/Mo (1:1) > Sn/Mo (1:2) > pure SnO_2 > pure MoO_3. The maximum ***k*** value of Sn/Mo (2:1) is 0.057 min^{-1} which is higher than pure SnO_2 (0.017 min^{-1}) and MoO_3 (0.007 min^{-1}). These findings confirm the synergy between SnO_2 and MoO_3, promoting ODS efficiency.

4.10 Characterization of the Oxidation Product

Figure 41 presents the solid-state FT-IR spectrum of the residual solid generated during the oxidation of dibenzothiophene. This analysis aids in identifying the type of sulfur oxidation product formed. The prominent absorptions observed at 1288 and 1165 cm^{-1} corresponded to the symmetrical and asymmetrical stretching vibrations of O←S→O in DBTO2, respectively, that confirm the presence of dibenzothiophene sulfone in the sample. Results similar to this were also reported by Chamack *et al.* (2015), Teimouri *et al.* (2018) and Tu *et al.* (2019).

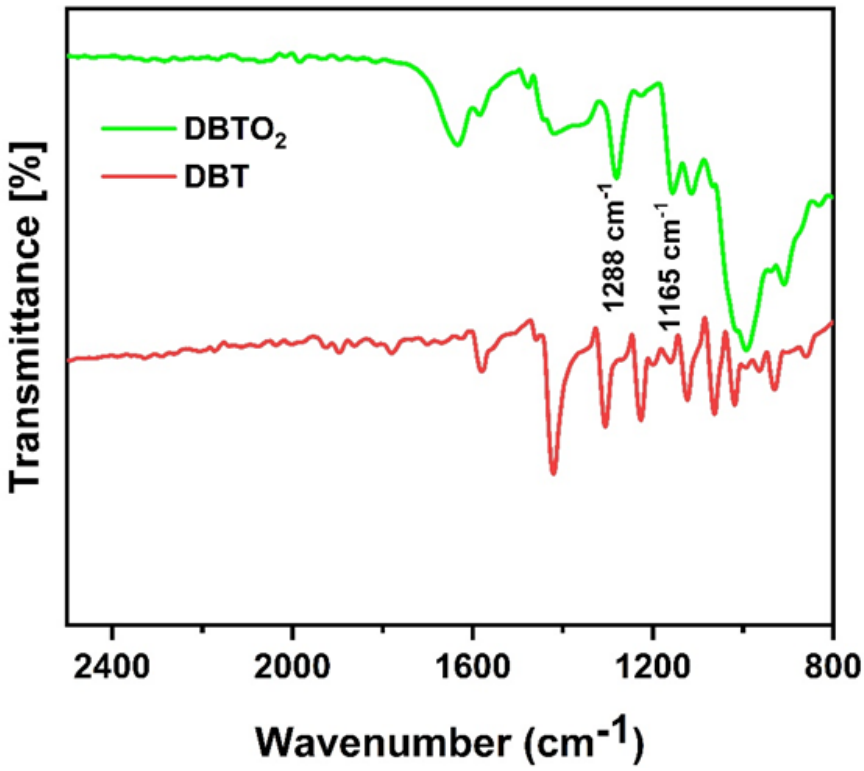

Figure 41: The FT-IR spectra of dibenzothiophene and corresponding sulfone

4.11 Catalyst reusability

The reusability of SnO_2-MoO_3 catalysts is crucial in industrial applications. Hence experiments were conducted to assess the catalysts' reusability under optimal conditions. Following the initial reaction run, the catalyst underwent centrifugation, followed by two washes with ethanol and drying at 80°C for 5 hours. Over subsequent runs, the efficacy of the catalyst in oxidizing DBT to DBT sulfone was slightly lower compared to the fresh catalyst, as indicated in (Fig. 42). The findings indicate that SnO_2-MoO_3 catalysts can be recycled up to five times for deep desulfurization. The gradual decrease in DBT conversion observed after each cycle may be attributed, at least in part, to the accumulation of DBTO2 on the catalyst surface, which can potentially block active sites (Ding *et al.,* 2011), and partly due to catalyst loss during washing.

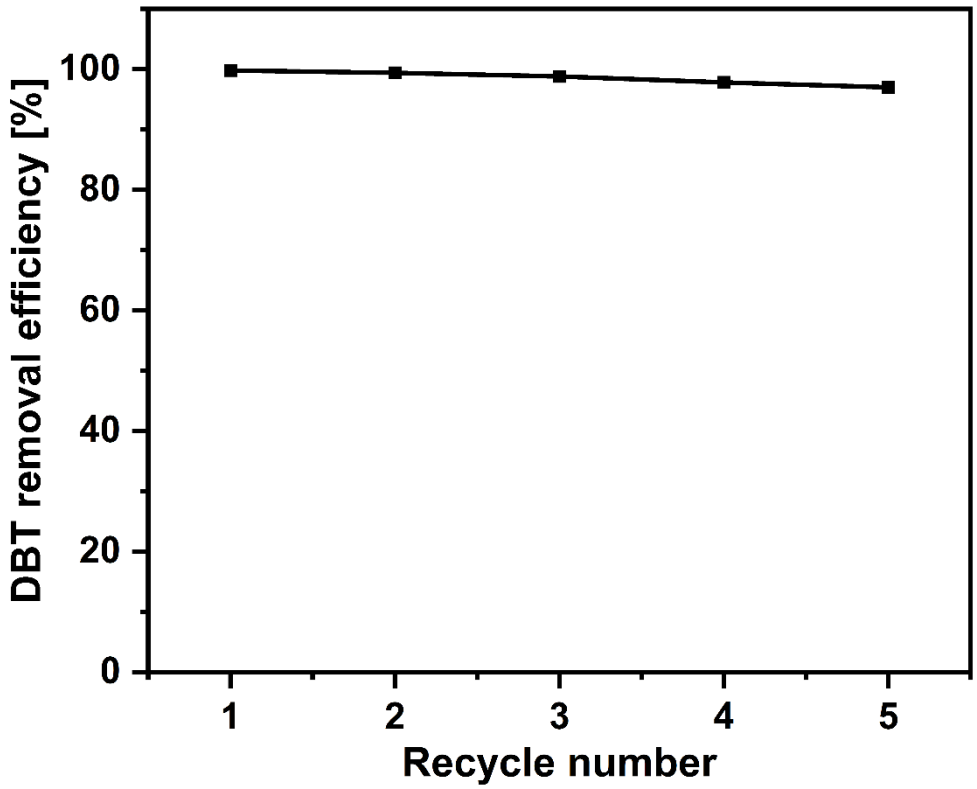

Figure 42: Catalyst recyclability under optimal ODS conditions

4.12 Proposed Mechanism of ODS of DBT in Model oil

Sulfur compounds are normally desulfurized oxidatively via simultaneous extraction and oxidation (Bernal & Caero, 2005). The reaction media contain two immiscible phases: an organic phase composed of heptane and dibenzothiophene and an aqueous phase composed of hydrogen peroxide, acetonitrile, and catalyst (Albayrak & Tavman, 2022; Mamaghani *et al.*, 2013). A series of tests were performed in Fig. 43 to evaluate the interaction between the oxidant and catalyst in our study's oxidation of DBT using SnO2-MoO3 catalyst materials. When acetonitrile and model diesel were used, there was 10% DBT removal due to liquid-liquid extraction processes (Verduzco *et al.*, 2004). When H_2O_2 or SnO_2-MoO_3 are added to the process alone, the removal efficiency is only 15% and 36%, respectively. This indicates that the catalyst and oxidant are essential in the reaction and that DBT can slightly be removed by adsorption function on the SnO_2-MoO_3 surface. Hence for DBT oxidation to occur, it needs both a catalyst and oxidant (Tharindu *et al.*, 2020; Yazu *et al.*, 2001) and in this work, 99.8% was removed when SnO_2-MoO_3 catalyst in the presence of hydrogen peroxide as an oxidant was used. According to González *et al.* (2018), oxygen vacancies and the acidity of the catalysts have a direct relationship with ODS capacity.

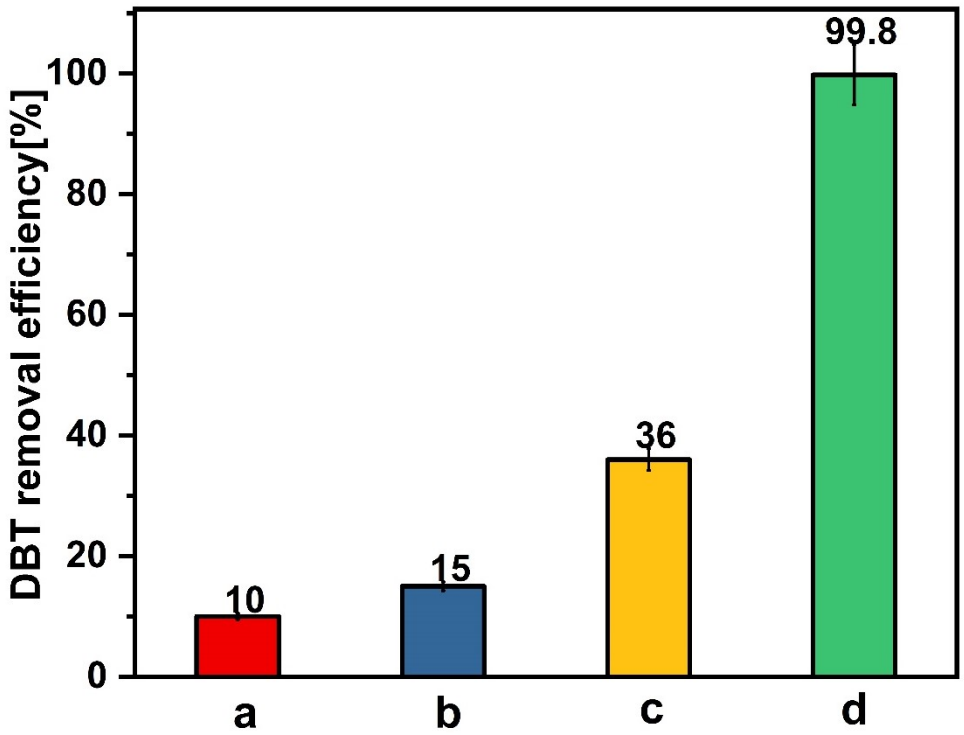

Figure 43: Oxidative desulfurization for DBT in different reaction conditions (a) acetonitrile and model diesel, (b) without catalyst, (c) without H_2O_2, (d) H_2O_2 and SnO_2-MoO_3 catalyst

The SnO_2-MoO_3 catalyst with Sn/Mo (2:1) mole ratio has high oxygen vacancies, which improves ODS efficiency. The S atom of DBT has a lone pair of electrons that can behave as Lewis bases or electron donors (González *et al.,* 2018). The SnO_2-MoO_3 catalyst is assumed to have Lewis's acid sites that receive electrons from the S atom of DBT in the ODS reaction via an acid-base reaction pathway, enhancing DBT chemisorption. On the other hand, upon interactions with the catalyst, in our case SnO_2-MoO_3, H_2O_2 in the ODS processes dissociates into two strong oxidant species: HO^- and HO_2^- ions. These are stronger oxidants than O_2 and thus react with them to produce DBT-sulfone (Kumar *et al.*, 2014; Wang *et al.*, 2010).

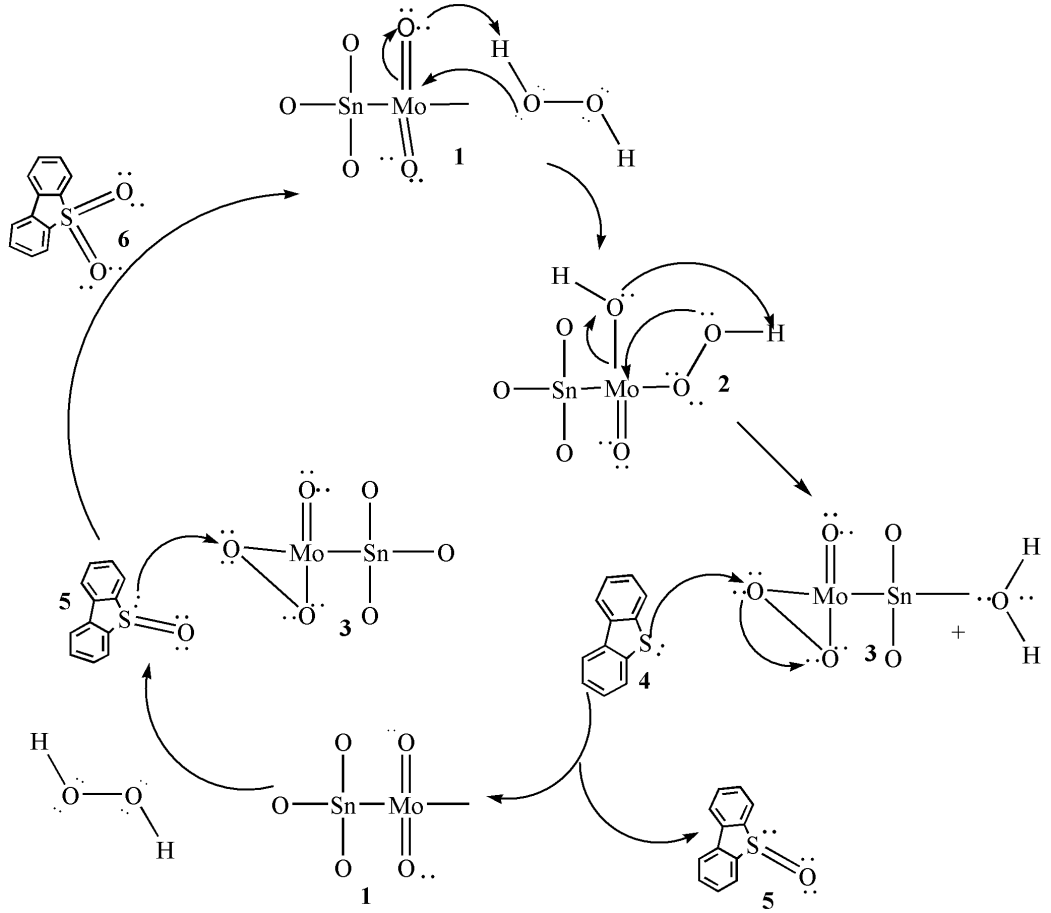

Scheme 3: A suggested reaction mechanism for DBT oxidation by H_2O_2 in the presence of SnO_2-MoO_3 catalyst

Scheme 3 shows the mechanism by which DBT is oxidized. The peroxo-complex intermediate with a much higher oxidation capacity than H_2O_2 (Chen & Schopfer, 1999; Wang *et al.,* 2010) is formed first. This occurs when a nucleophilic attack of H_2O_2 on the Mo=O bond of the catalyst surface (1), confirmed by Raman analysis, generates the active species of peroxometallic (2) intermediates. Water is eliminated from the hydro peroxymolybdate species to form peroxo species (3). Because the electron density of the sulfur atom is higher (4) (Wang *et al.,* 2003), it must be preceded by a nucleophilic attack of the sulfur atom on a peroxo species to form sulfoxide, DBTO (5) and recover molybdenum oxide species (1). Since hydrogen peroxide is abundant, the sulfoxide is further oxidized to generate the dibenzo sulfone, DBTO2 (6). Acetonitrile was used to extract the dibenzothiophene sulfone. The tin oxide (Sn) aids in removing electron density from Mo atoms, giving the molybdate species a more electrophilic nature. (Teimouri *et al.,* 2018).

CHAPTER FIVE

CONCLUSION AND RECOMMENDATION

5.1 Conclusion

In this work, the SnO_2–MoO_3 catalyst has been successfully synthesized from tin and molybdenum inorganic precursors by the sol-gel method. The effect of preparation conditions such as calcination temperature and precursor mole ratio had an important influence on materials' physical properties, such as porosity, crystallinity, crystallite size, lattice strain, specific surface area, oxygen vacancies, and acidic sites. The effect of operating parameters such as reaction time, oxidant ratio, reaction temperature and catalyst load were evaluated.

The following conclusion was made based on the result obtained.

(i) When calcination temperature was varied, the catalyst crystallinity increased, crystal size increased from 24 nm to 38 nm due to the Oswald ripening process, specific surface area and pore volume increased from 350 to 450ºC and then decreased from 550 to 650 ºC due to particle agglomerate as evidenced by SEM analysis.

(ii) The ODS reaction was done, and 450ºC was the optimal calcination temperature which resulted in 99.6% DBT removal from model diesel at the following conditions: 60ºC, 100 mg, 60 min, and 5 reaction temperature, catalyst loading, reaction time, and oxidant/sulfur ratio, correspondingly.

(iii) When mixing SnO_2 and MoO_3 oxides at different mole ratios, Sn/Mo (1:2), (1:1) and (2:1) crystal size varies from 29.9, 31.9 to 42.4 nm while surface area increased from 2.3, 10.7 to 50.4 m^2g^{-1}, furthermore morphological properties are improved from fused particles to cauliflower and agglomeration. The highest acidic site density of 49.3 $mEqg^{-1}$ was observed for the catalyst with mole ratio Sn/Mo (2:1), then 47.4 $mEqg^{-1}$ for Sn/Mo (1:1) and 46.7 $mEqg^{-1}$ for Sn/Mo (1:2).

(iv) The SnO_2-MoO_3 catalyst with a Sn/Mo mole ratio (2:1) at the calcination temperature of 450°C exhibited the highest catalytic activity and could remove 99.8% of dibenzothiophene under optimal conditions: catalyst dosage of 0.01 g, H_2O_2/DBT molar ratio of 5, reaction temperature of 60°C, and reaction time of 30 minutes.

(v) The improved catalytic activity demonstrated by the SnO_2-MoO_3 catalyst is due to surface defects increases because of particle agglomeration with decreased crystallite

size, resulting in a high surface area with high pore distribution around the mesopore region as well as the synergy between SnO_2 and MoO_3 oxide and the unsaturated coordination of tetragonal tin oxide to hexagonal molybdenum oxide, is believed to create Lewis acid sites that are essential for the adsorption of DBT and its subsequent conversion to DBT sulfone.

(vi) Kinetic studies show the ODS reaction follows pseudo-first-order kinetics with the Langmuir-Hinshelwood mechanism provide an insight into how the reaction proceeds and allows for the identification/determination of the rate law for the heterogeneous reaction.

(vii) The proposed sulfur removal efficiency mechanism consists of three steps: formation of a hydroperoxymolybdate, loss of water molecules to form a peroxo complex and nucleophilic attack on the peroxo complex by the sulfur molecule to form a sulfoxide and then sulfone.

(viii) The reusability experiments revealed that SnO_2-MoO_3 could be recycled five times for deep desulfurization.

(ix) The excellent ability of SnO_2-MoO_3 catalysts to efficiently oxidize sulfur in challenging molecules such as DBT, commonly present in diesel fuel, showcases their immense potential for large-scale desulfurization of transportation fuels. This potential holds significant promise in meeting stringent standards that ensure the protection of public health and the environment by reducing respiratory complications and minimizing infrastructure degradation associated with the decrease in SOx emissions.

5.2 Recommendations

This study evaluated the performance of tin molybdenum mixed metal oxide catalyst materials from tin and molybdenum inorganic precursors for sulfur removal in model diesel. Based on the findings of this study, we recommend the following:

(i) Future work should explore other oxidation catalytic reactions which can be performed using the synthesized catalysts.

(ii) A computation study should be done to compare the experimental and theoretical results.

(iii) Exploring the cost-benefit analysis of utilizing the catalyst in the oxidative desulfurization of practical heavy oil feedstocks, such as waste tire pyrolysis oil.

(iv) More study is needed to commercialize the employed catalyst's oxidative desulfurization process by addressing selectivity for the sulfides included in the fuel feedstock.

(v) A comparative report for kinetic analysis by Langmuir-Hinshelwood and Mars -van Krevelen model should be done.

(vi) Recovery and quantification of the sulphone, the waste product that can be used as a surfactant.

(vii) A solvent effect should be studied as the solvent has a significant effect on the result of the reaction, i.e., yields, by-product production, and reaction kinetics, and this effect is highly dependent on the catalyst type and substrate composition.

(viii) To determine whether the heating rate for the catalyst preparation will influence the catalyst's characteristics, which influence the activity.

REFERENCES

Abdul-Kadhim, W., Deraman, M. A., Abdullah, S. B., Tajuddin, S. N., Yusoff, M. M., Taufiq-Yap, Y. H., & Rahim, M. H. A. (2017). Efficient and reusable iron-zinc oxide catalyst for oxidative desulfurization of model fuel. *Journal of Environmental Chemical Engineering,* 5(2), 1645-1656.

Afify, H. H., Hassan, S. A., Abouelsayed, A., Demian, S. E., & Zayed, H. A. (2017). Coloration of molybdenum oxide thin films synthesized by spray pyrolysis technique. T*hin Solid Films*, 623, 40-47.

Agashe, C., Hüpkes, J., Schöpe, G., & Berginski, M. (2009). Physical properties of highly oriented spray-deposited fluorine-doped tin dioxide films as transparent conductor. *Solar Energy Materials and Solar Cells,* 93(8), 1256-1262.

Ahmadian, M., & Anbia, M. (2022). Highly efficient oxidative desulfurization catalyzed by copper-based materials using hydrogen peroxide as oxidant. *Fuel*, *324*, 124471. https://doi.org/10.1016/j.fuel.2022.124471

Al-Abduly, A., & Sharma, V. K. (2014). Oxidation of benzothiophene, dibenzothiophene, and methyl-dibenzothiophene by ferrate(VI). *Journal of Hazardous Materials*, 279, 296-301. https://doi.org/10.1016/j.jhazmat.2014.06.083

Al-Hammadi, S. A., Al-Amer, A. M., & Saleh, T. A. (2018). Alumina-carbon nanofiber composite as a support for MoCo catalysts in hydrodesulfurization reactions. *Chemical Engineering Journal*, 345, 242-251.

Al-Saadi, T. M., Hussein, B. H., Hasan, A. B., & Shehab, A. A. (2019). Study the structural and optical properties of Cr doped SnO2 nanoparticles synthesized by sol-gel method. *Energy Procedia,* 157, 457-465.

Albayrak, A. T., & Tavman, A. (2022). Sono-oxidative desulfurization of fuels using heterogeneous and homogeneous catalysts: A comprehensive review. *Ultrasonics Sonochemistry*, *83*, 105845. https://doi.org/10.1016/j.ultsonch.2021.105845

Ali, M. F., Al-Malki, A., El-Ali, B., Martinie, G., & Siddiqui, M. N. (2006). Deep desulphurization of gasoline and diesel fuels using non-hydrogen consuming techniques. *Fuel,* 85(10-11), 1354-1363.

Alonso, D. A., Nájera, C., & Varea, M. (2002). Simple, economical and environmentally friendly sulfone synthesis. *Tetrahedron Letters,* 43(19), 3459-3461.

Alvarez-Amparán, M. A., Cedeno-Caero, L., Cortes-Jácome, M. A., & Toledo-Antonio, J. A. (2017). Relationship between the catalytic activity and Mo–V surface species in bimetallic catalysts for the oxidative desulfurization of dibenzothiophenic compounds. *Reaction Kinetics, Mechanisms and Catalysis,* 122, 869-885.

Ameen, S., Akhtar, M. S., Godbole, R., & Shin, H. S. (2019). I*ntroductory Chapter: An Introduction to Nanoporous Materials. In Nanofluid Flow in Porous Media.* IntechOpen.

Arellano, U., Wang, J. A., Timko, M. T., Chen, L. F., Carrera, S. P., Asomoza, M., Vargas, O. G., & Llanos, M. E. (2014). Oxidative removal of dibenzothiophene in a biphasic system using sol–gel $FeTiO_2$ catalysts and H_2O_2 promoted with acetic acid. *Fuel*, 126, 16-25.

Atuchin, V. V., Gavrilova, T. A., Grigorieva, T. I., Kuratieva, N. V., Okotrub, K. A., Pervukhina, N. V., & Surovtsev, N. V. (2011). Sublimation growth and vibrational microspectrometry of α-MoO_3 single crystals. *Journal of Crystal Growth*, 318(1), 987-990.

Bai, J., Song, Y., Wang, C., Chen, H., Wei, D., Bai, L., Wang, W., Yang, L., Liang, Y., & Yang, H. (2021). Engineering the electronic structure of Mo sites in Mn–Mo–O mixed-metal oxides for efficient aerobic oxidative desulfurization. *Energy & Fuels,* 35(15), 12310-12318.

Bai, S., Chen, C., Zhang, D., Luo, R., Li, D., Chen, A., & Liu, C. C. (2014). Intrinsic characteristic and mechanism in enhancing H2S sensing of Cd-doped α-MoO3 nanobelts. *Sensors and Actuators B: Chemical,* 204, 754-762.

Baidya, T., Gupta, A., Deshpandey, P. A., Madras, G., & Hegde, M. S. (2009). High Oxygen Storage Capacity and High Rates of CO Oxidation and NO Reduction Catalytic Properties of Ce1− x Sn x O_2 and Ce0. 78Sn0. 2Pd0. 02O2-δ. *The Journal of Physical Chemistry C*, 113(10), 4059-4068.

Batrakova, E. V., & Kabanov, A. V. (2008). Pluronic block copolymers: Evolution of drug delivery concept from inert nanocarriers to biological response modifiers. *Journal of Controlled Release*, *130*(2), 98-106. https://doi.org/10.1016/j.jconrel.2008.04.013

Batzill, M., & Diebold, U. (2005). The surface and materials science of tin oxide. *Progress in Surface Science*, *79*(2), 47-154. https://doi.org/10.1016/j.progsurf.2005.09.002

Benak, K. R., Dominguez, L., Economy, J., & Mangun, C. L. (2002). Sulfonation of pyropolymeric fibers derived from phenol-formaldehyde resins. *Carbon,* 40(13), 2323-2332.

Gomez Bernal, H., & Cedeño Caero, L. (2005). Solvent effects during oxidation-extraction desulfurization process of aromatic sulfur compounds from fuels. *International Journal of Chemical Reactor Engineering,* 3(1), 1-14.

Bhadra, B. N., & Jhung, S. H. (2022). Enhancing the oxidative desulfurization efficiency of cobalt-loaded-porous carbon catalyst via nitrogen doping on carbon support. *Journal of Cleaner Production*, *360*, 132168. https://doi.org/10.1016/j.jclepro.2022.132168

Bharate, B. G. (2021). Synthesis of Molybdenum Oxide Nanoparticles by Sol-Gel Method for Ammonia Gas Sensing. *Biomedical Journal of Scientific &amp: Technical Research*, *37*(1), 29172-29175. https://doi.org/10.26717/BJSTR.2021.37.005957

Bi, F., Zhang, X., Du, Q., Yue, K., Wang, R., Li, F., Liu, N., & Huang, Y. (2021). Influence of pretreatment conditions on low-temperature CO oxidation over Pd supported UiO-66 catalysts. *Molecular Catalysis,* 509, 111633.

Blumberg, K. (2003). *Low-Sulfur Gasoline & Diesel: The Key to Lower Vehicle Emissions.* https://scholar.google.com

Boltes, K., Alonso del Aguila, R., & García-Calvo, E. (2013). Effect of mass transfer on biodesulfurization kinetics of alkylated forms of dibenzothiophene by Pseudomonas putida CECT5279. *Journal of Chemical Technology & Biotechnology*, 88(3), 422-431.

Boniek, D., Figueiredo, D., dos Santos, A. F. B., & de Resende Stoianoff, M. A. (2015). Biodesulfurization: A mini review about the immediate search for the future technology. *Clean Technologies and Environmental Policy*, 17, 29-37.

Brégeault, J. M. (2003). Transition-metal complexes for liquid-phase catalytic oxidation: some aspects of industrial reactions and of emerging technologies. *Dalton Transactions*(17), 3289-3302. https://doi.org/10.1039/B303073N

Brinker, C. J. (2013). *Sol-Gel Science: The Physics and Chemistry of Sol-Gel Processing.* Wiley Academic press.

Caero, L. C., Hernández, E., Pedraza, F., & Murrieta, F. (2005). Oxidative desulfurization of synthetic diesel using supported catalysts: Part I. Study of the operation conditions with a vanadium oxide based catalyst. *Catalysis Today,* 107, 564-569.

Cao, Y., Wang, H., Ding, R., Wang, L., Liu, Z., & Lv, B. (2020). Highly efficient oxidative desulfurization of dibenzothiophene using Ni modified MoO3 catalyst. *Applied Catalysis A: General*, 589, 117308.

Cao, Y., Wang, H., Ren, X., Li, F., Wang, J., Ding, R., Wang, L., Wu, J., Liu, Z., & Lv, B., (2019). Fe containing MoO_3 nanowires grown along the [110] direction and their fast selective adsorption of quasi-phenothiazine dyes. *CrystEngComm,* 21(34), 5106-5114.

Capel-Sanchez, M. C., Perez-Presas, P., Campos-Martin, J. M., & Fierro, J. L. G. (2010). Highly efficient deep desulfurization of fuels by chemical oxidation. *Catalysis Today,* 157(1-4), 390-396.

De Castro, I. A., Datta, R. S., Ou, J. Z., Castellanos-Gomez, A., Sriram, S., Daeneke, T., & Kalantar-zadeh, K. (2017). Molybdenum oxides–from fundamentals to functionality. *Advanced Materials,* 29(40), 1701619.

Chamack, M., Mahjoub, A. R., & Aghayan, H. (2015). Catalytic performance of vanadium-substituted molybdophosphoric acid supported on zirconium modified mesoporous silica in oxidative desulfurization. *Chemical Engineering Research and Design*, 94, 565-572.

Chan, N. Y., Lin, T. Y., & Yen, T. F. (2008). Superoxides: Alternative oxidants for the oxidative desulfurization process. *Energy & fuels,* 22(5), 3326-3328.

Charinpanitkul, T., Faungnawakij, K., & Tanthapanichakoon, W. (2008). Review of recent research on nanoparticle production in Thailand. *Advanced Powder Technology*, 19(5), 443-457.

Chen, J., Wang, M., Liao, X., Liu, Z., Zhang, J., Ding, L., Gao, L., & Li, Y. (2015). Large-scale synthesis of single-crystal molybdenum trioxide nanobelts by hot-wire chemical vapour deposition. *Journal of Alloys and Compounds*, 619, 406-410.

Chen, J. S., Cheah, Y. L., Madhavi, S., & Lou, X. W. (2010). Fast synthesis of α-MoO_3 nanorods with controlled aspect ratios and their enhanced lithium storage capabilities. *The Journal of Physical Chemistry C*, 114(18), 8675-8678.

Chen, K., Zhang, X. M., Yang, X. F., Jiao, M. G., Zhou, Z., Zhang, M. H., Wang, D. H., & Bu, X. H. (2018). Electronic structure of heterojunction MoO_2/g-C_3N4 catalyst for oxidative desulfurization. *Applied Catalysis B: Environmental,* 238, 263-273.

Chen, S. X., & Schopfer, P. (1999). Hydroxyl-radical production in physiological reactions. *European Journal of Biochemistry*, 260(3), 726-735. https://doi.org/10.1046/j.1432-1327.1999.00199.x

Chen, S., Zang, M., Li, L., Chen, J., Liu, Q., Feng, X., Sun, S., Zang, C., & Zhao, C. (2021). Efficient biodesulfurization of diesel oil by Gordonia sp. SC-10 with highly hydrophobic cell surfaces. *Biochemical Engineering Journal*, 174, 108094.

Chen, Y., Zhao, S., & Song, Y. F. (2013). An efficient heterogeneous catalyst based on highly dispersed Na7H2LaW10O36· $32H_2O$ nanoparticles on mesoporous silica for deep desulfurization. *Applied Catalysis A: General,* 466, 307-314.

Choodamani, C., Nagabhushana, G. P., Rudraswamy, B., & Chandrappa, G. T. (2014). Thermal effect on magnetic properties of Mg-Zn ferrite nanoparticles. *Materials Letters,* 116, 227-230.

Chuenchom, L., Kraehnert, R., & Smarsly, B. M. (2012). Recent progress in soft-templating of porous carbon materials. *Soft Matter,* 8(42), 10801-10812.

Cristoni, S., Armelao, L., Gross, S., Tondello, E., & Traldi, P. (2001). Electrospray ionization in the study of sol-gel processes: The polycondensation of Ti (O-n-Bu) 4 in the presence of Si (OEt) 4. *Rapid Communications in Mass Spectrometry*, 15(6), 386-392.

Dai, T., Ren, Y., Qian, L., & Liu, X. (2018). Characterization of molybdenum oxide thin films grown by atomic layer deposition. *Journal of Electronic Materials,* 47, 6709-6715.

Dale, S. (2019). *BP Statistical Review of World Energy.* BP Plc, London, United Kingdom

Dammala, P., Machado, J., Rani, B., Murali, S., Devi, S., Luwang, M. N., & Sahu, N. K. (2019). Synthesis of biphasic nanomaterials based on ZnO and SnO2: Application towards photocatalytic degradation of acid red dye. *Nano-Structures & Nano-Objects*, 18, 100292.

Dartt, C. B., & Davis, M. E. (1994). Catalysis for Environmentally Benign Processing. *Industrial & Engineering Chemistry Research*, *33*(12), 2887-2899.

Das, S., & Jayaraman, V. (2014). SnO2: A Comprehensive Review on Structures and Gas Sensors. *Progress in Materials Science*, 66, 1-17.

Delmon, B., & Ruiz, P. (1987). Synergy in selective catalytic oxidation. *Reaction Kinetics and Catalysis Letters*, *35*(1), 303-314. https://doi.org/10.1007/BF02062166

Dieguez, A., Romano-Rodrıguez, A., Vila, A., & Morante, J. R. (2001). The complete Raman spectrum of nanometric SnO_2 particles. *Journal of Applied Physics,* 90(3), 1550-1557.

Ding, Y., Zhu, W., Li, H., Jiang, W., Zhang, M., Duan, Y., & Chang, Y. (2011). Catalytic oxidative desulfurization with a hexatungstate/aqueous H 2 O 2/ionic liquid emulsion system. *Green Chemistry*, 13(5), 1210-1216.

Khodadadi Dizaji, A., Mortaheb, H. R., & Mokhtarani, B. (2019). Extractive-catalytic oxidative desulfurization with graphene oxide-based heteropolyacid catalysts: investigation of affective parameters and kinetic modeling. *Catalysis Letters,* 149, 259-271.

Dong, L., Dai, X., Peng, C., Yang, C., Li, G., Chen, S., Miao, G. and Xiao, J. (2022). Ultra-deep catalytic adsorptive desulfurization of diesel fuel using Ti-silica gel adsorbent at low Ti-loading. *AIChE Journal*, 68(2), e17493.

Dos-Santos, T. V., da Silva Avelino, D. O., Meneghetti, M. R., & Meneghetti, S. M. P. (2018). Mixed oxides based on SnO_2 impregnated with MoO_3: A robust system to apply in fructose conversion. *Catalysis Communications,* 114, 120-123.

Dos-Santos, T. V., da Silva Avelino, D. O., Pryston, D. B., Meneghetti, M. R., & Meneghetti, S. M. (2022). Tin, molybdenum and tin-molybdenum oxides: Influence of Lewis and Bronsted acid sites on xylose conversion. *Catalysis Today*, 394, 125-132.

Dumesic, J. A. (2008). *Principles of Heterogeneous Catalysis*. https://scholar.google.com

Dumon, A. S., Sahu, A., & Raybaud, P. (2021). Hydrogenolysis and β: Elimination mechanisms for CS bond scission of dibenzothiophene on CoMoS edge sites. *Journal of Catalysis,* 403, 32-42.

Egorova, M., & Prins, R. (2004). Hydrodesulfurization of dibenzothiophene and 4,6-dimethyldibenzothiophene over sulfided NiMo/γ-Al_2O_3, CoMo/γ-Al_2O_3, and Mo/γ-Al_2O_3 catalysts. *Journal of Catalysis*, 225(2), 417-427.

Elhi, F., Gantman, M., Nurk, G., Schulz, P. S., Wasserscheid, P., Aabloo, A., & Põhako-Esko, K. (2020). Influence of carboxylate anions on phase behavior of choline ionic liquid mixtures. *Molecules,* 25(7), 1691.

Ethan Boechler. (2021). *Energy Education*. University of Galary Press.

Evans, D. F. (1988). Self-organization of amphiphiles. *Langmuir*, *4*(1), 3-12.

Fahlman, B. D. (2007). *Solid-State Chemistry.* https://scholar.google.com

Fan, X., Zhang, G., & Zhang, F. (2015). Multiple roles of graphene in heterogeneous catalysis. *Chemical Society Reviews,* 44(10), 3023-3035.

Fogler, H. (2020). *Elements of Chemical Reaction Engineering, 6th Edition*. Pearson. https://books.google.co.tz/books?id=jWX7zQEACAAJ

Fraile, J. M., Gil, C., Mayoral, J. A., Muel, B., Roldán, L., Vispe, E., Calderón, S., & Puente, F. (2016). Heterogeneous titanium catalysts for oxidation of dibenzothiophene in hydrocarbon solutions with hydrogen peroxide: On the road to oxidative desulfurization. *Applied Catalysis B: Environmental*, 180, 680-686.

Frewer, L. J., Gupta, N., George, S., Fischer, A. R. H., Giles, E. L., & Coles, D. (2014). Consumer attitudes towards nanotechnologies applied to food production. *Trends in Food Science & Technology*, 40(2), 211-225.

Gavrilova, N., Myachina, M., Poluboyarinova, K., Novaeva, E., & Nazarov, V. (2020). Colloidal Characteristics of Molybdenum Blue Nanoparticles Dispersion for Catalytic Applications. *Materials Proceedings,* 4(1), 24-36.

Gawande, M. B., Pandey, R. K., & Jayaram, R. V. (2012). Role of mixed metal oxides in catalysis science: Versatile applications in organic synthesis. *Catalysis Science & Technology,* 2(6), 1113-1125.

Ghashang, M., Mansoor, S. S., Mohammad Shafiee, M. R., Kargar, M., Najafi Biregan, M., Azimi, F., & Taghrir, H. (2016). Green chemistry preparation of MgO nanopowders: Efficient catalyst for the synthesis of thiochromeno [4, 3-b] pyran and thiopyrano [4, 3-b] pyran derivatives. *Journal of Sulfur Chemistry,* 37(4), 377-390.

Ghouri, Z. K., Barakat, N. A., Obaid, M., Lee, J. H., & Kim, H. Y. (2015). Co/CeO_2-decorated carbon nanofibers as effective non-precious electro-catalyst for fuel cells application in alkaline medium. *Ceramics International,* 41(2), 2271-2278.

Ghubayra, R., Nuttall, C., Hodgkiss, S., Craven, M., Kozhevnikova, E. F., & Kozhevnikov, I. V. (2019). Oxidative desulfurization of model diesel fuel catalyzed by carbon-supported heteropoly acids. *Applied Catalysis B: Environmental,* 253, 309-316.

Gokel, G. W., Gerdes, H. M., & Dishong, D. M. (1980). Sulfur heterocycles. Heterogeneous, phase-transfer, and acid-catalyzed potassium permanganate oxidation of sulfides to sulfones and a survey of their carbon-13 nuclear magnetic resonance spectra. *The Journal of Organic Chemistry,* 45(18), 3634-3639.

Gong, H. P., Hua, W. M., Yue, Y. H., & Gao, Z. (2017). Graphene oxide for acid catalyzed-reactions: Effect of drying process. *Applied Surface Science,* 397, 44-48.

Gong, L., & Haur, S. C. (2017). On demand rapid patterning of colored amorphous molybdenum oxide using a focused laser beam. *Journal of Materials Chemistry C*, *5*(8), 2090-2097. https://doi.org/10.1039/C6TC04580D

González, J., Chen, L. F., Wang, J. A., Manríquez, M., Limas, R., Schachat, P., Navarrete, J., & Contreras, J. L. (2016). Surface chemistry and catalytic properties of VOX/Ti-MCM-41 catalysts for dibenzothiophene oxidation in a biphasic system. *Applied Surface Science,* 379, 367-376.

González, J., Wang, J. A., Chen, L., Manríquez, M., Salmones, J., Limas, R., & Arellano, U. (2018). Quantitative determination of oxygen defects, surface lewis acidity, and catalytic properties of mesoporous MoO_3/SBA-15 catalysts. *Journal of Solid State Chemistry*, 263, 100-114.

Goyal, R., Singh, O., Agrawal, A., Samanta, C., & Sarkar, B. (2022). Advantages and limitations of catalytic oxidation with hydrogen peroxide: From bulk chemicals to lab scale process. *Catalysis Reviews,* 64(2), 229-285.

Granato, D. B., Caraveo-Frescas, J. A., Alshareef, H. N., & Schwingenschlögl, U. (2013). Enhancement of p-type mobility in tin monoxide by native defects. *Applied Physics Letters,* 102(21), 1-16.

Rad, A. G., Abbasi, H., & Afzali, M. H. (2011). Gold nanoparticles: Synthesising, characterizing and reviewing novel application in recent years. *Physics Procedia*, 22, 203-208.

Gray, K. A., Mrachko, G. T., & Squires, C. H. (2003). Biodesulfurization of fossil fuels. *Current Opinion in Microbiology,* 6(3), 229-235.

Green, M. (1994). *An Introduction to the Chemistry of Molybdenum.* https:// scholar. google. com

Grønborg, S. S., Šarić, M., Moses, P. G., Rossmeisl, J., & Lauritsen, J. V. (2016). Atomic scale analysis of sterical effects in the adsorption of 4, 6-dimethyldibenzothiophene on a CoMoS hydrotreating catalyst. *Journal of Catalysis,* 344, 121-128.

Gross, L., Mohn, F., Moll, N., Meyer, G., Ebel, R., Abdel-Mageed, W. M., & Jaspars, M. (2010). Organic structure determination using atomic-resolution scanning probe microscopy. *Nature chemistry,* 2(10), 821-825.

Guan, X., Wang, Y., Luo, P., Yu, Y., Chen, D., & Li, X. (2019). Incorporating N atoms into SnO2 nanostructure as an approach to enhance gas sensing property for acetone. *Nanomaterials,* 9(3), 445.

Guo, L., Tian, Y., Li, J., Zhao, D., Yu, X., Ding, T., Jiang, Z. and Li, X. (2020). Effect of Sn-rich and Ce-rich Sn1− xCexO2 supports of Pd catalysts on CO oxidation. *Catalysis Today*, 355, 358-365.

Guo, Y., Liang, J., Liu, Y., Liu, Y., Xu, X., Fang, X., Zhong, W., & Wang, X. (2019). Identifying surface active sites of SnO_2: Roles of surface O_2–, O_{22}–anions and acidic species played for toluene deep oxidation. *Industrial & Engineering Chemistry Research,* 58(40), 18569-18581.

Gürü, M. (2007). Oxidative Desulfurization of Aşkale Coal by Nitric Acid Solution. *Energy Sources, Part A: Recovery, Utilization, and Environmental Effects*, *29*(5), 463-469. https://doi.org/10.1080/009083190966054

Haneda, M., Ota, Y., Doi, Y., & Hattori, M. (2016). Preparation, characterization, and activity of SnO 2 nanoparticles supported on $Al_2 O_3$ as a catalyst for the selective reduction of NO with $C_3 H_6$. *Journal of Materials Science,* 51, 10949-10959.

Hao, R., Yang, S., Yuan, B., & Zhao, Y. (2017). Simultaneous desulfurization and denitrification through an integrative process utilizing $NaClO_2/Na_2S2O_8$. *Fuel Processing Technology*, 159, 145-152.

Harold, K. (1989). *Transition Metal Oxides: Surface Chemistry and Catalysis*. https:// scholar. google. com

Harrison, R. M., & Yin, J. (2000). Particulate matter in the atmosphere: which particle properties are important for its effects on health? *Science of The Total Environment*, *249*(1), 85-101. https://doi.org/10.1016/S0048-9697(99)00513-6

Haw, K. G., Bakar, W. A. W. A., Ali, R., Chong, J. F., & Kadir, A. A. A. (2010). Catalytic oxidative desulfurization of diesel utilizing hydrogen peroxide and functionalized-activated carbon in a biphasic diesel–acetonitrile system. *Fuel Processing Technology,* 91(9), 1105-1112.

Hosseini, S. M., Hosseini-Monfared, H., Abbasi, V., & Khoshroo, M. R. (2016). Selective oxidation of hydrocarbons under air using recoverable silver ferrite–graphene ($AgFeO_2$–G) nanocomposite: A good catalyst for green chemistry. *Inorganic Chemistry Communications,* 67, 72-79.

Houda, S., Lancelot, C., Blanchard, P., Poinel, L., & Lamonier, C. (2018). Oxidative desulfurization of heavy oils with high sulfur content: A review. *Catalysts,* 8(9), 344.

Hu, H., Deng, C., Xu, J., Zhang, K., & Sun, M. (2015). Metastable h-MoO3 and stable α-MoO3 microstructures: Controllable synthesis, growth mechanism and their enhanced photocatalytic activity. *Journal of Experimental Nanoscience,* 10(17), 1336-1346.

Huang, H. C., Shown, I., Chang, S. T., Hsu, H. C., Du, H. Y., Kuo, M. C., Wong, K. T., Wang, S. F., Wang, C. H., Chen, L. C., & Chen, K. H. (2012). Pyrolyzed Cobalt Corrole as a Potential Non-Precious Catalyst for Fuel Cells. *Advanced Functional Materials,* 22(16), 3500-3508.

Huang, H., Zhou, Z., Qin, J., Li, Y., Liu, G., & Wu, W. (2020). A facile synthesis of mesoporous Mo–Al oxides for desulfurization of dibenzothiophene in the extractive

catalytic oxidative desulfurization system. *Reaction Kinetics, Mechanisms and Catalysis*, 130, 363-379.

Hussein, A. K. (2016). Applications of nanotechnology to improve the performance of solar collectors: Recent advances and overview. *Renewable and Sustainable Energy Reviews*, *62*, 767-792. https://doi.org/10.1016/j.rser.2016.04.050

Hutchings, G. (2004). *Heterogeneous Catalyst Preparation.* https://scholar.google.com

Il'in, A. A., Dao, K. K., Rumyantsev, R. N., Il'in, A. P., Petukhova, K. A., & Goryanskaya, V. A. (2017). Synthesis of SnO_2–MoO_3 solid solution and its properties in the reaction of methanol dehydrogenation. *Russian Journal of Applied Chemistry*, 90, 1433-1438.

Inmanee, T., Pinthong, P., & Jongsomjit, B. (2017). Effect of calcination temperatures and Mo modification on nanocrystalline (γ-χ)-Al_2O_3 catalysts for catalytic ethanol dehydration. *Journal of Nanomaterials*, 2017.30-45.

Jarzebski, Z. M., & Marton, J. P. (1976). Physical Properties of SnO_2 Materials: I . Preparation and Defect Structure. *Journal of The Electrochemical Society*, 123(7), 199-205. https://doi.org10.1149/1.2133010

Jeevanandam, J., Barhoum, A., Chan, Y. S., Dufresne, A., & Danquah, M. K. (2018). Review on nanoparticles and nanostructured materials: history, sources, toxicity and regulations. *Beilstein Journal of Nanotechnology,* 9(1), 1050-1074.

Jiang, W., An, X., Xiao, J., Yang, Z., Liu, J., Chen, H., Li, H., Zhu, W., Li, H., & Dai, S. (2022). Enhanced oxygen activation achieved by robust single chromium atom-derived catalysts in aerobic oxidative desulfurization. *ACS Catalysis,* 12(14), 8623-8631.

Jiang, X., Li, H., Zhu, W., He, L., Shu, H., & Lu, J. (2009). Deep desulfurization of fuels catalyzed by surfactant-type decatungstates using H_2O_2 as oxidant. *Fuel,* 88(3), 431-43

Jin, G., Weng, W., Lin, Z., Dummer, N. F., Taylor, S. H., Kiely, C. J., Bartley, J. K., & Hutchings, G. J. (2012). $Fe_2(MoO_4)3/MoO_3$ nano-structured catalysts for the oxidation of methanol to formaldehyde. *Journal of Catalysis*, 296, 55-64.

Jittiarporn, P., Sikong, L., Kooptarnond, K., & Taweepreda, W. (2015). Influence of calcination temperature on the structural and photochromic properties of

nanocrystalline MoO_3. *Digest Journal of Nanomaterials and Biostructures*, 10, 1237-1248.

Jolivet, J. P., Cassaignon, S., Chanéac, C., Chiche, D., Durupthy, O., & Portehault, D. (2010). Design of metal oxide nanoparticles: Control of size, shape, crystalline structure and functionalization by aqueous chemistry. *Comptes Rendus Chimie*, 13(1-2), 40-51.

Jose, N., Sengupta, S., & Basu, J. K. (2011). Optimization of oxidative desulfurization of thiophene using Cu/titanium silicate-1 by box-behnken design. *Fuel,* 90(2), 626-632.

Kargar, H., Ghahramaninezhad, M., Shahrak, M. N., & Balula, S. S. (2021). An effective magnetic catalyst for oxidative desulfurization of model and real fuels: Fe_3O_4/ZIF-8/TiO_2. *Microporous and Mesoporous Materials*, 317, 110992.

Kazemi, M., Ghobadi, M., & Mirzaie, A. (2018). Cobalt ferrite nanoparticles ($CoFe_2O_4$ MNPs) as catalyst and support: Magnetically recoverable nanocatalysts in organic synthesis. *Nanotechnology Reviews,* 7(1), 43-68.

Khodadadi, A., Torabiangaji, M., Talebizadeh Rafsanjani, A., & Yonesi, A. (2012, March). *Adsorptive Desulfurization of Diesel Fuel with Nano Copper Oxide (CuO). In Proceedings of the 4th International Conference on Nanostructures (ICNS4) (pp. 12-14).* https://scholar.google.com

Kirkham, M., Wang, X., Wang, Z. L., & Snyder, R. L. (2007). Solid Au nanoparticles as a catalyst for growing aligned ZnO nanowires: A new understanding of the vapour–liquid–solid process. *Nanotechnology,* 18(36), 365304

Králik, M. (2014). Adsorption, chemisorption, and catalysis. *Chemical Papers*, *68*(12), 1625-1638. https://doi.org/10.2478/s11696-014-0624-9

Kulkarni, P. S., & Afonso, C. A. M. (2010). Deep desulfurization of diesel fuel using ionic liquids: current status and future challenges. *Green Chemistry*, *12*(7), 1139-1149. https://doi.org/10.1039/C002113J

Kumar, S., Srivastava, V. C., & Badoni, R. P. (2014). Oxidative desulfurization of dibenzothiophene by zirconia-based catalysts. *International Journal of Chemical Reactor Engineering,* 12(1), 295-302.

Kung, H. H. (1989). *Transition Metal Oxides: Surface Chemistry and Catalysis.* https://scholar.google.com/

Lavalley, J. C. (1996). Infrared spectrometric studies of the surface basicity of metal oxides and zeolites using adsorbed probe molecules. *Catalysis Today*, *27*(3), 377-401. https://doi.org/10.1016/0920-5861(95)00161-1

Leal, G. F., Lima, S., Graça, I., Carrer, H., Barrett, D. H., Teixeira-Neto, E., Curvelo, A. A.S., Rodella, C.B., & Rinaldi, R. (2019). Design of nickel supported on water-tolerant Nb_2O_5 catalysts for the hydrotreating of lignin streams obtained from lignin-first biorefining. *Iscience,* 15, 467-488.

Lee, S. C.*, et al.* (2011). A novel tin oxide-based recoverable thick film SO2 gas sensor promoted with magnesium and vanadium oxides. *Sensors and Actuators B: Chemical,* 160(1), 1328-1334. https://doi.org/10.1016/j.snb.2011.09.070

Lei, J., Chen, L., Yang, P., Du, X., & Yan, X. (2013). Oxidative desulfurization of diesel fuel by mesoporous phosphotungstic acid/SiO 2: the effect of preparation methods on catalytic performance. *Journal of Porous Materials,* 20, 1379-1385.

Leofanti, G., Padovan, M., Tozzola, G., & Venturelli, B. J. C. T. (1998). Surface area and pore texture of catalysts. *Catalysis Today*, 41(1-3), 207-219.

Lermusiaux, L., Mazel, A., Carretero-Genevrier, A., Sanchez, C., & Drisko, G. L. (2022). Metal-Induced Crystallization in Metal Oxides. A*ccounts of Chemical Research,* 55(2), 171-185.

Li, C., Liu, Y., Wan, W., Li, Y., Ma, Y., Zhang, J., Ren, X., & Zhao, H. (2020). Hydrothermal synthesis of novel porous butterfly-like hierarchical SnO2 architecture with excellent gas-sensing performance to acetaldehyde. *Sensors and Actuators B: Chemical*, 318, 128209.

Li, D., Lin, Y. S., & Guliants, V. V. (2010). Synthesis and characterization of ordered meso-macro-porous silica membranes on a porous alumina support. *Tsinghua Science and Technology,* 15(4), 377-384.

Li, F., Xu, J., Yu, X., Chen, L., Zhu, J., Yang, Z., & Xin, X. (2002). One-step solid-state reaction synthesis and gas sensing property of tin oxide nanoparticles. *Sensors and Actuators B: Chemical*, 81(2-3), 165-169.

Li, K. T., Yen, C. S., & Shyu, N. S. (1997). Mixed-metal oxide catalysts containing iron for selective oxidation of hydrogen sulfide to sulfur. *Applied Catalysis A: General,* 156(1), 117-130.

Li, X., Gu, Z., Cho, J., Sun, H., & Kurup, P. (2011). Tin–copper mixed metal oxide nanowires: Synthesis and sensor response to chemical vapors. S*ensors and Actuators B: Chemical,* 158(1), 199-207.

Li, X., Zhang, J., Zhou, F., Wang, Y., Yuan, X., & Wang, H. (2018). Oxidative desulfurization of dibenzothiophene and diesel by hydrogen peroxide: Catalysis of $H_3PMo_{12}O_{40}$ immobilized on the ionic liquid modified SiO_2. *Molecular Catalysis,* 452, 93-99.

Liu, A., Zhu, M., & Dai, B. (2019). A novel high-performance SnO2 catalyst for oxidative desulfurization under mild conditions. *Applied Catalysis A: General,* 583, 117134.

Liu, L. Z., Li, T. H., Wu, X. L., Shen, J. C., & Chu, P. K. (2012). Identification of oxygen vacancy types from Raman spectra of SnO2 nanocrystals. *Journal of Raman Spectroscopy,* 43(10), 1423-1426.

Liu, X., Zhang, D., Zhang, Y., & Dai, X. (2010). Preparation and characterization of p-type semiconducting tin oxide thin film gas sensors. *Journal of Applied Physics,* 107(6), 1-12.

Liu, Y., Chu, J., Lian, L., Chen, X., An, S., Hong, L., Wang, D., & Chen, W. (2021). Ultrafast oxidative desulfurization of diesel fuels by mass transfer enhancement of polyoxometalate modified alumina catalysts. *Energy & Fuels,* 35(3), 2110-2120.

Livage, J., Henry, M., & Sanchez, C. (1988). Sol-gel chemistry of transition metal oxides. *Progress in Solid State Chemistry*, 18(4), 259-341.

Luna, M. L., Taboada-Ortega, M. A., Alvarez-Amparán, M. A., & Cedeño-Caero, L. (2022). Effect of iron incorporation on W based catalysts for oxidative desulfurization of dibenzothiophene compounds. *Catalysis Today*, 394, 336-347.

Lü, H., Zhang, Y., Jiang, Z., & Li, C. (2010). Aerobic oxidative desulfurization of benzothiophene, dibenzothiophene and 4, 6-dimethyldibenzothiophene using an Anderson-type catalyst $[(18H_{37})_2N(CH_3)_2]5\ [IMo_6O_{24}]$. *Green Chemistry,* 12(11), 1954-1958.

Luo, Q., Zhou, Q., Lin, Y., Wu, S., Liu, H., Du, C., Zhong, Y. and Yang, C. (2019). Fast and deep oxidative desulfurization of dibenzothiophene with catalysts of MoO_3–TiO_2@ MCM-22 featuring adjustable Lewis and Brønsted acid sites. *Catalysis Science & Technology,* 9(21), 6166-6179.

Luo, S., Fan, J., Liu, W., Zhang, M., Song, Z., Lin, C., Wu, X., & Chu, P. K. (2006). Synthesis and low-temperature photoluminescence properties of SnO_2 nanowires and nanobelts. *Nanotechnology,* 17(6), 1695.

Lupan, O., Trofim, V., Cretu, V., Stamov, I., Syrbu, N. N., Tiginyanu, I., Mishra, Y. K., & Adelung, R. (2014). Investigation of optical properties and electronic transitions in bulk and nano-microribbons of molybdenum trioxide. *Journal of Physics D: Applied Physics,* 47(8), 085302.

Lv, G., Deng, S., Yi, Z., Zhang, X., Wang, F., Li, H., & Zhu, Y. (2019). One-pot synthesis of framework W-doped TS-1 zeolite with robust Lewis acidity for effective oxidative desulfurization. *Chemical Communications,* 55(33), 4885-4888.

Ma, C., Chen, D., Liu, F., Sun, X., Xiao, F., & Dai, B. (2015). Oxidative desulfurization of a model fuel using ozone oxidation generated by dielectric barrier discharge plasma combined with Co_3 O_4/γ-A_{l2} O_3 catalysis. *RSC Advances*, 5(117), 96945-96952.

Ma, X. S., & Shi, Y. J. (1987). Study of Operating Condition Affecting Mass Transfer Rate in Liquid Surfactant Membrane Process. *Separation Science and Technology*, *22*(2-3), 819-829. https://doi.org/10.1080/01496398708068983

Da Silva Madeira, L., Ferreira-Leitão, V. S., & Da Silva Bon, E. P. (2008). Dibenzothiophene oxidation by horseradish peroxidase in organic media: Effect of the DBT: H_2O_2 molar ratio and H_2O_2 addition mode. *Chemosphere,* 71(1), 189-194.

Madhu Mohan, V., Bin, H., & Chen, W. (2010). Enhancement of electrochemical properties of MoO 3 nanobelts electrode using PEG as surfactant for lithium battery. *Journal of Solid State Electrochemistry*, 14, 1769-1775.

Madras, G., & McCoy, B. J. (2004). Temperature effects on the transition from nucleation and growth to Ostwald ripening. *Chemical Engineering Science*, *59*(13), 2753-2765. https://doi.org/10.1016/j.ces.2004.03.022

Majewski, A. (2020). *What is Diesel Fuel*. https://dieselnet.com/tech/fuel_diesel.php

Mallesham, B., Rangaswamy, A., Rao, B. G., Rao, T. V., & Reddy, B. M. (2020). Solvent-free production of glycerol carbonate from bioglycerol with urea over nanostructured promoted SnO 2 catalysts. *Catalysis Letters,* 150, 3626-3641.

Malliaris, A., Le Moigne, J., Sturm, J., & Zana, R. (1985). Temperature dependence of the micelle aggregation number and rate of intramicellar excimer formation in aqueous surfactant solutions. *The Journal of Physical Chemistry,* 89(12), 2709-2713.

M Marte, A., Indolfi, P., Ficociello, C., Russo, D., Oreste, M., Bottigliero, G., Gualdiero, G., Barone, C., Vigliar, E., Indolfi, C., & Casale, F. (2013). Inflammatory myofibroblastic bladder tumor in a patient with wolf-hirschhorn syndrome. *Case reports in Urology*, 2013, 20-37

Mamatha, K. M., Ravikumar, C. R., Murthy, H. A., Kumar, V. D., Kumar, A. N., & Jahagirdar, A. A. (2022). Facile green synthesis of Molybdenum oxide nanoparticles using Centella Asiatica plant: Its photocatalytic and electrochemical lead sensor applications. *Sensors International,* 3, 100153.

Manjunathan, P., Marakatti, V. S., Chandra, P., Kulal, A. B., Umbarkar, S. B., Ravishankar, R., & Shanbhag, G. V. (2018). Mesoporous tin oxide: An efficient catalyst with versatile applications in acid and oxidation catalysis. *Catalysis Today,* 309, 61-76.

Martos, M., Morales, J., & Sánchez, L. (2000). Cation-deficient MoySnxO2 oxides as anodes for lithium ion batteries. *Electrochimica Acta,* 46(1), 83-89.

Matsumoto, S. I., Ikeda, Y., Suzuki, H., Ogai, M., & Miyoshi, N. (2000). NOx storage-reduction catalyst for automotive exhaust with improved tolerance against sulfur poisoning. *Applied Catalysis B: Environmental,* 25(2-3), 115-124.

Mishra, R. (2019). *Nanoporous Materials.* https://scholar.google.com

Mohebali, G., & Ball, A. S. (2008). Biocatalytic desulfurization (BDS) of petrodiesel fuels. *Microbiology*, *154*(8), 2169-2183. https://doi.org/10.1099/mic.0.2008/017608-0

Mohebali, G., & Ball, A. S. (2016). Biodesulfurization of diesel fuels: Past, present and future perspectives. *International Biodeterioration & Biodegradation*, *110*, 163-180. https://doi.org/10.1016/j.ibiod.2016.03.011

Wan Abdullah, W. N., Wan Abu Bakar, W. A., Ali, R., & Embong, Z. (2015). Oxidative desulfurization of commercial diesel catalyzed by tert-butyl hydroperoxide polymolybdate on alumina: Optimization by Box-Behnken design. Clean Technologies and Environmental Policy, 17, 433-441.

Niederberger, M. (2009). *Metal Oxide Nanoparticles in Organic Solvents: Synthesis, Formation, Assembly and Application*. https://scholar.google.com/

Nilsson, A. (2011). *Chemical Bonding at Surfaces and Interfaces*. https://scholar.google.com/

Noh, J. S., & Schwarz, J. A. (1990). Effect of HNO_3 treatment on the surface acidity of activated carbons. *Carbon*, *28*(5), 675-682.

Okamoto, Y., Oh-Hiraki, K., Imanaka, T., & Teranishi, S. (1981). X-ray photoelectron spectroscopic study of mixed oxide catalysts containing molybdenum: SnO_2-MoO*3* catalysts. *Journal of Catalysis,* 71(1), 99-110.

lutoye, M. A., & Hameed, B. H. (2016). Kinetics and deactivation of a dual-site heterogeneous oxide catalyst during the transesterification of crude jatropha oil with methanol. *Journal of Taibah University for Science,* 10(5), 685-699.

Optenhostert, T., Puthenkalam, S., Stegmann, N., Steffen, M., & Schmidt, W. (2021). Catalytic Hydrodesulfurization of Gaseous Fuels with Autogenously Formed Hydrogen. *Chemie Ingenieur Technik,* 93(6), 1028-1032.

Otsuki, S., Nonaka, T., Takashima, N., Qian, W., Ishihara, A., Imai, T., & Kabe, T. (2000). Oxidative desulfurization of light gas oil and vacuum gas oil by oxidation and solvent extraction. *Energy & fuels,* 14(6), 1232-1239.

Owen, K. C. (1995). *Automotive Fuels Reference Book*. Warrendale, PA.

Pal, N., & Bhaumik, A. (2013). Soft templating strategies for the synthesis of mesoporous materials: Inorganic, organic–inorganic hybrid and purely organic solids. *Advances in Colloid and Interface Science*, *189-190*, 21-41.

Pal, N., & Bhaumik, A. (2013). Soft templating strategies for the synthesis of mesoporous materials: Inorganic, organic–inorganic hybrid and purely organic solids. *Advances in Colloid and Interface Science*, 189, 21-41.

Palaić, N., Sertić-Bionda, K., Margeta, D., & Podolski, Š. (2015). Oxidative desulphurization of diesel fuels. *Chemical and Biochemical Engineering Quarterly*, 29(3), 323-327.

Pandey, S., & Srivastava, V. C. (2018). Oxidative-extractive desulfurization of liquid fuel using stannous chloride-acetic acid mixture as catalyst. *Petroleum Science and Technology*, *36*(1), 40-47. https://doi.org/10.1080/10916466.2017.1403451

Perinelli, D. R., Cespi, M., Lorusso, N., Palmieri, G. F., Bonacucina, G., & Blasi, P. (2020). Surfactant self-assembling and critical micelle concentration: One approach fits all? *Langmuir,* 36(21), 5745-5753.

Pitto-Barry, A., & Barry, N. P. E. (2014). Pluronic® block-copolymers in medicine: From chemical and biological versatility to rationalisation and clinical advances. *Polymer Chemistry*, *5*(10), 3291-3297. https://doi.org/10.1039/C4PY00039K

Pletnev, M. (2001). Chemistry of Surfactants. https://scholar.google.com

Polarz, S., & Smarsly, B. (2019). An Introduction to Nanoporous Materials. *Journal of Nanoscience and Nanotechnology*, *2*(6), 581-612. https://doi.org/10.1166/jnn.2002.151

Pouladi, B., Fanaei, M. A., & Baghmisheh, G. (2019). Optimization of oxidative desulfurization of gas condensate via response surface methodology approach. *Journal of Cleaner Production,* 209, 965-977.

Poyraz, A. S., & Dag, Ö. (2009). Role of Organic and Inorganic Additives on the Assembly of CTAB-P123 and the Morphology of Mesoporous Silica Particles. *The Journal of Physical Chemistry C*, *113*(43), 18596-18607. https://doi.org/10.1021/jp907303a

Poyraz, A. S., Kuo, C. H., Biswas, S., King'ondu, C. K., & Suib, S. L. (2013). A general approach to crystalline and monomodal pore size mesoporous materials. *Nature Communications*, 4(1), 2952.

P Pradeesh, G., Ponnuswamy, V., Gowtham, B., Suresh, R., & Chandrasekaran, J. (2018). Influence of annealing temperature on the properties of molybdenum oxide nanoparticles prepared through chemical precipitation method for pn junction diode application. *Optik,* 175, 217-227.

Mohana-Priya, S., Geetha, A., & Ramamurthi, K. (2016). Structural, morphological and optical properties of tin oxide nanoparticles synthesized by sol–gel method adding hydrochloric acid. *Journal of Sol-Gel Science and Technology,* 78, 365-372.

Purkayastha, M. D., & Manhar, A. K. (2016). *Nanotechnological Applications in Food Packaging, Sensors and Bioactive Delivery Systems.* https://scholar.google.com

Qi, L., Zheng, P., Zhao, Z., Duan, A., Xu, C., & Wang, X. (2022). Insights into the intrinsic kinetics for efficient hydrodesulfurization of 4, 6-dimethyldibenzothiophene over mesoporous CoMoS2/ZSM-5. *Journal of Catalysis,* 408, 279-293.

Qin, X., Huang, Y., Wang, K., Xu, T., Wang, Y., Liu, P., Kang, Y., & Zhang, Y. (2019). Novel hierarchically porous Ti-MOFs/nitrogen-doped graphene nanocomposite served as high efficient oxygen reduction reaction catalyst for fuel cells application. *Electrochimica Acta,* 297, 805-813.

Qiu, J., Wang, G., Zhang, Y., Zeng, D., & Chen, Y. (2015). Direct synthesis of mesoporous $H_3PMo1_2O_{40}/SiO_2$ and its catalytic performance in oxidative desulfurization of fuel oil. *Fuel,* 147, 195-202.

Rafiee, E., & Rahpeyma, N. (2015). Selective Oxidation of Sulfurs and Oxidation Desulfurization of Model Oil by 12-Tungstophosphoric Acid on Cobalt-Ferrite Nanoparticles as Magnetically Recoverable Catalyst. *Chinese Journal of Catalysis, 36*(8), 1342. https://doi.org/10.1016/S1872-2067(15)60862-2

Rajendran, A., Fan, H. X., Cui, T. Y., Feng, J., & Li, W. Y. (2021). Enrichment of polymeric WOx species in WOx@ SnO_2 catalysts for ultra-deep oxidative desulfurization of liquid fuels. *Fuel,* 290, 120036.

Rao, C., Shen, J., Wang, F., Peng, H., Xu, X., Zhan, H., Fang, X., Liu, J., Liu, W., & Wang, X. (2018). SnO_2 promoted by alkali metal oxides for soot combustion: The effects of surface oxygen mobility and abundance on the activity. *Applied Surface Science*, 435, 406-414.

Rao, C. N. R., Müller, A., & Cheetham, A. K. (Eds.). (2006). *The chemistry of Nanomaterials: Synthesis, Properties and Applications*. John Wiley & Sons.

Rapp, B. E. (2017). *Chapter 20-Surface Tension. Rapp Mechanics and Mathematics, BEBT-M. M, editor. Micro and Nano Technologies*. Elsevier, 421-44.

Reddy, R. K. K., Kailasa, S., Rani, B. G., Jayarambabu, N., Yasuhiko, H., Ramana, G. V., & Rao, K. V. (2019). Hydrothermal approached 1-D molybdenum oxide nanostructures for high-performance supercapacitor application. *SN Applied Sciences*, 1, 1-9.

Ren, Y., Ma, Z., & Bruce, P. G. (2012). Ordered mesoporous metal oxides: Synthesis and applications. *Chemical Society Reviews*, 41(14), 4909-4927.

Rivoira, L., Martínez, M. L., Anunziata, O., & Beltramone, A. (2017). Vanadium oxide supported on mesoporous SBA-15 modified with Al and Ga as a highly active catalyst in the ODS of DBT. *Microporous and Mesoporous Materials,* 254, 96-113.

Rodriguez, J. A. (2003). Electronic and chemical properties of mixed-metal oxides: basic principles for the design of DeNOx and DeSOx catalysts. *Catalysis Today*, *85*(2), 177-192. https://doi.org/10.1016/S0920-5861(03)00385-7

Rivoira, L., Martínez, M. L., Anunziata, O., & Beltramone, A. (2017). Vanadium oxide supported on mesoporous SBA-15 modified with Al and Ga as a highly active catalyst in the ODS of DBT. *Microporous and Mesoporous Materials,* 254, 96-113.

Rosi, N. L., & Mirkin, C. A. (2005). Nanostructures in Biodiagnostics. *Chemical Reviews*, *105*(4), 1547-1562. https://doi.org/10.1021/cr030067f

Ruel-Gariépy, E., & Leroux, J.-C. (2004). In situ-forming hydrogels: Review of temperature-sensitive systems. *European Journal of Pharmaceutics and Biopharmaceutics*, *58*(2), 409-426. https://doi.org/10.1016/j.ejpb.2004.03.019

Safa, M. A., Bouresli, R., Al-Majren, R., Al-Shamary, T., & Ma, X. (2019). Oxidative desulfurization kinetics of refractory sulfur compounds in hydrotreated middle distillates. *Fuel,* 239, 24-31.

Safa, M. A., & Ma, X. (2016). Oxidation kinetics of dibenzothiophenes using cumene hydroperoxide as an oxidant over MoO_3/Al_2O_3 catalyst. *Fuel*, *171*, 238-246. https://doi.org/10.1016/j.fuel.2015.12.050

Sagadevan, S., Lett, J. A., Fatimah, I., Lokanathan, Y., Léonard, E., Oh, W. C., Hossain, M. M., & Johan, M. R. (2021). Current trends in the green syntheses of tin oxide nanoparticles and their biomedical applications. *Materials Research Express,* 8(8), 082001.

Saha, B., Vedachalam, S., & Dalai, A. K. (2021). Review on recent advances in adsorptive desulfurization. *Fuel Processing Technology,* 214, 106685.

Sakthikumar, K., Ede, S. R., Mishra, S., & Kundu, S. (2016). Shape-selective synthesis of $Sn(MoO_4)_2$ nanomaterials for catalysis and supercapacitor applications. *Dalton Transactions,* 45(21), 8897-8915.

Saleh, T. A. (2021). Carbon nanotube-incorporated alumina as a support for MoNi catalysts for the efficient hydrodesulfurization of thiophenes. *Chemical Engineering Journal*, 404, 126987. https://doi.org/10.1016/j.cej.2020.126987

Sangeetha, P., Sasirekha, V., & Ramakrishnan, V. (2011). Micro-Raman investigation of tin dioxide nanostructured material based on annealing effect. *Journal of Raman Spectroscopy,* 42(8), 1634-1639.

Sato, K., Hyodo, M., Aoki, M., Zheng, X. Q., & Noyori, R. (2001). Oxidation of sulfides to sulfoxides and sulfones with 30% hydrogen peroxide under organic solvent-and halogen-free conditions. *Tetrahedron,* 57(13), 2469-2476.

Satterfield, C. (1991). *Heterogeneous Catalysis in Industrial Practice (2nd edition)*. New York, NY (United States); McGraw Hill Book Co.

Seguin, L., Figlarz, M., Cavagnat, R., & Lassègues, J. C. (1995). Infrared and Raman spectra of MoO3 molybdenum trioxides and $MoO_3 \cdot xH_2O$ molybdenum trioxide hydrates. *Spectrochimica Acta Part A: Molecular and Biomolecular Spectroscopy*, 51(8), 1323-1344.

Sen, S. K., Dutta, S., Khan, M. R., Manir, M. S., Dutta, S., Al Mortuza, A., Razia, S., & Hakim, M. A. (2019). Characterization and antibacterial activity study of hydrothermally synthesized h-MoO_3 nanorods and α-MoO_3 nanoplates. *Bionanoscience,* 9, 873-882.

Sengupta, A., Kamble, P. D., Basu, J. K., & Sengupta, S. (2012). Kinetic study and optimization of oxidative desulfurization of benzothiophene using mesoporous titanium silicate-1 catalyst. *Industrial & Engineering Chemistry Research*, 51(1), 147-157.

Sengupta, J., Sahoo, R. K., Bardhan, K. K., & Mukherjee, C. D. (2011). Influence of annealing temperature on the structural, topographical and optical properties of sol–gel derived ZnO thin films. *Materials Letters,* 65(17-18), 2572-2574.

Shaabani, A., Behnam, M., & Rezayan, A. H. (2009). Tungstophosphoric acid (H3PW12O40) catalyzed oxidation of organic compounds with $NaBrO_3$. *Catalysis Communications,* 10(7), 1074-1078.

Shafi, R., & Hutchings, G. J. (2000). Hydrodesulfurization of hindered dibenzothiophenes: an overview. *Catalysis Today*, *59*(3), 423-442.

Shan, W., Liu, F., He, H., Shi, X., & Zhang, C. (2011). Novel cerium–tungsten mixed oxide catalyst for the selective catalytic reduction of NO_x with NH_3. *Chemical Communications,* 47(28), 8046-8048.

Shchukin, E. D., Pertsov, A. V., Amelina, E. A., & Zelenev, A. S. (2001). *Structure, Stability and Degradation of Various Lyophobic Disperse Systems.* https://scholar.google.com

Shehzad, K., Shah, N. A., Amin, M., Abbas, M., & Syed, W. A. (2018). Synthesis of SnO2 nanowires forCO, CH4 and CH3OH gases sensing. *International Journal of Distributed Sensor Networks*, 14(8), 1550147718790750.

Shen, D., Dai, Y., Han, J., Gan, L., Liu, J., & Long, M. (2018). A nanocellulose template strategy for the controllable synthesis of tungsten-containing mesoporous silica for ultra-deep oxidative desulfurization. *Chemical Engineering Journal,* 332, 563-571.

Shi, P., Zhang, H., Lin, L., Song, C., Chen, Q., & Li, Z. (2019). Molecular dynamics simulation of four typical surfactants in aqueous solution. *RSC Advances*, 9(6), 3224-3231.

Shylesh, S., Schünemann, V., & Thiel, W. R. (2010). Magnetically separable nanocatalysts: bridges between homogeneous and heterogeneous catalysis. *Angewandte Chemie International Edition,* 49(20), 3428-3459.

Siciliano, T., Tepore, A., Filippo, E., Micocci, G., & Tepore, M. (2009). Characteristics of molybdenum trioxide nanobelts prepared by thermal evaporation technique. *Materials Chemistry and Physics,* 114(2-3), 687-691.

Sing, K. (1982). Reporting Physisorption Data for Gas/Solid Systems with Special Reference to the Determination of Surface Area and Porosity. *Pure and Applied Chemistry*, *54*, 2201-2218. https://doi.org/10.1351/pac198254112201

Sing, K. (1985). Reporting physisorption data for gas/solid systems with special reference to the determination of surface area and porosity (Recommendations 1984). *Pure and Applied Chemistry*, *57*(4), 603-619. https://doi.org/10.1351/pac198557040603

Kothaplamoottil-Sivan, S., Padinjareveetil, A. K., Padil, V. V., Pilankatta, R., George, B., Senan, C., Černík, M., & Varma, R. S. (2019). Greener assembling of MoO_3 nanoparticles supported on gum arabic: Cytotoxic effects and catalytic efficacy towards reduction of p-nitrophenol. *Clean Technologies and Environmental Policy,* 21, 1549-1561.

Soleimani, M., Bassi, A., & Margaritis, A. (2007). Biodesulfurization of refractory organic sulfur compounds in fossil fuels. *Biotechnology Advances,* 25(6), 570-596.

Song, C., & Ma, X. (2004). Ultra-deep Desulfurization of Liquid Hydrocarbon Fuels: Chemistry and Process. *International Journal of Green Energy*, *1*, 167-191. https://doi.org/10.1081/GE-120038751

Speight, J. G. (2020). Petroleum Refining and Environmental Control and Environmental Effects. In R. Malhotra (Ed.), *Fossil Energy* (pp. 101-131). Springer New York. https://doi.org/10.1007/978-1-4939-9763-3_70

Spivey, A. C., Weston, M., & Woodhead, S. (2002). Celastraceae sesquiterpenoids: biological activity and synthesis. *Chemical Society Reviews*, 31(1), 43-59.

Srivastava, V. C. (2012). An evaluation of desulfurization technologies for sulfur removal from liquid fuels. *RSC Advances*, *2*(3), 759-783. https://doi.org/10.1039/C1RA00309G

Strukul, G. (1992). *Catalytic Oxidations with Hydrogen Peroxide as Oxidant*. Springer Netherlands. https://books.google.co.tz/books?id=Lmt3x9CyfLgC

Subhan, S., Rahman, A. U., Yaseen, M., Rashid, H. U., Ishaq, M., Sahibzada, M., & Tong, Z. (2019). Ultra-fast and highly efficient catalytic oxidative desulfurization of dibenzothiophene at ambient temperature over low Mn loaded Co-Mo/Al_2O_3 and Ni-Mo/Al_2O_3 catalysts using NaClO as oxidant. *Fuel*, 237, 793-805.

Sui, Y., Huang, X., Ma, Z., Li, W., Qiao, F., Chen, K., & Chen, K. (2003). The effect of thermal annealing on crystallization in a-Si: H/SiO2 multilayers by using layer by layer plasma oxidation. *Journal of Physics: Condensed Matter,* 15(34), 5793.

Švachula, J., Králíková, B., Tichý, J., & Machek, J. (1991). Acid-base properties of Sn− Mo− Ox catalysts. *Reaction Kinetics and Catalysis Letters,* 44(1), 45-49.

Svensson, B., Alexandridis, P., & Olsson, U. (1998). Self-assembly of a poly (ethylene oxide)/poly (propylene oxide) block copolymer (pluronic P104,(EO) 27 (PO) 61 (EO) 27) in the presence of water and xylene. *The Journal of Physical Chemistry B*, 102(39), 7541-7548.

Takita, Y., Ozaki, A., & Moro-oka, Y. (1972). Catalytic oxidation of olefins over oxide catalysts containing molybdenum: V. Relation between the surface concentration of acidic sites and the catalytic activity to form acetone. *Journal of Catalysis,* 27(2), 185-192.

Tam, P. S. (1990). Desulfurization of fuel Relation between the surface concentration of acidic sites and the catalytic activity oil by oxidation and extraction. 1. Enhancement of extraction oil yield. *Industrial & Engineering Chemistry Research*, *29*(3), 321-324. https://doi.org/10.1021/ie00099a002

Tanabe, K., Itoh, M., Morishige, K., & Hattori, H. (1976). *The Effect of Preparation Method on the Acidity of Mixed Oxides.* https://scholar.google.com

Tang, X., Li, Y., Huang, X., Xu, Y., Zhu, H., Wang, J., & Shen, W. (2006). MnOx–CeO2 mixed oxide catalysts for complete oxidation of formaldehyde: Effect of preparation method and calcination temperature. *Applied Catalysis B: Environmental,* 62(3-4), 265-273.

Tazikeh, S., Akbari, A., Talebi, A., & Talebi, E. (2014). Synthesis and characterization of tin oxide nanoparticles via the Co-precipitation method. *Materials Science-Poland,* 32, 98-101.

Teimouri, A., Mahmoudsalehi, M., & Salavati, H. (2018). Catalytic oxidative desulfurization of dibenzothiophene utilizing molybdenum and vanadium oxides supported on MCM-41. *International Journal of Hydrogen Energy*, 43(31), 14816-14833

Thalgaspitiya, W. R., Kapuge, T. K., He, J., Rathnayake, D., Kerns, P., & Suib, S. L. (2020). Mesoporous Molybdenum–Tungsten Mixed Metal Oxide: A Solid Acid Catalyst for Green, Highly Efficient sp3–sp2 C–C Coupling Reactions. *ACS Applied Materials & Interfaces,* 12(5), 5990-5998.

Thangasamy, P., Ilayaraja, N., Jeyakumar, D., & Sathish, M. (2017). Electrochemical cycling and beyond: Unrevealed activation of MoO3 for electrochemical hydrogen evolution reactions. *Chemical Communications,* 53(14), 2245-2248.

Thalgaspitiya, W. R., Kapuge, T. K., He, J., Rathnayake, D., & Suib, S. L. (2020). High surface area mesoporous tungsten oxide for fast, green oxidation of organosulfur compounds in crude oil. *Applied Materials Today,* 19, 100616.

Tjong, S. (2013). *Nanocrystalline Materials: Their Synthesis-Structure-Property Relationships and Applications*. https://scholar.google.com/

Tran, D. T., Palomino, J. M., & Oliver, S. R. (2018). Desulfurization of JP-8 jet fuel: Challenges and adsorptive materials. *RSC Advances,* 8(13), 7301-7314.

Trifirò, F. (1998). The chemistry of oxidation catalysts based on mixed oxides. *Catalysis Today*, *41*(1), 21-35. https://doi.org/10.1016/S0920-5861(98)00035-2

Tu, Y., Li, T., Yu, G., Wei, L., Ta, L., Zhou, Z., & Ren, Z. (2019). Study on modification and desulfurization performance of a molybdenum-based catalyst. *Energy & Fuels*, 33(9), 8503-8510.

Vedachalam, S., Baquerizo, N., & Dalai, A. K. (2022). Review on impacts of low sulfur regulations on marine fuels and compliance options. *Fuel,* 310, 122243.

Ramirez-Verduzco, L. F., Torres-Garcia, E., Gomez-Quintana, R., Gonzalez-Pena, V., & Murrieta-Guevara, F. (2004). Desulfurization of diesel by oxidation/extraction scheme: influence of the extraction solvent. *Catalysis Today,* 98(1-2), 289-294.

Vinogradov, S. V., Bronich, T. K., & Kabanov, A. V. (2002). Nanosized cationic hydrogels for drug delivery: preparation, properties and interactions with cells. *Advanced Drug Delivery Reviews*, 54(1), 135-147.

Vioux, A. (1997). Nonhydrolytic Sol−Gel Routes to Oxides. *Chemistry of Materials*, *9*(11), 2292-2299. https://doi.org/10.1021/cm970322a

Vioux, A. (2016). Nonhydrolytic Sol-Gel Technology. In L. Klein, M. Aparicio, & A. Jitianu (Eds.), *Handbook of Sol-Gel Science and Technology* (pp. 1-27). Springer International Publishing. https://doi.org/10.1007/978-3-319-19454-7_28-1

Wang, B. B., Zhu, K., Feng, J., Wu, J. Y., Shao, R. W., Zheng, K., & Cheng, Q. J. (2016). Low-pressure thermal chemical vapour deposition of molybdenum oxide nanorods. *Journal of Alloys and Compounds,* 661, 66-71.

Wang, D., & Astruc, D. (2014). Fast-Growing Field of Magnetically Recyclable Nanocatalysts. *Chemical Reviews*, *114*(14), 6949-6985. https://doi.org/10.1021/cr500134h

Wang, D., Qian, E. W., Amano, H., Okata, K., Ishihara, A., & Kabe, T. (2003). Oxidative desulfurization of fuel oil: Part I. Oxidation of dibenzothiophenes using tert-butyl hydroperoxide. *Applied Catalysis A: General,* 253(1), 91-99.

Wang, F., & Ueda, W. (2009). High Catalytic Efficiency of Nanostructured Molybdenum Trioxide in the Benzylation of Arenes and an Investigation of the Reaction Mechanism. *Chemistry: A European Journal*, *15*(3), 742-753.

Wang, H., & Prins, R. (2008). HDS of benzothiophene and dihydrobenzothiophene over sulfided Mo/γ-Al2O3. *Applied Catalysis A: General*, *350*(2), 191-196.

Wang, J., Zhao, D., & Li, K. (2010). Oxidative desulfurization of dibenzothiophene using ozone and hydrogen peroxide in ionic liquid. *Energy & Fuels,* 24(4), 2527-2529.

Wang, L., Li, M. C., Zhang, G. H., & Xue, Z. L. (2020). Morphology evolution and quantitative analysis of β-MoO_3 and α-MoO_3. *High Temperature Materials and Processes*, 39(1), 620-626.

Wang, X., Li, Z., Zhang, Z., Li, Q., Guo, E., Wang, C., & Yin, L. (2015). Mo-doped SnO_2 mesoporous hollow structured spheres as anode materials for high-performance lithium ion batteries. *Nanoscale,* 7(8), 3604-3613.

Wang, Y., Bi, F., Wang, Y., Jia, M., Tao, X., Jin, Y., & Zhang, X. (2021). MOF-derived CeO2 supported Ag catalysts for toluene oxidation: The effect of synthesis method. *Molecular Catalysis,* 515, 111922.

Wei, S., He, H., Cheng, Y., Yang, C., Zeng, G., Kang, L., Qian, H., & Zhu, C., 2017. Preparation, characterization, and catalytic performances of cobalt catalysts supported on KIT-6 silicas in oxidative desulfurization of dibenzothiophene. *Fuel,* 200, 11-21.

Weiss, W., & Ranke, W. (2002). Surface chemistry and catalysis on well-defined epitaxial iron-oxide layers. *Progress in Surface Science*, *70*(1), 1-151.

Wilson, K., & Lee, A. F. (2016). Catalyst design for biorefining. *Philosophical Transactions of the Royal Society A: Mathematical, Physical and Engineering Sciences*, *374*(2061), 20150081. https://doi.org/10.1098/rsta.2015.0081

Wolkenstein, T. (2012). *Electronic Processes on Semiconductor Surfaces during*. https://scholar.google.com

Wu, L., Li, Y., Fu, Z., & Su, B. L. (2020). Hierarchically structured porous materials: Synthesis strategies and applications in energy storage. *National Science Review,* 7(11), 1667-1701.

Xiao, X., Zhong, H., Zheng, C., Lu, M., Zuo, X., & Nan, J. (2016). Deep oxidative desulfurization of dibenzothiophene using a flower-like $WO_3ĚH_2O$ catalyst in an organic biphasic system. *Chemical Engineering Journal,* 304, 908-916.

Xu, H., Zhang, D., Wu, F., & Cao, R. (2017). Deep oxidative desulfurization of fuels based on [C_4mimCl] CoCl2 ionic liquid oxone solutions at room temperature. *Fuel,* 208, 508-513.

Xu, J. M., Li, L., Wang, S., Ding, H. L., Zhang, Y. X., & Li, G. H. (2013). Influence of Sb doping on the structural and optical properties of tin oxide nanocrystals. *CrystEngComm,* 15(17), 3296-3300.

Xu, K., Zeng, D., Tian, S., Zhang, S., & Xie, C. (2014). Hierarchical porous SnO2 micro-rods topologically transferred from tin oxalate for fast response sensors to trace formaldehyde. *Sensors and Actuators B: Chemical,* 190, 585-592.

Yadav, G. D., & Pujari, A. A. (1999). Friedel–Crafts acylation using sulfated zirconia catalyst. *Green Chemistry*, *1*(2), 69-74. https://doi.org/10.1039/A808891H

Yang, H., Jiang, B., Sun, Y., Zhang, L., Huang, Z., Sun, Z., & Yang, N. (2017). Heterogeneous oxidative desulfurization of diesel fuel catalyzed by mesoporous polyoxometallate-based polymeric hybrid. *Journal of Hazardous Materials,* 333, 63-72.

Yang, P., Zhao, D., Margolese, D. I., Chmelka, B. F., & Stucky, G. D. (1999). Block copolymer templating syntheses of mesoporous metal oxides with large ordering lengths and semicrystalline framework. *Chemistry of Materials,* 11(10), 2813-2826.

Yang, W., Zhou, W., Xu, W., Li, H., Huang, W., Jiang, B., Zhou, Z., & Yan, Y. (2012). Synthesis and characterization of a surface molecular imprinted polymer as a new adsorbent for the removal of dibenzothiophene. *Journal of Chemical & Engineering Data*, 57(6), 1713-1720.

Yang, Z., Lu, Y., & Yang, Z. (2009). Mesoporous materials: Tunable structure, morphology and composition. *Chemical Communications*, (17), 2270-2277.

Yansheng, C., Changping, L., Qingzhu, J., Qingshan, L., Peifang, Y., Xiumei, L., & Welz-Biermann, U. (2011). Desulfurization by oxidation combined with extraction using acidic room-temperature ionic liquids. *Green Chemistry*, 13(5), 1224-1229.

Yazu, K., Yamamoto, Y., Furuya, T., Miki, K., & Ukegawa, K. (2001). Oxidation of dibenzothiophenes in an organic biphasic system and its application to oxidative desulfurization of light oil. *Energy & Fuels,* 15(6), 1535-1536.

Yu, K. N., Xiong, Y., Liu, Y., & Xiong, C. (1997). Microstructural change of nano-SnO_2 grain assemblages with the annealing temperature. *Physical Review B*, 55(4), 2666.

Yu, X., Han, P., & Li, Y. (2018). Oxidative desulfurization of dibenzothiophene catalyzed by α-MnO_2 nanosheets on palygorskite using hydrogen peroxide as oxidant. *RSC Advances,* 8(32), 17938-17943.

Zakharova, G. S., Täschner, C., Volkov, V. L., Hellmann, I., Klingeler, R., Leonhardt, A., & Büchner, B. (2007). $MoO_{3-\delta}$ nanorods: synthesis, characterization and magnetic properties. *Solid State Sciences,* 9(11), 1028-1032.

Zha, J., & Roggendorf, H. (1991). Sol–gel science, the physics and chemistry of sol–gel processing, Ed. by C. J. Brinker and G. W. Scherer, Academic Press, Boston 1990, xiv, 908 pp., bound—ISBN 0-12-134970-5. *Advanced Materials*, *3*(10), 522-522. https://doi.org/10.1002/adma.19910031025

Zhang, J., Wang, A., Li, X., & Ma, X. (2011). Oxidative desulfurization of dibenzothiophene and diesel over [Bmim] 3PMo12O40. *Journal of Catalysis,* 279(2), 269-275.

Z Zhang, Q., Zhang, J., Yang, H., Dong, Y., Liu, Y., Yang, L., Wei, D., Wang, W., Bai, L., & Chen, H. (2019). Efficient aerobic oxidative desulfurization over Co–Mo–O bimetallic oxide catalysts. *Catalysis Science & Technology,* 9(11), 2915-2922.

Zhang, X., Bi, F., Zhu, Z., Yang, Y., Zhao, S., Chen, J., Lv, X., Wang, Y., Xu, J., & Liu, N. (2021). The promoting effect of H_2O on rod-like MnCeOx derived from MOFs for toluene oxidation: A combined experimental and theoretical investigation. *Applied Catalysis B: Environmental*, 297, 120393.

Zhang, X., Hou, F., Yang, Y., Wang, Y., Liu, N., Chen, D., & Yang, Y. (2017). A facile synthesis for cauliflower like CeO_2 catalysts from Ce-BTC precursor and their catalytic performance for CO oxidation. *Applied Surface Science,* 423, 771-779.

Zhang, X., Xiang, S., Du, Q., Bi, F., Xie, K., & Wang, L. (2022). Effect of calcination temperature on the structure and performance of rod-like MnCeOx derived from MOFs catalysts. *Molecular Catalysis,* 522, 112226.

Zhang, Y., Li, G., Kong, L., & Lu, H. (2018). Deep oxidative desulfurization catalyzed by Ti-based metal-organic frameworks. *Fuel,* 219, 103-110.

Zhao, D., & Wan, Y. (2007). Chapter 8 - The Synthesis of Mesoporous Molecular Sieves. In J. Čejka, H. van Bekkum, A. Corma, & F. Schüth (Eds.), *Studies in Surface Science and Catalysis* (Vol. 168, pp. 241-III). Elsevier.

Zhao, L., Qin, H., Wu, R. A., & Zou, H. (2012). Recent advances of mesoporous materials in sample preparation. *Journal of Chromatography A,* 1228, 193-204.

Zhao, W., Zheng, X., Liang, S., Zheng, X., Shen, L., Liu, F., Cao, Y., Wei, Z., & Jiang, L. (2018). Fe-doped γ-Al_2O_3 porous hollow microspheres for enhanced oxidative desulfurization: Facile fabrication and reaction mechanism. *Green Chemistry,* 20(20), 4645-4654.

Zheng, L., Xu, Y., Jin, D., & Xie, Y. (2009). Novel metastable hexagonal MoO3 nanobelts: Synthesis, photochromic, and electrochromic properties. *Chemistry of Materials,* 21(23), 5681-5690.

Zheng, P., Duan, A., Chi, K., Zhao, L., Zhang, C., Xu, C., Zhao, Z., Song, W., Wang, X., & Fan, J. (2017). I. Influence of sulfur vacancy on thiophene hydrodesulfurization mechanism at different MoS2 edges: A DFT study. *Chemical Engineering Science*, 164, 292-306.

Zhou, J., Lin, N., Wang, L., Zhang, K., Zhu, Y., & Qian, Y. (2015). Synthesis of hexagonal MoO 3 nanorods and a study of their electrochemical performance as anode materials for lithium-ion batteries. *Journal of Materials Chemistry A,* 3(14), 7463-7468.

Zhu, D. M., Feng, K. I., & Schelly, Z. A. (1992). Reverse micelles of Triton X-100 in cyclohexane: effects of temperature, water content, and salinity on the aggregation behavior. *The Journal of Physical Chemistry,* 96(5), 2382-2385.

Zhu, W., Zhu, G., Li, H., Chao, Y., Zhang, M., Du, D., ... & Zhao, Z. (2013). Catalytic kinetics of oxidative desulfurization with surfactant-type polyoxometalate-based ionic liquids. *Fuel Processing Technology,* 106, 70-76.

Zhuang, J., Hu, B., Tan, J., & Jin, X. (2014). Deep oxidative desulfurization of dibenzothiophene with molybdovanadophosphoric heteropolyacid-based catalysts. *Transition Metal Chemistry*, 39, 213-220.

Zuo, M., Huang, X., Li, J., Chang, Q., Duan, Y., Yan, L., Xiao, Z., Mei, S., Lu, S., & Yao, Y. (2019). Oxidative desulfurization in diesel via a titanium dioxide triggered thermocatalytic mechanism. *Catalysis Science & Technology,* 9(11), 2923-2930.

RESEARCH OUTPUTS

(i) Publication

Lesafi, F. J., Pogrebnaya, T., & King'ondu, C. K. (2022). Effect of the calcination temperature on SnO2-MoO3 crystal structure and catalytic activity in desulfurization of model diesel. *Fuel*, 330, 125601.

Lesafi F., Pogrebnaya T., & King'ondu C.K, (2022). *Mesoporous SnO_2-MoO_3 catalysts for diesel oxidative desulfurization: Impact of the SnO_2/MoO_3 mole ratio on catalytic efficiency (accepted for publication by the Heliyon).*

(ii) Poster Presentation